FIBER ADSORBENTS FOR TERT-BUTYL MERCAPTAN REMOVAL FROM PIPELINE GRADE NATURAL GAS

A Thesis
Presented to
The Academic Faculty

by

Grace Chen

In Partial Fulfillment
of the Requirements for the Degree
Master of Science in the
School of Chemical & Biomolecular Engineering

Georgia Institute of Technology
December 2013

FIBER ADSORBENTS FOR T-BUTYL MERCAPTAN REMOVAL

FROM PIPELINE GRADE NATURAL GAS

Approved by:

Dr. Christopher W. Jones
School of Chemical &
Biomolecular Engineering
Georgia Institute of Technology

Dr. William J. Koros
School of Chemical &
Biomolecular Engineering
Georgia Institute of Technology

Dr. Yoshiaki Kawajiri
School of Chemical &
Biomolecular Engineering
Georgia Institute of Technology

Date Approved: June 25, 2013

ACKNOWLEDGEMENTS

I would like to thank my family, my advisers Dr. Christopher Jones and Dr. William Koros, my friends, my committee member Dr. Yoshiaki Kawajiri, and General Electric for their assistance and support in completing this project.

TABLE OF CONTENTS

LIST OF TABLES

LIST OF FIGURES

NOMENCLATURE

13X	Zeolite 13X Sorbent
a	Annular Void Space around Fiber
A	Cross Sectional Area
ads	Adsorption Step
Bi_m	Biot Mass Number
BMC	Bare Module Cost
p	Pellet
c	Center Channel between Fibers
CA	Cellulose Acetate Polymer
cooling	Cooling Step
c_{TBM}	Concentration of TBM
CH_4	Methane
C_p	Specific Heat Capacity
d	Diameter
D	Diffusion Coefficient
des	Desorption Step
E	Base Equipment Cost
E’	Purchased Equipment Cost
F_m	Materials Factor
F_p	Pressure Factor
eq	Equilibrium
f	Fiber

G	Guthrie Method Factoring Estimation
ΔH_{vap}	Heat of Vaporization
heating	Heating Step
i	Interstitial
k	Mass Transfer Coefficient
k_B	Boltzmann Constant
L	Length
L (Appendix B only)	Labor
$_m$	Fiber Module
m	Mass
$\dot{m}$	Mass Flow Rate
M	Direct Field Materials
MW	Molecular Weight
n	Moles
$\dot{n}$	Molar Flow Rate
N	Number
NG	Natural Gas
NMP	N-Methyl-2-Pyrrolidone
OC	Operating Cost
p	Pellet
P	Pressure
P (Appendix B only)	Page Method Factoring Estimation
PL	Parasitic Load
Q	Heat
r	Radius

R	Gas Constant
Re	Reynolds Number
res	Residence Time
s	Superficial
SA	Surface Area
Sc	Schmidt Number
SF	Shape Factor
Sh	Sherwood Number
T	Temperature
TBM	t-Butyl Mercaptan Odorant
TCI	Total Capital Investment
TDC	Total Direct Cost
TIC	Total Installed Cost
TNC	Total Indirect Cost
tot	Whole System
v	Gas Velocity
V	Volume
$\dot{V}$	Volumetric Flow Rate
w	Weight Fraction
x	Capacity
α	Thermal Diffusivity
Δ	Change
ε	Void or Porosity
λ	Mean Free Path
κ	Thermal Conductivity

μ	Viscosity
ρ	Density
σ	Collision Diameter
τ	Tortuosity
φ	Volume Fraction
Ω	Collision Integral

SUMMARY

The purpose of this thesis study is to assess the feasibility of using a fiber sorbent module system to remove t-butyl mercaptan (TBM), a common odorant, from pipeline grade natural gas. Odorants such as mercaptans are added to natural gas for safety reasons, but their combustion products are corrosive and decrease the lifetime of the gas turbines in which they are combusted. Therefore, it is desirable to remove the odorants to extend this lifetime and improve efficiency.

A TBM removal system attached to a single 85 MW GE 7EA gas turbine process burning natural gas at a flow rate of approximately 15,000 standard cubic feet per minute (SCFM) serves as the basis for this system design and process analysis study. The concentration of odorants in natural gas is typically 10 ppm or less. For the purposes of this study, the upper limit of 10 ppm TBM was used. Zeolite 13X was selected as the model adsorbent for this study due to its high sorption capacity for mercaptans and its ease of incorporation into both fibers and pellets.

Design calculations were performed to optimize and determine the feasibility of fiber modules for TBM removal, as well as assess their advantages over conventional pellet packed beds. An understanding of how critical parameters such as heat and mass transfer resistances and pressure drop are affected by design specifications such as fiber sorbent and bed dimensions, allows an optimal design for the needs of the model turbine to be developed. Based on these design equations, a fiber sorbent module configuration that selectively and continuously removes TBM from natural gas was developed.

Additionally, different sorbent regeneration modes were considered and an economic analysis was performed on these systems to determine the best option. The capital and operating costs of the fiber sorbent treatment system and an equivalent pellet packed bed system were estimated for comparison purposes. Finally, the capital cost of the 85 MW turbine was also estimated and compared with that of the fiber sorbent system to determine the costs and savings of implementation. Based on these cost estimations, the fiber sorbent system has the potential to offer a simple, low-cost way to prevent corrosion in turbines, and are more economically and spatially attractive than traditional pellet packed bed technology.

CHAPTER 1

INTRODUCTION

1.1 Current Energy Scenario

A brief glimpse into the global history of energy shows the discovery and explosive growth of fossil fuel consumption since the 19th century, especially in the United States. The development of coal mining techniques in the U.S. in the late 18th century followed by government tax exemptions and subsidies for the coal industry in the mid-1900s led to coal becoming a dominant fuel source in the United States. The rise of petroleum and natural gas fuel soon followed the discovery of large reserves of these natural resources and the invention of the internal combustion engine. Eventually, federal energy tax policies led to petroleum and natural gas consumption surpassing coal by 1950. Together, these three fossil fuels are still the major source of the energy consumed in the United States today. The constant, rapid increase in energy demands coupled with energy independence and climate change concerns in the U.S. has encouraged the planned gradual conversion to clean fuel alternatives. As such, natural gas has recently come into the spotlight as a clean, economical, and domestically abundant energy source. However, the corrosiveness of the combustion products of sulfur impurities and added odorants in natural gas negatively impacts its economic benefits. Efficient removal of these impurities can relieve this problem and support the conversion from oil and coal to natural gas.

1.1.1 United States Energy Consumption by Source

As mentioned previously, the United States currently relies primarily on three fossil fuels, coal, oil, and natural gas, for most of its total energy needs. Electricity generation consumes a large fraction of this energy at 39.2% of the total energy consumed, relying primarily on coal, nuclear, and natural gas as a supply. As seen in Figure 1, coal is the largest contributor at 18.0% of the total energy supplied for electricity generation, followed by nuclear at 8.26% and natural gas at 7.74%[1]. However, a conscious effort has been made recently to reduce the use of coal, which releases high levels of air pollutants such as carbon dioxide, sulfur dioxide (SO_2), nitrogen oxides (NO_x), soot or ash, mercury and other heavy metals, and facilitate a major switch from coal to natural gas. Natural gas burns cleaner than other fossil fuels, is easier to transport, and has an increasing domestic supply[2]. Compared with coal usage at the power plant, natural gas produces half as much CO2, less than one third as much NO_x, and a negligible amount of SO_2 and mercury[3].

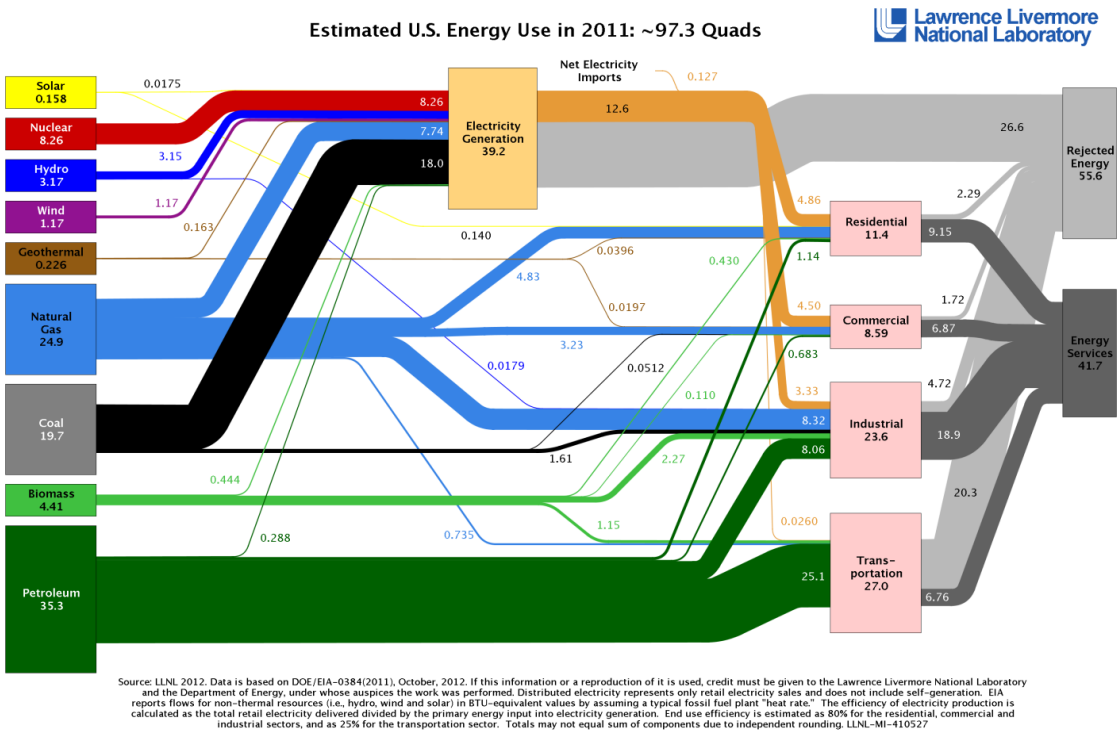

Figure 1: Energy flow diagram of the total energy supply and consumption in the United States in 2011. The left side indicates sources of energy while the right side indicates how much of each source is used in a particular sector. Almost 40% of the total energy consumed went towards electricity generation, and was supplied mainly by coal, natural gas, and nuclear sources. Source: Lawrence Livermore National Laboratory, 2011.

With these new policies and a continued increase in natural gas production with low prices, the natural gas industry is projected to grow significantly within the next few decades as the use of coal declines[4]. This, of course, will be largely seen in the electric power sector, which shows a strong growth in natural gas consumption[4]. The numbers displayed in Figure 2 track this projected growth, implying that natural gas for electricity generation will only become more significant with time.

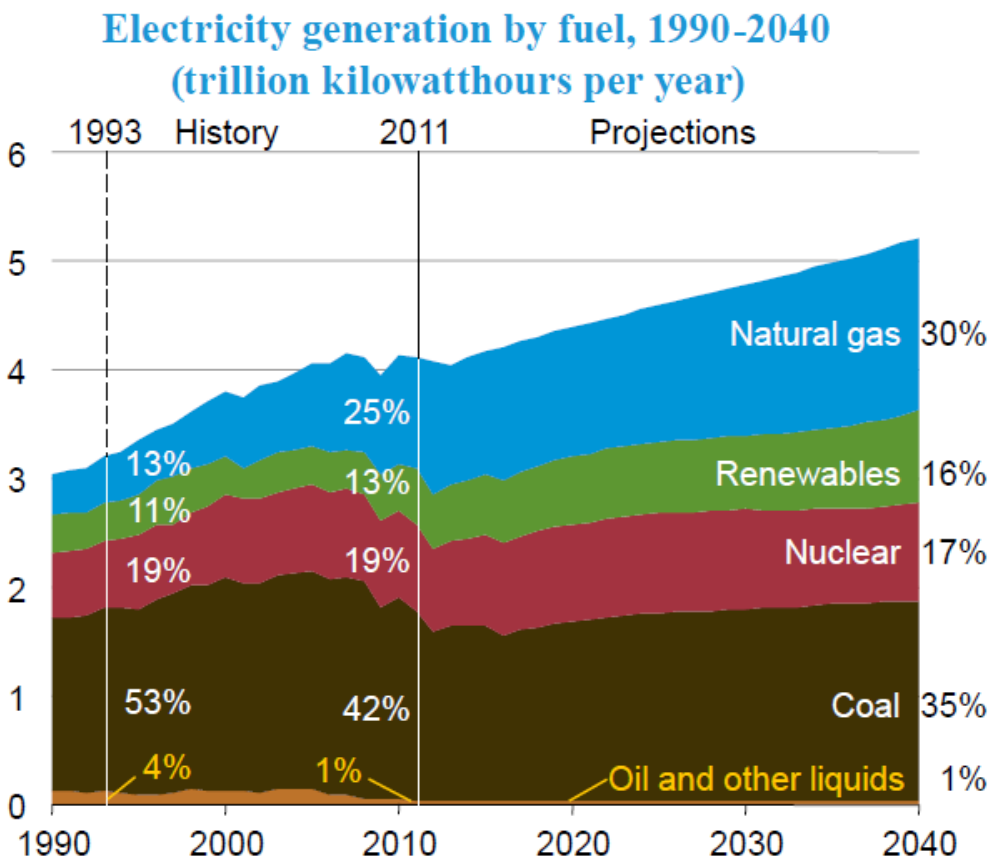

Figure 2: United States electricity generation by fuel type from 1990 to 2011, and projected onwards to 2040. Source: U.S. Energy Information Administration, Annual Energy Outlook, 2011.

1.1.2 Natural Gas-Fueled Power Plants

The increase in natural gas production coupled with new power plant emissions regulations will cause an increase in the use of natural gas for electricity generation. There already exists over 300,000 miles of natural gas transmission pipelines in the United States[5]. As shown in Figure 3, these pipelines form a highly integrated cross-country network that can supply natural gas to any location for any purpose. An increasing number of new power plants being built are fitted for natural gas fuel, in addition to current coal-fired power stations being replaced with natural gas units[6, 7].

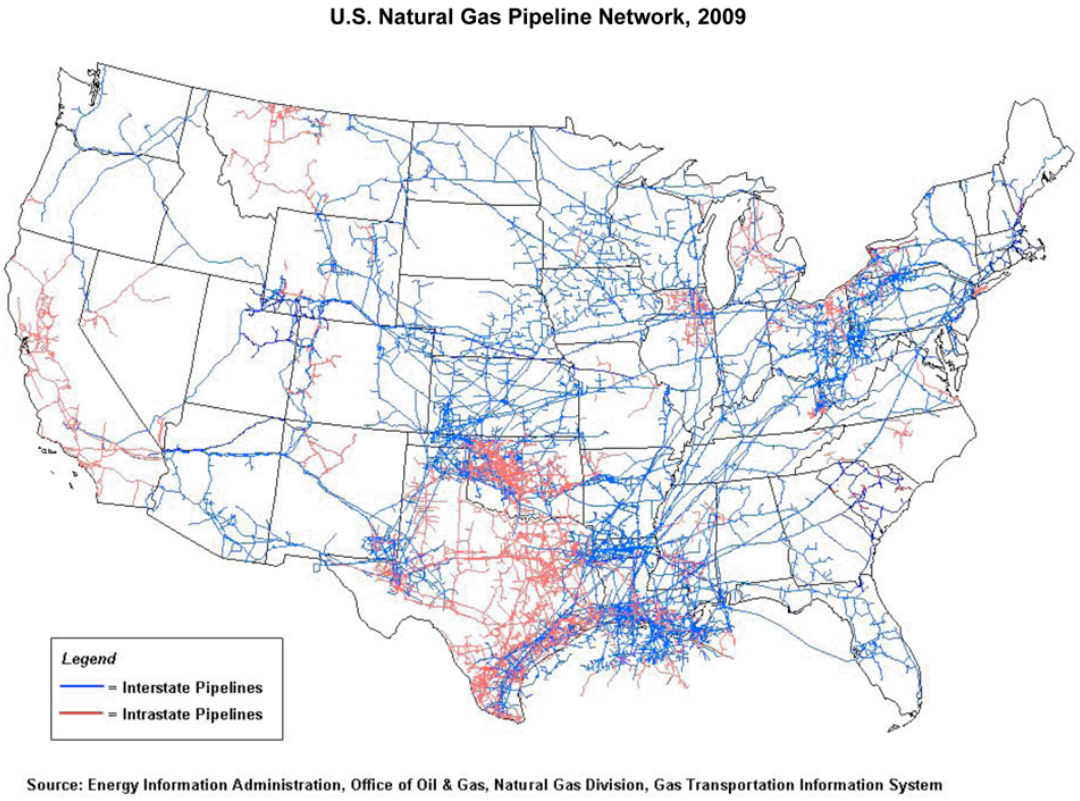

Figure 3: U.S. natural gas pipeline network, 2009. Source: Energy Information Administration, Office of Oil & Gas, Natural Gas Division, Gas Transportation Information System, 2009.

Commercially, the most common method used to generate electricity from natural gas is through electromagnetic induction, where mechanical energy created and supplied by a turbine is transformed into electricity. A gas turbine, or combustion turbine, uses hot, high pressure gases generated from the burning of natural gas to spin the turbine and generate electricity. An excess of air enters the turbine and is compressed before being mixed with natural gas and burned directly. On the other hand, a steam turbine first burns the natural gas in a boiler and uses the heat to create steam to turn the turbine and generate electricity. Alone, gas turbines and steam turbines are not very efficient, with only about 30-35% of the thermal energy generated being transformed to useful electricity. Today, many natural gas-fueled power plants operate in a combined cycle, as illustrated in Figure 4, integrating both a gas turbine and a steam turbine. The gas turbine

operates normally, but the waste heat is used to produce steam for use in the steam turbine, which then generates additional electricity. This leads to a thermal efficiency greater than that of a gas or steam turbine alone. Combined cycle plants can be as much as 50 to 60% efficient[6].

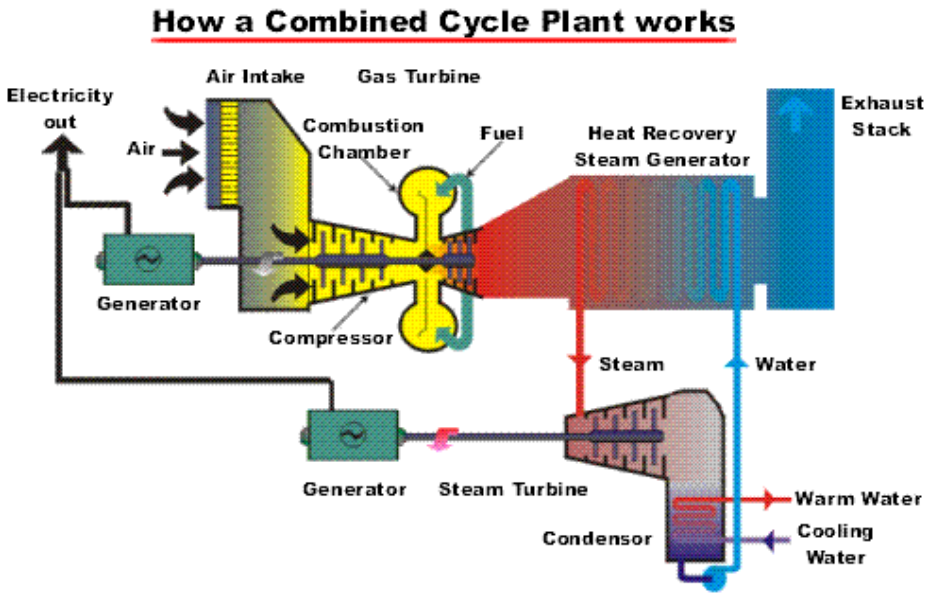

Figure 4: Diagram of a natural gas fueled combined cycle power plant. Source: Nooter/Eriksen Inc.

1.1.3 Odorants and their Combustion Products in Pipeline Natural Gas (evidence for corrosion and prevention strategies)

Raw natural gas, composed mostly of methane, is colorless and odorless, making leak detection difficult. The aftermath of a 1937 natural gas explosion in a Texas school led to U.S. legislature mandating the use of mercaptans as odorants in natural gas for ease of detection. The lower explosive limit (LEL) of natural gas in air is 5%, and regulations specify that the gas must be detectable at one-fifth of this limit. Therefore, according to this, the odorized natural gas must be detectable by an average person at a maximum

concentration of 1% in air[8]. However, while the mercaptans are useful for safety reasons, they are organosulfur compounds whose combustion products corrode the turbines and transmission / distribution pipelines in which they are used.

The combustion gas turbine in combined cycle power plants experiences a great deal of corrosion during use. Much of this corrosion happens because the sulfur present in the fuel reacts with alkali material taken in from the surrounding environment during combustion. The combustion product is a molten reactive residue containing alkaline sulfates. This residue settles and accumulates over turbine rotor blades, nozzle guide vanes, and other hot-section components, reacting with the oxide layer on the surface and demolishing it[9]. Figure 5 shows three different types of hot corrosion that may happen on combustion turbine surfaces. The large amount of air taken in by a gas turbine for combustion results in a highly oxidizing atmosphere in the turbine's combustion zone, which also contributes to corrosion[10]. Even a small amount of sulfur (as low as 0.05% by weight) in the fuel can effectively diffuse into the metal of the turbine and cause the devastating accelerated oxidation-corrosion reaction commonly known as "hot corrosion." The most common source of the alkali matter is salt (sodium chloride) in the large quantities of air taken into the compressor side of the gas turbine. This salt may come directly from seawater spray or from sea salt particles carried by the wind[9].

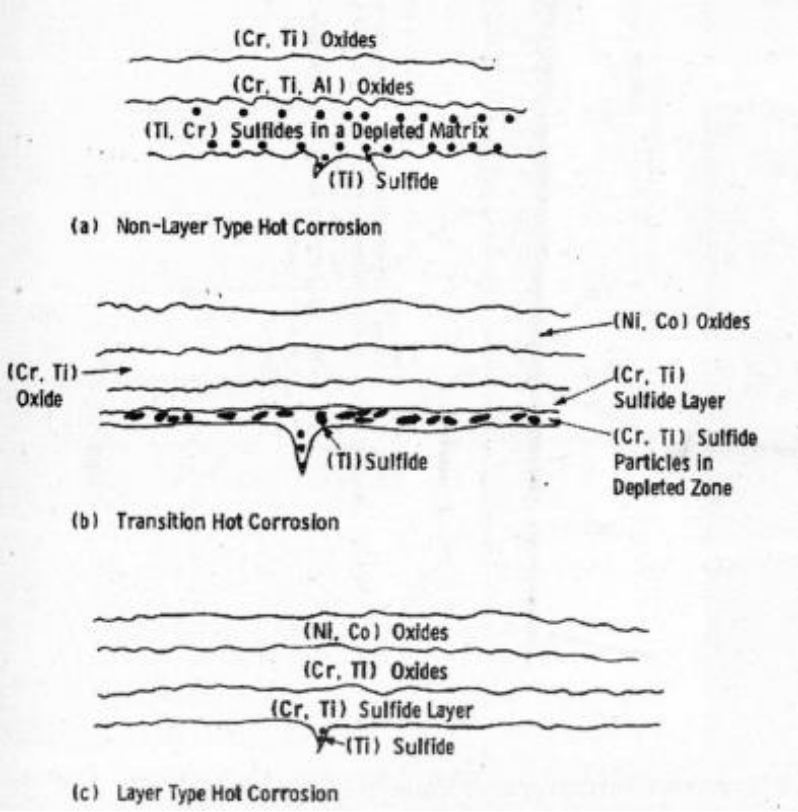

Figure 5: Schematic characterization of corrosion products found at areas typical of the three different hot corrosion regions. Source: Viswanathan R. *Case Histories on Integrity and Failures in Industry*, 1999.

Hot corrosion of combustion turbine surfaces reduces the overall turbine efficiency through surface roughening and profile thickening of blades and other parts[11]. As shown in Table 1, combustion turbine corrosion, as well as corrosion of generators and transmission structures, costs industry millions of dollars per year.

Table 1: A short compiled list of the costs of corrosion problems affecting broad sectors of the electric power industry for 1998. Highest costs are listed first. The corrosion costs to the combustion turbine and transmission sector are substantial. Source: Corrosion Inspection and Monitoring, 2007.

Corrosion problem	Sector	$ Millions	Percent (%)
Turbine corrosion fatigue (CF) and SCC	Fossil and nuclear	792	6.75
Corrosion in electric generators	Fossil and nuclear	459	3.91
Flow-accelerated corrosion	Fossil and nuclear	422	3.60
Oxide particle erosion of turbines	Fossil	360	3.07
Corrosion of tower footings, anchor rods, and tower structures	Transmission	99	0.84
Hot corrosion of combustion turbine (CT) blades and vanes	Combustion turbine	93	0.79
Hot oxidation of CT blades and vanes	Combustion turbine	35	0.30
HRSG flow-accelerated corrosion and underdeposit corrosion	Combustion turbine	20	0.18
Heat recovery steam generator (HRSG) CF	Combustion turbine	20	0.17
Corrosion of CT compressor section and CT exhaust section	Combustion turbine	18	0.16
Conductor deterioration	Transmission	18	0.15
Corrosion of splices and shield wires	Transmission	18	0.15
Corrosion of substation equipment	Transmission	5	0.04

Additionally, Figure 6 shows the results of another corrosion study done in 2002, which indicates the widespread problem of corrosion in all types of economic sectors. Particularly of interest to this work are the corrosion of gas and liquid transmission pipelines costing approximately $7.0 billion dollars per year, the corrosion during gas distribution costing approximately $5.0 billion dollars per year, and the corrosion in the electrical utilities sector costing approximately $6.9 billion dollars per year.

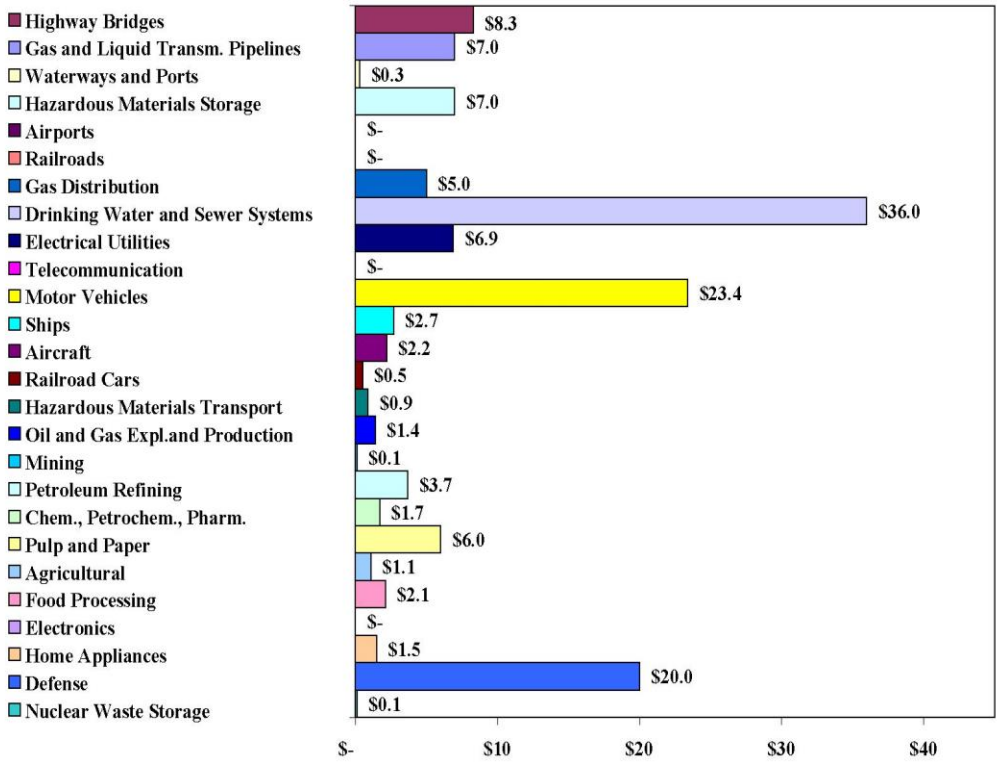

Figure 6: Cost of corrosion analyzed by economic sector in billions of dollars in year 2002. Source: NACE Cost of Corrosion Study, 2002.

To combat corrosion in turbines, several methods have been suggested. In the cases of light surface corrosion, reconditioning of the affected areas by cleaning and removing the chromium depleted zone can extend turbine life[9]. However, this requires on-going periodic monitoring by metallographic analysis (or even visual inspection) to determine when reconditioning is necessary. This can be both time-consuming and costly, as it requires a complete shutdown and opening of the turbine for an extended period of time. Another option would be to use high temperature corrosion resistant alloys in the manufacturing of turbine blades and other parts, however, the process of selecting these alloys can be complex and time consuming. There is often disagreement over which alloys are best to use for any application and if various alloys have different degrees of resistance depending on operating conditions such as temperature. Misunderstanding and improper selection of alloys can lead to equipment failure and

corrosion, or conversely lead to the selection of a more expensive alloy than necessary[12]. Studies have found that increasing the chromium content in various alloys will increase corrosion resistance at high (800 to 950°C) and lower (670-750°C) temperatures, but other than that, there is not much consensus on the positive effects of other metals[9, 10]. As hot corrosion requires both sulfur and an alkali to be present at high temperatures to form the reactive residue, it has been recommended that sulfur and / or alkali compounds be carefully removed from both the fuel and the surrounding environment before introduction into the turbine. For the intake air, efficient air filters must be used to capture the trace amounts of salt and / or sulfur compounds (such as H_2S, COS, SO_2) before entering the compression chamber. However, the composition of ambient air is constantly changing and it may be difficult to design a filter to sufficiently and selectively remove the desired compounds. The other option would be to remove sulfur compounds from the natural gas. Much of the sulfur present in treated natural gas comes from the mercaptans added for safety, though a trace amount may also come from naturally occurring hydrogen sulfide impurities[6]. This method will be explored in more detail in the following sections.

1.2 Sulfur Removal from Pipeline Natural Gas

Some of the difficulties associated with sulfur removal from odorized natural gas include the large amount of high pressure gas that needs to be processed as well at the ultra-low concentrations of odorants generally present. Some common techniques used to remove sulfur compounds from natural gas and other fuels are discussed below.

1.2.1 Catalytic Hydrodesulfurization (HDS)

A common method used to remove sulfur from natural gas and other fuels before combusting them is a two-step catalytic hydrodesulfurization process such as the one show in Figure 7. This is generally employed in the fuel refining process to reduce sulfur dioxide (SO_2) emissions from the exhaust gases of motor vehicles and other fuel combustion processes, as well as remove sulfur as a poisonous species in catalytic converters[13]. The process involves adding hydrogen to the sulfur compound in the presence of a Ni-Mo/Al_2O_3 or Co-Mo/ Al_2O_3 catalyst to cleave the carbon-sulfur bond and replace it with a carbon-hydrogen bond with hydrogen sulfide (H_2S) produced as a by-product[14]. In the second step, the H_2S must then be removed through adsorption on an amine contactor, zinc-oxide, or other sorbent[14, 15].

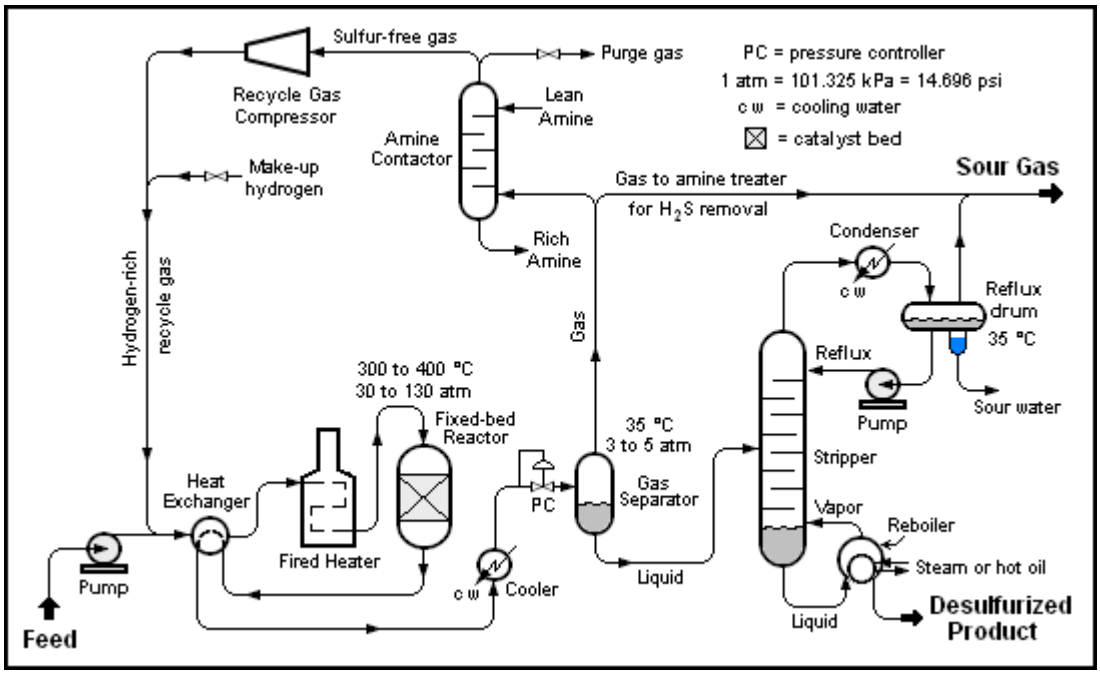

Figure 7: Schematic diagram of a hydrodesulfurization unit. The fuel feed is heated and pressurized before introduction into a fixed-bed reactor filled with catalyst where hydrodesulfurization happens. The H2S-containing hydrogen-rich product gas is treated with amines (or other sorbent) before being recycled back to the system. Source: Beychok, M. *Hydrodesulfurization*, 2006.

Industrially, the process takes place at high temperatures between 300-400°C and high pressures between 30-40 atmospheres. This process is efficient in sulfur removal with high sorption capacities, and is good for treating large volumes of gas with long cycle times[16]. However, this method is not only complex, but also energy intensive and expensive due to the need to keep both the catalyst and the adsorbent at the elevated temperature, and the need to add and recycle hydrogen to the system[14]. Additionally, zinc oxide needs to be replaced periodically and the process takes a long time to start up and it is generally not a good option for low concentrations of sulfur or small scale processes[17].

1.2.2 Selective Catalytic Oxidation (SCO)

Another approach uses activated carbon catalysts to selectively oxidize organosulfur compounds. For H_2S containing fuels, the products are water and elemental sulfur, which can then be separated from the fuel and sold[18]. An example of this process can be seen in Figure 8. For other organosulfur compounds, the electrophilic addition of oxygen to the sulfur atoms produces sulfoxides and sulfones, which can also be easily removed from the fuel stream. Air is commonly used as an oxidant for its oxygen content, but peroxides, peracids, and alkanols have also been used[19].

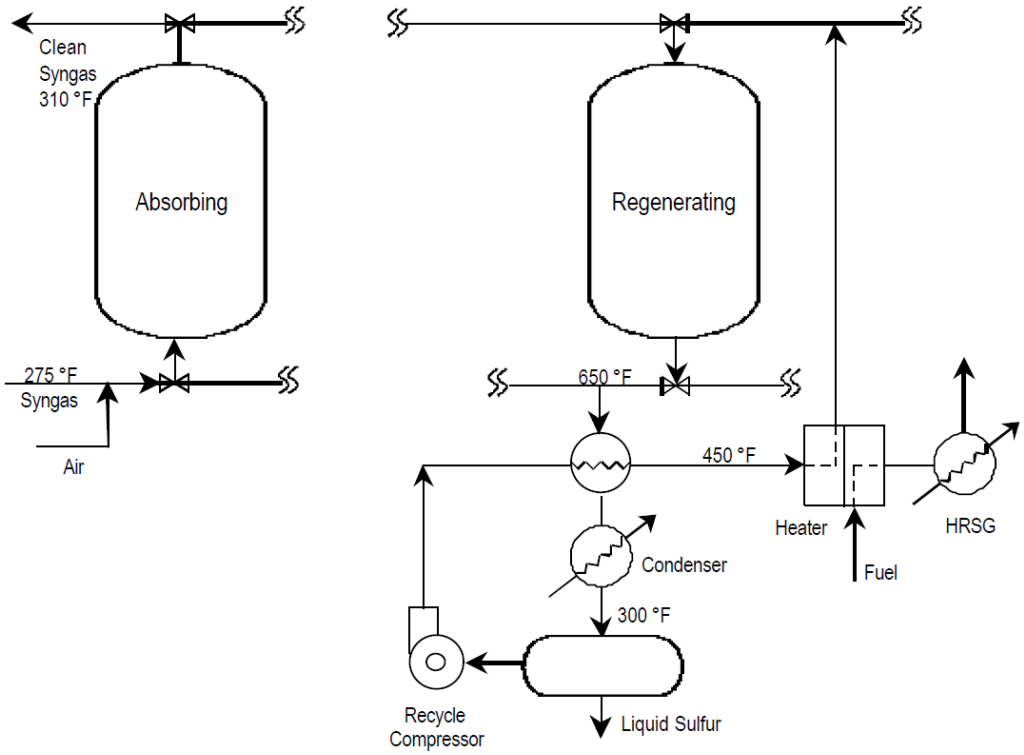

Figure 8: Simplified diagram of a selective catalytic oxidation process for H_2S removal. The heated fuel feed (depicted as syngas in this example) is mixed with air before introduction into a fixed-bed reactor filled with microporous catalyst where oxidation happens. The elemental sulfur product is continuously stored within the catalyst pores until they are saturated, at which point the catalyst is thermally regenerated with high temperature nitrogen. Source: DOE-NETL Proceedings Accession Number DE2004-832829, 2004.

This process requires the addition of heat to operate at temperatures of 150-280°C[20]. It is good for removing trace amounts of H2S and other organosulfur compounds from gas streams and the process can operate continuously[18, 21]. However, the formation of poisonous byproducts such as SO_2 and COS and the need for their removal is a problem[16, 21], and heating the catalyst bed for both the reaction and regeneration process is energy intensive.

1.2.3 Adsorption on Solid Sorbents

The last major approach for sulfur removal from fuels is selective adsorption on solid adsorbents such as metal oxides, metal-containing zeolites, and metal-containing aluminum oxide. This method does not convert the sulfur compounds to a different species before separation; instead, the acidic sulfur compounds are simply adsorbed onto the surface by its attraction to the basic surface sites of the adsorbent[14, 22]. There are two common modes of operation: temperature swing adsorption (TSA) process with low temperature adsorption and high temperature desorption, and pressure swing adsorption (PSA) process with high pressure adsorption and low pressure desorption[23]. Both kinds of desorption serves to regenerate the sorbent for subsequent cycles of adsorption. An example of TSA is depicted in Figure 9.

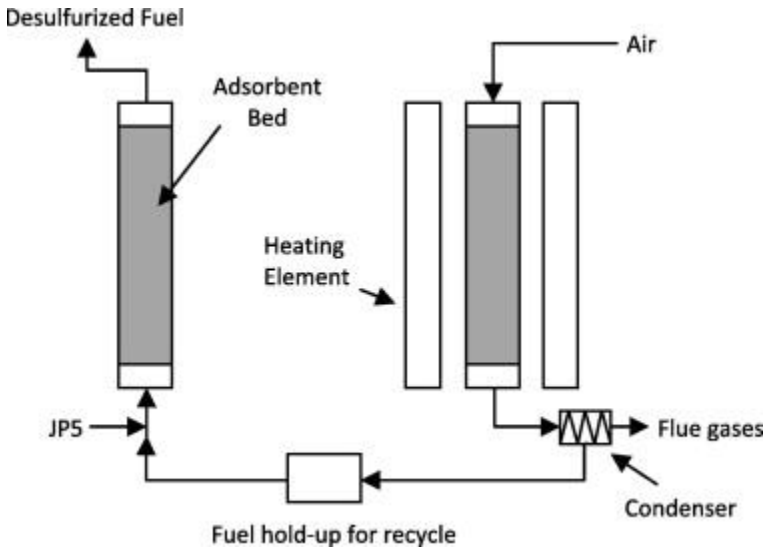

Figure 9: Schematic diagram of a laboratory scale adsorption-regeneration unit used for desulfurization using TSA. The fuel (depicted as JP5 in this example) is fed into a column packed with sorbent, where the sulfur compounds are adsorbed until breakthrough. Desulfurized fuel comes out of the back end of the bed. During desorption, the bed temperature was raised to 450C while air flowed through as a stripping medium. Source: Fuel 89(11), 2010

Much of this method can operate at ambient temperatures and pressures, with only high pressures needed for the adsorption cycle of a PSA process and high temperatures needed for the desorption cycle of a TSA process. This makes the process much more energy and cost efficient than either HDS or SCO. This process is also good for removing trace amounts of sulfur from fuel, something that HDS is unable to offer[22]. Overall, the process is also simple; no hydrogen gas is necessary and the sulfur compounds do not get converted to other hazardous products so there is no need for a second separation step to remove byproducts. However, sulfur uptake capacity on the sorbent is often low, so that large quantities of sorbent are required[16] and there may be difficulties in selecting an appropriate sorbent. Selectivity for the sulfur compounds over the fuel can also be a problem. Overall though, the advantages that solid sorbents offer to efficiently and effectively remove sulfur from fuels significantly outweigh their disadvantages.

1.3 Materials and Methods for Selective Adsorption

Some common solid sorbents used in selective adsorption of sulfur compounds are: ion-exchanged or metal-containing zeolites, supported metals, metal oxides, metal-containing aluminum oxide, activated carbons, and modified mesoporous silica.

Zeolites are attractive sorbents due to their large pores and surface area, polarity, high thermal stability, and surface acidity and basicity that leads to high removal ratios. Zeolites X, Y, ZSM-5, USY have been successful in many studies for adsorbing various sulfur compounds[15, 17, 22]. The exchange of ions and metals such as Cu^{+}, Ag^{+}, Zn^{2+}, Na^{+}, Fe^{2+}, AgNO3, Ag-Mn, and others typically increases the desulfurization performance of the zeolites, though the performance and selectivity is as much dependent on the composition of the sulfur and fuel species present as on the composition of the zeolite[14,

[24-26]. The capacity of ion-exchanged zeolites is generally higher than that of activated carbon and metal-containing activated alumina, but they can be difficult to apply under water containing conditions due to their hydrophilicity[14, 26]. However, it has been found that exchanging with silver species can help with adsorptivity, capacity, and selectivity for sulfur compounds even in the presence of water, and that less hydrophilic zeolites, such as ZSM-5, have capacities and removal efficiencies that are more resistant to adverse water effects in high humidity conditions[24]. Zeolites can be regenerated with air, but typically need high temperatures (around 400-500°C) for complete regeneration, which can be costly[27].

Metal oxides are highly efficient at removing sulfur in fuel down to sub-ppmv levels, but require high temperatures to do so[22]. Manganese oxide specifically is easily reduced at high temperatures so the range for temperature swing desorption is limited[17]. Also, metal oxides alone do not have a high sulfur capacity when compared to other sorbents[26]. A combination of metal-exchanged metal and aluminum oxide ($Cu/ZnO/Al_2O_3$) can have greater sorption capacity than either metal-exchanged metal oxide (Cu/ZnO), metal-exchanged aluminum oxide (Cu/Al2O3), or any other configurations (ZnO/Al_2O_3, ZnO)[14, 28]. Activated alumina alone has good adsorptive properties but tends to have a lower selectivity for sulfur compounds over fuel species. Supported metals have a high sulfur capacity, but also require operating at high temperatures around 200 ˚C to reach these capacities[22].

Activated carbons are inexpensive and have high surface area and pore volume. However, alone they do not have high adsorption capacity for sulfur compounds[17, 26]. The capacity of activated carbon is determined by physical, porous, and chemical structure, and can be increased by metal impregnation or oxidation[20]. A lower temperature (around 200°C) is needed for full regeneration of activated carbons compared to zeolites[27]. Similar to ion-exchanged zeolites, different types of metal modified activated carbons will be differently selective for sulfur compounds, and will

have varying degrees of desulfurization performance depending on the composition of the sulfur-containing fuel. These sorbents have been mainly used for liquid fuels[20, 22].

Metal modified mesoporous silica adsorbents show higher capacity than mesoporous silica without modification, but overall, the capacities are still generally lower than that of metal-exchanged zeolites. However, they can be regenerated at low temperatures around 100°C and the absence of aluminum should make them more water resistant[25, 27].

The ability of solid sorbents to remove trace amounts of sulfur from fuel and for the process to operate at low temperatures and pressures gives them a significant advantage over traditional hydrodesulfurization and catalytic oxidation approaches. Adsorption is also relatively simple compared to the other two processes. However, the energy savings gained from low operating temperatures and pressures can be counterbalanced by the use of the sorbents in pellet packed beds. Typically, the beds are temperature or pressure controlled columns filled with stationary adsorbent pellets. Gas is fed into one end of the bed and the species of interest is adsorbed through its contact with the pellets, such that the exit gas is free of the adsorbed species. Flow through these packed beds often causes a high pressure drop and particle attrition, especially at higher volumetric flow rates. A typical natural gas-fueled combined cycle power plant unit such as the 840 MW units used at Plant McDonough-Atkinson (Smyrna, GA) must process gas at a flow rate of approximately 180,000 standard cubic feet per minute (SCFM). Even a single 85 MW GE 7EAQ gas turbine has a flow rate of approximately 15,000 SCFM. Pressure drop in packed beds is directly affected by feed velocity and pellet size. In order to lower the pressure drop in sorbent packed beds for applications with such massive flow rates, the flow would have to be significantly decreased or the sorbent pellet size would have to be increased[29, 30].

Additionally, the pellet packed bed configuration can be difficult for heat and mass transfer equilibration, leading to long cycle times and underutilization of the

sorbent. The overall mass transfer resistance in the packed bed determines the speed at which adsorption occurs, and is a sum of three mass transfer resistances: the external resistance in the bulk phase, the internal resistance through the pellet, and the internal resistance through the sorbent. It is often controlled by the internal resistance of the pellets, which is proportional to the pellet size. Therefore, a trade-off appears with regard to pellet size, where increasing their size leads to a lower pressure drop, but also leads to a larger mass transfer resistance[29-31].

A way to circumvent the disadvantages of a pellet packed bed system is to use fiber sorbents instead. Here, sorbent crystals are spun into fibers instead of shaped into pellets, and are bundled into modules similar to that in a packed bed. Fiber-based adsorbents have been shown previously to have significantly lower pressure drop and better heat and mass transfer rates than packed bed adsorbers[31].

1.4 Research Objectives

This Master's thesis is part of a larger work that is envisioned to include a PhD project with an overall goal to create a fiber sorbent module system to remove sulfur-containing odorants from pipeline grade natural gas. These fiber sorbents, combining the high sulfur capture capacity of powder adsorbents with the cost effectiveness and ease of manufacturing of established fiber membrane production, will be created and tested in a subsequent PhD project. The envisioned fiber sorbents will comprise porous solid polymer fibers embedded with a zeolite sorbent, bundled together into a module as shown in Figure 10.

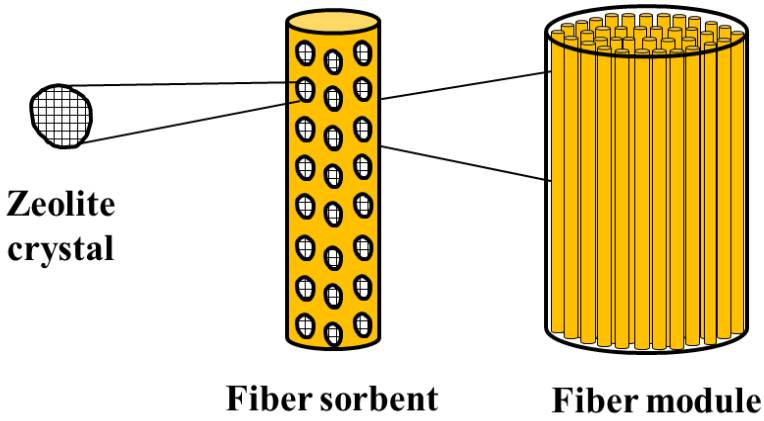

Figure 10: Schematic of a fiber sorbent module showing microporous zeolite crystals distributed within a polymer fiber. The fibers are then packed into a module for use in the TSA process.

The fiber sorbent module system will operate in a TSA mode with natural gas passing over the fibers in parallel flow as will be discussed in later chapters. This configuration leads to a pressure drop that is significantly lower than in a pellet packed bed system. Hot regeneration gas and a cooling gas will be used for regeneration and cooling of the fibers respectively. The small diameter of the fibers used and the nature of the gas flow through such a system will also result in faster heat and mass equilibration times, and therefore more efficient use of the sorbent, than a packed bed.

To ensure efficient progress on the PhD project, the main objective of the current MS research is to model, design, and optimize solid fiber sorbent modules for selective and continuous TBM removal from natural gas, as well as assess their advantages over other conventional and developing technologies. The insights gained from the evaluation of fiber sorbents for this application in the current MS study will guide the detailed experimentally intense PhD project that will be pursued after completing the current MS project.

1.5 References

1. *Annual Energy Outlook*, 2012, U.S. Energy Information Administration.
2. Drajem, M. and B. Olson, *The future of oil, coal, and gas under Obama*, in *Bloomberg Businessweek*2012.
3. *Clean Energy: Natural Gas*, 2012, U.S. Environmental Protection Agency.
4. *Natural Gas Year-in-Review* in *Natural Gas Monthly*2012, U.S. Energy Information Administration.
5. *Corrosion costs and preventive strategies in the United States* 2002, NACE International.
6. *Overview of Natural Gas: Electric generation using natural gas*, 2011, Natural Gas Supply Association.
7. *About Energy: Natural Gas: Featured Plant Profile: Plant McDonough-Atkinson.*, Georgia Power.
8. Ivanov, I., J. Strmen, and L. Jones, *Pre-odorization or pickling of new natural gas pipe.* Pipeline & Gas Journal, 2009. 236(11): p. 1-4.
9. Casanova, M., *Corrosion problems in turbines.* Proceedings of the Second Turbomachinery Symposium, 1973: p. 83-90.
10. *High Temperature Corrosion and Materials Application* 2007, ASM International: Materials Park, Ohio. p. 249-258.
11. Bammert, K. and H. Santstede, *Measurements concerning the influence of surface roughness and profile changes on the performance of gas turbines.* Journal of Engineering for Gas Turbines and Power, 1972. 94(3): p. 207-213.
12. Craig, B.D. and L. Smith, *Corrosion resistant alloys (CRA) in the oil and gas industry – selection guidelines update, 3rd Edition*, in *Nickel Institute Technical Series* 2011.

13. Brunet, S., et al., *On the hydrodesulfurization of FCC gasoline: a review.* Applied Catalysis a-General, 2005. 278(2): p. 143-172.

14. Kang, S.-H., et al., *Effective removal of odorants in gaseous fuel for the hydrogen station using hydrodesulfurization and adsorption.* Energy & Fuels, 2007. 21(6): p. 3537-3540.

15. Alptekin, G., et al., *Regenerable sorbent for natural gas desulfurization.* Journal of Materials Engineering and Performance, 2006. 15(4): p. 433-438.

16. Ratnasamy, C., et al., *Removal of sulfur compounds from natural gas for fuel cell applications using a sequential bed system.* Catalysis Today, 2012. 198(1): p. 233-238.

17. Wakita, H., Y. Tachibana, and M. Hosaka, *Removal of dimethyl sulfide and t-butylmercaptan from city gas by adsorption on zeolites.* Microporous and Mesoporous Materials, 2001. 46(2-3): p. 237-247.

18. Gardner, T.H., et al., *Fuel processor integrated H2S catalytic partial oxidation technology for sulfur removal in fuel cell power plants.* Fuel, 2002. 81(17): p. 2157-2166.

19. Chica, A., et al., *Selective catalytic oxidation of organosulfur compounds with tert-butyl hydroperoxide.* Chemistry-a European Journal, 2006. 12(7): p. 1960-1967.

20. Cui, H., S.Q. Turn, and M.A. Reese, *Removal of sulfur compounds from utility pipelined synthetic natural gas using modified activated carbons.* Catalysis Today, 2009. 139(4): p. 274-279.

21. Wu, X.X., et al., *Activated carbons for selective catalytic oxidation of hydrogen sulfide to sulfur.* Carbon, 2005. 43(5): p. 1087-1090.

22. Shen, Y., et al., *Selective adsorption for removing sulfur: a potential ultra-deep desulfurization approach of jet fuels.* Rsc Advances, 2012. 2(5): p. 1700-1711.

23. Clausse, M., J. Bonjour, and F. Meunier, *Adsorption of gas mixtures in TSA adsorbers under various heat removal conditions.* Chemical Engineering Science, 2004. 59(17): p. 3657-3670.

24. Hwang, C.-L. and N.-H. Tai, *Removal of dimethylsulfide by adsorption on ion-exchanged zeolites.* Applied Catalysis B-Environmental, 2010. 93(3-4): p. 363-367.

25. Ko, C.H., et al., *Selective removal of sulfur compounds in city-gas by adsorbents.* Korean Journal of Chemical Engineering, 2007. 24(6): p. 1124-1127.

26. Satokawa, S., Y. Kobayashi, and H. Fujiki, *Adsorptive removal of dimethylsulfide and t-butylmercaptan from pipeline natural gas fuel on Ag zeolites under ambient conditions.* Applied Catalysis B-Environmental, 2005. 56(1-2): p. 51-56.

27. Koriakin, A., Y.-H. Kim, and C.-H. Lee, *Adsorptive Desulfurization of Natural Gas Using Lithium-Modified Mesoporous Silica.* Industrial & Engineering Chemistry Research, 2012. 51(44): p. 14489-14495.

28. Kim, H.-T., et al., *Desulfurization of odorant-containing gas: Removal of t-butylmercaptan on Cu/ZnO/Al2O3.* International Journal of Hydrogen Energy, 2007. 32(15): p. 3603-3608.

29. Feng, X.S., et al., *Hollow-fiber-based adsorbers for gas separation by pressure-swing adsorption.* Aiche Journal, 1998. 44(7): p. 1555-1562.

30. Gilleskie, G.L., J.L. Parker, and E.L. Cussler, *GAS SEPARATIONS IN HOLLOW-FIBER ADSORBERS.* Aiche Journal, 1995. 41(6): p. 1413-1425.

31. Bhandari, D.A., N. Bessho, and W.J. Koros, *Hollow Fiber Sorbents for Desulfurization of Natural Gas.* Industrial & Engineering Chemistry Research, 2010. 49(23): p. 12038-12050.

CHAPTER 2

BACKGROUND AND THEORY

2.1 Fiber Sorbent Modules and Their Potential Advantages

Fiber sorbents are relatively new gas and liquid separation materials that offer many potential advantages over conventional pellet packed beds in some cases. Fiber sorbents have been created with a wet spinning process and consist of a porous polymer support structure embedded with a selective sorbent such as a zeolite[1]. The typically inexpensive polymer gives the fiber its structure and flexibility while the zeolite or other filler performs the separation through selective adsorption of the species of interest. Fiber sorbents have been spun with high sorbent-to-polymer loadings of up to 75 wt. % [2]. Traditionally, fiber sorbents have been spun in a hollow form, with a water and gas impermeable barrier layer added to either the bore side or shell side of the fiber after spinning for thermal cycling[3]. This barrier layer allows for a heating or cooling fluid to be passed through or around each of the fibers to control the temperature during adsorption and desorption. The feed and sweep gases are then passed on the other side. In adsorption mode, for example, the feed gas may be passed over the shell of the fibers as a cooling fluid such as water is passed through bore of the fibers to accept the heat of adsorption and keep the fibers isothermal throughout the adsorption. Subsequent heating/desorption and cooling steps also use the barrier layer configuration with a heating or cooling fluid such as steam or hot and cold water, and an inert sweep gas over the fibers to desorb the adsorbed species and then return the fibers back to the sorption temperature[4].

However, in the case of trace amounts of the adsorbing species in an otherwise inert gas feed, the overall heat of adsorption may be so low that the fibers stay practically isothermal during the sorption step even without the use of a cooling fluid. In this case,

the fibers could potentially be spun as porous solid fibers instead of hollow fibers, and hot and cool inert gas streams flowing over the fibers used for the subsequent regeneration steps instead of water or steam. This modification makes the fiber spinning process, the module fabrication process, and the actual separation process much simpler. Essentially the fiber module becomes akin to a monolith, but with much greater flexibility in fabrication, as the fiber dimensions and packing fraction in the bed can be easily changed.

Fiber sorbent modules can offer several advantages over traditional beds packed with spherical pellets. As mentioned in Section 1.3, one of the most important advantages is a lower pressure drop across the bed due to a simpler flow pattern[5]. This is important for maintaining the high delivery pressure of the pipeline natural gas so that no additional pumps or compressors are needed to feed the gas to the turbines, therefore reducing the operating cost. Another advantage is faster heat and mass transfer equilibration times due to the smaller critical dimensions that can be used for the fibers and a simpler and more uniform flow path[6, 7]. This is good for high flow rate applications where large volumes of gas must be processed quickly. The lower pressure drops associated with fiber modules allows the diameter of a fiber sorbent to be made much smaller than the diameter of a sorbent pellet since pressure drop scales inversely with diameter[8]. Moreover, since the flow pattern in fiber sorbents can be parallel to the fiber axis, form drag can be further minimized in comparison to pellet beds. Even a fiber with a diameter as small as 300 μm will not incur a pressure drop as large as a 1 mm pellet (see Appendix A for example calculations). Lastly, the gas is able to contact the sorbent in a fiber module more uniformly than in a pellet packed bed so that channeling and dead spaces within the bed are minimized[9]. Due to the rapid equilibration times and lower pressure drop (which also scales with velocity in both pellet and fiber systems), smaller (or fewer) beds are needed for fiber sorbents than for pellets to process the same amount of gas.

2.2 Transport Properties of Fiber Sorbents

The transport properties of porous solid sorbents usually determine their adsorption and desorption rates. Two major transport mechanisms that are commonly present with fiber sorbents are: molecular diffusion and Knudsen diffusion. Molecular diffusion occurs in the external boundary layer surrounding the fiber and within large pores of the fiber. Knudsen or transition diffusion occurs within small pores of the fiber and within the pores of the individual sorbent particles[6].

There are three distinct regions for gas transport in and around a fiber sorbent: external, internal meso or macropore, and internal micropore. High surface area zeolite crystals (particle sizes typically 0.1-1 μm) intrinsically contain small, uniform micropores. Traditionally, these crystalline powders are compressed into pellets (diameters typically 1-3 mm) with or without an inert binding material to decrease the pressure drop in packed bed adsorbers, which forms a new network of macropores from the intergranular void space[10]. In this work, the zeolite powder will be spun into porous polymer fibers (diameters typically 100-400 μm) such that the macropores will be located within the void space of the fibers. As discussed previously, the use of a fiber sorbent morphology rather than pelletized sorbents has the advantage of decreasing the pressure drop even more.

The three regions for gas transport are depicted in Figure 11. The first region involves the diffusion of the adsorbing species through a stagnant boundary layer that surrounds the external surface of the sorbent. The transport within this region is referred to as the external, or interphase diffusion. The second region involves diffusion of the adsorbing species through the meso and macropores of the fiber, while the third region encompasses diffusion of the species through the micropores of the powder adsorbent, in this case, zeolite. Transport within the second and third regions are referred to as internal,

or intraphase diffusion. Both external and internal transport regions may provide significant resistances when considering adsorption rates[10, 11].

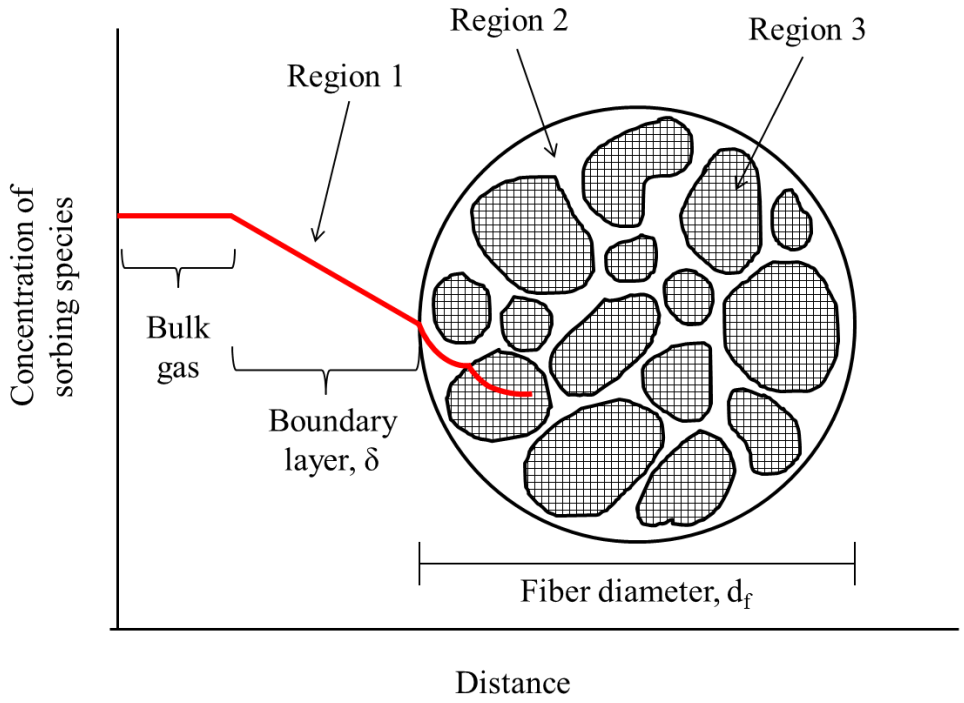

Figure 11: General concentration profile of the sorbing gas species around and within the cross-section of a porous fiber sorbent (figure lengths not drawn to scale). The three main regions for mass transfer are indicated. Region 1 depicts external diffusive mass transport through the stagnant film (or boundary) layer surrounding the fiber. Region 2 depicts internal diffusive mass transport through fiber meso and macropores. Region 3 depicts internal diffusive mass transfer and subsequent adsorption onto zeolite crystal micropores.

2.2.1 External (Bulk) Transport through Boundary Layer

External or bulk diffusion involves the transport of gas molecules from the bulk gas stream to the outer surface of the sorbent. The diffusion occurs through a stagnant boundary layer of thickness δ that surrounds the fiber sorbent. Fick's First Law can be written for a two component gas mixture for this region of transport:

$$\nabla C_A = \frac{1}{D_{AB}}\left[X_A(N_A + N_B) - N_A\right] \tag{1.1}$$

where C_A is the concentration of species A, D_{AB} is the diffusivity of species A in B, X_A is the mole fraction of species A, and N_A and N_B are the fluxes of species A and B respectively. When equimolar counter-diffusion or a very dilute concentration of species A is assumed, equation (1.1) simplifies to:

$$N_A = -D_{AB}\nabla C_A \tag{1.2}$$

Further assuming a very thin boundary layer relative to the radius of curvature of the fiber, the equation can be simplified to just one dimension. Solving that equation with the appropriate boundary conditions returns the flux of species A through the film layer in the direction of interest (denoted as x here)[10]:

$$N_{Ax} = \frac{-D_{AB}}{\delta}(C_{A\delta} - C_{AS}) \tag{1.3}$$

where δ is the boundary layer thickness, and $C_{A\delta}$ and C_{AS} are the concentrations of species A in the bulk gas phase and at the surface of the sorbent respectively. The magnitude of the boundary layer thickness is unknown, such that a mass-transfer coefficient is typically used instead. This will be discussed further in Section 2.3.

Molecular Diffusion

Molecular diffusion occurs when collisions between the diffusing molecules dominates the mass transport, such as in the external boundary layer. Molecular diffusivity, D_M or D_{AB} in a two component gaseous system can be fairly accurately calculated from the Chapman-Enskog equation as follows[10, 12]:

$$D_M = D_{AB} = \frac{1.858\times10^{-27}T^{3/2}}{P\sigma_{12}^2\Omega}\left(\frac{1}{M_1}+\frac{1}{M_2}\right)^{1/2} \tag{1.4}$$

where T is temperature in Kelvin, P is total pressure of the gas mixture in atmospheres, σ_{12} is the average collision diameter in meters given by $\sigma_{12} = 0.5(\sigma_1 + \sigma_2)$, Ω is the

dimensionless temperature-dependent collision integral, and M_1 and M_2 are the molecular weights of the two species in the gas mixture in g/mol. This equation shows that the molecular diffusivity in binary gas mixtures is independent of concentration, but varies inversely with pressure, meaning that this diffusion coefficient is expected to be small for the high pressure system of this work.

2.2.2 Internal (Mesopore and Macropore) Transport through Fiber Pores

In highly porous solid adsorbents like zeolites, most of the adsorption sites are contained within the pore network, so mass transport within these enclosed spaces generally controls the adsorption rate. At the fiber surface and within the pores of the sorbent, there is generally negligible bulk flow, such that transport can be considered to happen only through diffusion. Additionally, there is generally only diffusion through the pores of the sorbent, and no transport through the solid sorbent itself. Fick's First Law can again be written in one dimension to describe transport within the particle in terms of the effective diffusivity D_p^{eff} through the pores (such that the flux happens only through the area of the pores and not through the solid)[10, 13]:

$$N_A = -D_p^{eff} \frac{\partial c}{\partial x} \tag{1.5}$$

The void space within a sorbent fiber or pellet can be considered as a randomly oriented interwoven network of pores through which diffusion takes place. This pore diffusivity can be defined as[10, 13]:

$$D_p^{eff} = \frac{D\varepsilon_p}{\tau} \tag{1.6}$$

where D_p is the pore diffusivity, D is the diffusivity that would exist in a straight cylindrical pore at the same conditions, ε_p is the overall porosity in the solid sorbent (ratio

of void volume to total volume of a fiber or pellet), and τ is the tortuosity factor that accounts for random pore orientation and any variations in pore diameter. The tortuosity factor normally ranges between 2 to 6, and is commonly inversely proportional to porosity. The diffusivity D that would be used in equation (1.6) depends on the mechanism of transport within the meso/macropores. These different contributing mechanisms are described below in more detail.

Molecular Diffusion

Molecular diffusion inside of a fiber sorbent can occur within the large pores of the fiber, but unlike molecular diffusion in the external boundary layer, it will be subject to the effects of tortuosity and porosity and will therefore be effectively smaller. For molecular diffusion to take place internally, the mean free path of a gas molecule must be smaller than the pore diameter of the adsorbent[13]. Otherwise, Knudsen or transition diffusion will occur.

Knudsen Diffusion

Knudsen diffusion occurs when collisions between the diffusing molecules and the pore walls of the sorbent dominates the mass transport. This results when the mean free path of the gases exceeds the pore diameter and molecules become more likely to collide with the pore walls than with other molecules. From kinetic theory and the ideal gas law, the mean free path, λ, of a molecule may be calculated as[14, 15]:

$$\lambda = \frac{k_B T}{\sqrt{2}\pi d_A^2 P} \tag{1.7}$$

where k_B is Boltzmann's constant in J/K, T is temperature in Kelvins, P is pressure in Pascals, d_A is the diameter of the gas molecule of interest in meters.

Typically, Knudsen diffusion is important with small sorbent pores and at low pressures. For the current system sorbing a large gas molecule at high pressure, this type of diffusion is unlikely to be important, but is still mentioned here for completeness. Knudsen diffusivity can be estimated with the following equation[10, 13]:

$$D_K = 9700 r_p \sqrt{\frac{T}{M}} \tag{1.8}$$

where r_p is the mean sorbent pore radius in centimeters, T is temperature in Kelvin, and M is the molecular weight of the species of interest.

Transition Region Diffusion

When molecular diffusivity and Knudsen diffusivity are equally important, both must be accounted for to accurately describe mass transport within the sorbent macropores. In the case of a binary gas mixture with equimolar counter diffusion, the diffusivity in the transition region may be approximated as[10, 15]:

$$\frac{1}{D_{transition}} = \frac{1}{D_M} + \frac{1}{D_K} \tag{1.9}$$

Because the mean free path of any molecule depends on pressure, any adsorbent-adsorbate pair can experience a transition from molecular to Knudsen diffusion. Table 2 summarizes the mean free path conditions relative to the pore radius in which the three main types of diffusion will dominate[6, 16].

Table 2: Range of conditions under which different types of diffusion are important

Diffusion Region	Condition for Diffusion Type
Molecular	$\lambda < 0.1\ r_p$
Transition	$10\ r_p > \lambda > 0.1\ r_p$
Knudsen	$\lambda > 10\ r_p$

2.2.3 Internal (Micropore) Transport through Sorbent (Zeolite) Pores

A second region of internal transport exists within the micropores of the powder sorbent supported within the polymer fiber network. The kinetic selectivity of sorbents such as the zeolites studied in this work is dependent on the micropore diffusion that occurs in the intracrystalline pores. Zeolites are crystalline, highly porous aluminosilicate materials with frameworks made out of SiO_4 and AlO_4 tetrahedra. The 3D pore system has precisely defined diameters due to its crystal structure. The silicon to aluminum ratio in zeolites, which is always 1 or greater, determines the affinity for polar molecules such as water; lower Si / Al ratios result in more hydrophilic materials while higher ratios result in more hydrophobic materials. Exchangeable cations on negatively charged sites contribute to different adsorptive properties.

Diffusion through zeolites is an activated process, such that diffusion can only happen when enough energy is supplied to desorb an adsorbed molecule. Arrhenius' equation can be used to describe the temperature dependence of this type of diffusion[13]:

$$D_s = D_0 e^{-E/RT} \tag{1.10}$$

where D_s is the diffusivity of the zeolite sorbent crystal, D_0 is a diffusion pre-factor in cm^2/s similar to the pre-exponential factor in the Arrhenius equation for rate constants, E is the activation energy in J/mol, R is the gas constant, and T is temperature in Kelvin.

The crystalline structure of these zeolite frameworks and the cations within them are critical to the diffusivity of guest molecules. The framework determines the free

diameter(s) of the pores in the crystalline structure of the zeolite, which in turn restricts the size of molecules that are able to pass through. However, the effective diameters are usually larger than the free diameters due to vibrations in both the framework and the diffusing molecule. This allows molecules with critical diameters slightly larger than the free diameter of the zeolite to diffuse in. Cations on the surface of the framework block the pores and reduce their diameters, further reducing the diffusivity of guest molecules. Varying the type and number of exchangeable cations on these surface sites can change this diffusivity.

Zeolites X and Y have effective diameters of 8.5 Å and zeolites ZSM-5 and silicalite have effective diameters of 6.0 Å. The presence of sodium cations on zeolites X (NaX or 13X) and Y (NaY) decreases their effective diameters. Because the Si/Al ratio in zeolite X is close to 1, there is a greater amount of sodium cations than in zeolite Y, which has a Si/Al ratio close to 2. The effective diameter of zeolite NaX is about 8.3 Å. All of these diameters are large enough to allow the easy passage of large molecules such as t-butyl mercaptan (TBM), which has a critical diameter of 5.6 Å. As there is no significant barrier for the entrance of TBM molecules through the pores, diffusion is very fast. Reasonably, the diffusivities of molecules are generally larger for zeolites X and Y than for ZSM-5[13]. The diffusivities of large pore X and Y zeolites are typically around 10^{-6} to 10^{-8} cm^2/s. Figure 12 shows the structure of zeolites X and Y, which are used in this work.

Figure 12: Framework structure of zeolite X and Y (faujasite) unit where each vertex represents a Si or Al atom and each line represents an O atom. The free diameter of the window is about 7.4 angstroms, but due to vibrations within the zeolite crystal structure and the diffusing guest molecule, the effective diameter is slightly larger at 8.5 angstroms. Cations on the surface will reduce this diameter. Source: International Zeolite Association

With the Si/Al ratio of zeolite X being close to 1, polar molecules such as TBM will preferentially adsorb over nonpolar methane in pipeline natural gas. However, the presence of molecules with larger dipole moments such as water in the natural gas may present a problem, as zeolite X will preferentially adsorb these species over weakly polar TBM.

2.3 Mass Transfer Influences on Sorption Kinetics

The physical adsorption and desorption rates at the surface of porous adsorbents are usually very high in comparison to the mass transfer resistance and other non-idealities such as channeling and axial dispersion. As such, the adsorption process is considered to be diffusion-limited or diffusion-controlled rather than reaction (sorption)-limited. As discussed in section 2.2, there are three regions for gas transport associated with fiber sorbents, and thus, it follows that there are also three mass transfer resistances associated with each of the regions. Externally, in binary gas mixtures, mass transfer resistance exists in the boundary layer circumscribing the fiber. Internally, diffusional

mass transfer resistance exists in the micropores of the zeolite crystals and in the macropores of the fiber. The sorption rate of the system can be affected by any combination of these resistances with other non-idealities, and the overall dynamics of the fiber sorbent module controls the effectiveness of the sorption process[13]. This section briefly discusses the overall system response to these resistances and how they are compounded, followed by an elaboration of the resistances in each region and how the equilibration times are affected. Section 2.4 will further elaborate on breakthrough curve responses and other patterns in an adsorption bed.

2.3.1 Breakthrough Curves

In an ideal plug flow situation, the concentration signal at the outlet of the bed would be identical to the input with only a time delay difference due to the time it takes to reach adsorption equilibrium in the bed. In real systems however, the outlet concentration signal will be dispersed due to the effects of mass transfer resistances and/or axial dispersion. Studies of adsorption beds can be carried out using a step change to the concentration of the adsorbing species at the inlet and measuring the response at the outlet, called a breakthrough curve. Another common option is to inject a pulse of the adsorbing species at the inlet and measure the response at the outlet, called a chromatographic response[13]. An example of both an ideal (perfect) and real breakthrough curve in response to an inlet step change is shown in Figure 13.

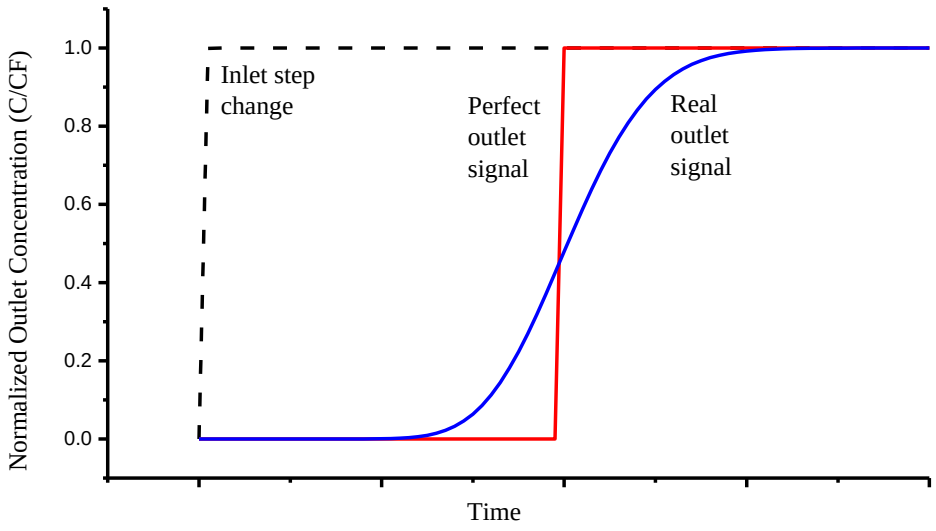

Figure 13: Representative breakthrough curve in response to a step change in inlet concentration of the adsorbing species. The y-axis plots the normalized concentration – the concentration measured at the inlet and outlet divided by the concentration in the feed gas. The perfect outlet signal shows only the time delay due to adsorption in the bed until saturation. The real outlet signal shows both the time delay and spreading due to mass transfer resistances and non-idealities in the bed.

The spread of the outlet response to a perfect step or pulse injection at the inlet is directly related to the resistances and any axial dispersion. In a breakthrough curve, the adsorbate concentration at the outlet is zero until the breakthrough time. The time delay in both cases is due to adsorption; the adsorbing species only shows up in the effluent once the bed has been saturated[17].

2.3.2 Resistance in Series

The overall outlet response can be said to be affected by the overall mass transfer coefficient encompassing external and internal resistances, and by axial dispersion, if it exists. The resistances and non-idealities add up in series to create an overall response.

This can be represented by the following relationship in which all resistances and dispersion are considered to be important[13]:

$$\frac{1}{Kk'} = \frac{D_L}{v_s^2}\left(\frac{1-\varepsilon_b}{\varepsilon_b}\right) + \frac{R_f}{3k_c} + \frac{R_f^2}{15\varepsilon_f D_p} + \frac{r_s^2}{15KD_s} \tag{1.11}$$

where k' is an overall effective rate coefficient that relates diffusion, dispersion, and mass transfer coefficients (s), K is the dimensionless Henry's law constant (or adsorption equilibrium constant) for linear adsorption isotherm (q=Kc), v_s is the superficial velocity of the fluid in the bed (cm/s), D_L is the axial dispersion coefficient (cm^2/s), ε_b is the bed porosity, R_f is the radius of the fiber (cm), k_c is the external mass transfer coefficient (cm/s), ε_f is the fiber porosity, D_p is the diffusion coefficient through the fiber pores (cm^2/s), r_s is the radius of the zeolite crystals (cm), and D_s is the diffusion coefficient through the micropores of the zeolite crystal (cm^2/s). The first term on the right-hand side of the equation represents the axial dispersion contribution to the overall effective rate, the second term represents the external film resistance contribution, the third term represents the internal macropore (fiber) resistance contribution, and the last term represents the internal micropore (zeolite) resistance contribution. If no axial dispersion is assumed, equation (1.11) can be simplified to[13]:

$$\frac{1}{Kk} = \frac{R_f}{3k_c} + \frac{R_f^2}{15\varepsilon_f D_p} + \frac{r_s^2}{15KD_s} \tag{1.12}$$

where k is the overall mass transfer coefficient and all other terms remain the same.

The time, t, it takes to reach mass transfer equilibrium in any of the regions can be estimated from[16]:

$$t \approx c\frac{L^2}{D} \tag{1.13}$$

where L is the characteristic length (cm) and D is the diffusion coefficient (cm^2/s) associated with that region, and c is a dimensionless constant that varies with each region.

2.3.3 External Resistance and Mass Transfer Coefficient

External mass transfer resistance can occur in binary component systems as a stagnant boundary layer or film layer forms around the outer surface of the fiber sorbent. The velocity of the gas flowing parallel to the fibers will change depending on its position relative to the fiber outer surface, decreasing with proximity to the fiber radius. This is due to the no-slip constraint at the fiber surface. The boundary layer is defined as the distance from the fiber where the concentration of the adsorbing species is 99% of the concentration in the bulk or feed gas[18]. The external resistance occurs as a result of the adsorbing species in the feed gas having to diffuse through this film layer to reach the fiber.

As discussed in Section 2.2.1, the flux of the adsorbing species can be described by equation (1.3). However, it is difficult to determine the thickness of the boundary layer, so a mass transfer coefficient is typically used instead to describe the flux of the species from the bulk gas to the sorbent surface[10, 19]:

$$N_A = k_c(C_{A\delta} - C_{AS}) \tag{1.14}$$

where N_A is the average molar flux in the x-direction (moles/cm^2-s), and k_c is the external mass transfer coefficient (cm/s). This external mass transfer coefficient can be estimated from appropriate Sherwood correlations relating the properties and velocity of the flowing fluid to the dimensions of the sorbent. The Sherwood number is defined as[8]:

$$Sh = \frac{k_c d_f}{D_M} \tag{1.15}$$

where d_f is the fiber diameter and D_M is the molecular diffusivity. For flow outside and parallel to a bundle of fibers, the Sherwood number can be correlated as[20]:

$$Sh = 1.45\left[ReSc\frac{d_f}{L_b} \right]^{0.33} \tag{1.16}$$

where L_b is the length of the fiber bed and the fibers, Re is the Reynolds number used to characterize different flow regimes, and Sc is the Schmidt number used to characterize the importance of viscosity versus diffusivity in fluid flows, defined as[19]:

$$Re = \frac{\rho d_f v_s \varepsilon_b}{\mu} \tag{1.17}$$

$$Sc = \frac{\mu}{\rho D_M} \tag{1.18}$$

where μ and ρ are the viscosity and density of the moving fluid respectively, v_s is the fluid superficial velocity, and ε_b is the porosity of the fiber bed. As can be seen from equations (1.15) to (1.17), the external mass transfer coefficient is a function of fluid velocity and other fiber and module properties.

Based on equation (1.13), the characteristic diffusion time for this region external to the fibers is proportional to the square of the thickness of the boundary layer (δ) divided by molecular diffusivity (D_M) [16]:

$$t_{external} \propto \frac{\delta^2}{D_M} \tag{1.19}$$

2.3.4 Internal Resistances

In composite fiber sorbents, internal resistance may arise from the micropores, meso/macropores, or both. The micropore resistance comes from the adsorbing species needing to diffuse through the zeolite pores and onto the adsorption sites. The meso/macropore resistance comes from the adsorbing species needing to diffuse through the fiber pores to reach the sorbent[6]. However, because the dimensions of the zeolite 13X crystals are so small (0.1-1 μm) compared to that of the fibers (100-400 μm), the

characteristic diffusion time from equation (1.13) for the micropores of this system is much faster than the diffusion time for the meso/macropores, as shown below[16]:

$$t_{macropore} \propto \frac{R_f^{\,2}}{D_p^{eff}} \tag{1.20}$$

$$t_{micropore} \propto \frac{r_s^{\,2}}{D_s} \tag{1.21}$$

where R_f is the radius of the fiber, D_{eff} is the effective diffusivity in the fiber pores, r_s is the radius of the zeolite, and D_s is the diffusivity in the sorbent. It is clear from these equations that even in the case of very low diffusivities in the zeolite, the mass transfer equilibration time would still be much faster in the sorbent crystals, such that the macropore resistance is considered to be the dominant internal resistance. This leads to a concentration profile or gradient within the fiber, but a uniform concentration within the zeolite crystals. In this case, the sorption rate will be dependent on fiber diameter[13].

2.4 Adsorption Properties and Patterns in Fiber Sorbents

As mentioned previously, the intrinsic properties of the feed gas, fiber materials, and fiber morphology directly control the mass transfer of adsorbate from the bulk feed gas to the adsorption sites within the sorbent. The shape and timing of the breakthrough curve as it is influenced by mass transfer resistances and dispersion, is then closely related to how efficiently the bed and the sorbent itself is utilized, and the types of patterns that will be observed within the bed. These patterns can be characterized a number of ways so as to describe bed performance, and will be discussed further in this section.

2.4.1 Mass Transfer Zone and Length of Unused Bed

The spreading of the breakthrough curve response at the outlet of the bed can be correlated to one side of the concentration front moving faster than the other inside the bed, as shown in

Figure 14. The breakthrough concentration in an adsorption bed is a user chosen point at which the concentration of the adsorbing species in the outlet reaches a maximum allowable level. The time it takes to reach this point is called the breakthrough time, t_b. The stoichiometric time point, t_s, represents the time at which the ideal concentration front (no spreading) would reach the end of the bed such that the breakthrough curve response would be identical to the inlet step function. This ideal concentration front can be applied to the previous stages of the bed before breakthrough as well, in the middle of the actual concentration front, such that the bed area in the side that moves faster is equal to the bed area in the side that moves slower. The equilibration time, t_e, is the time at which the adsorbent reaches its saturation capacity and the adsorbate concentration in the effluent becomes the same as that in the feed.

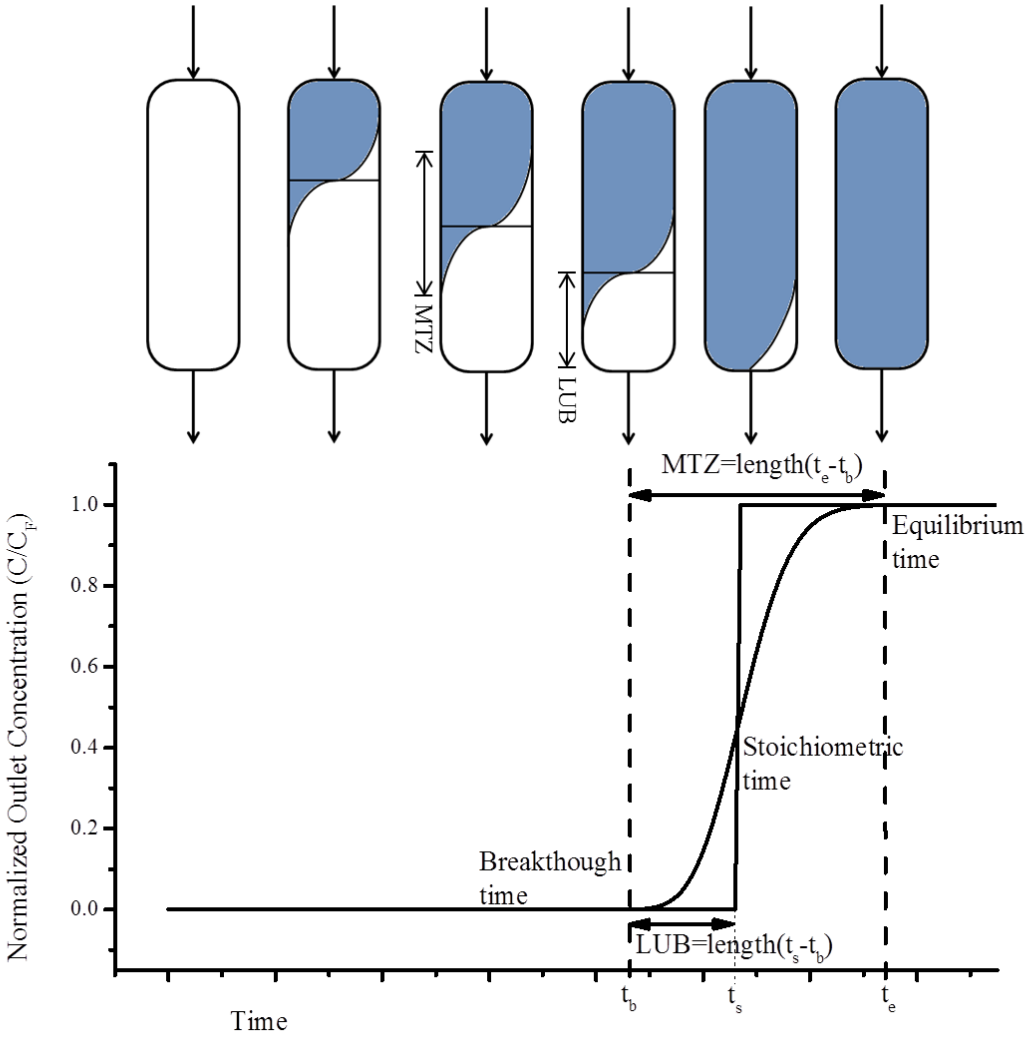

Figure 14: Adsorption over time of the species of interest in a bed and its corresponding breakthrough curve showing breakthough time tb, stoichiometric time ts, and equilibrium time te. Figure adapted from Seader and Henley, 1998 [21].

The length equilibrium section (LES) is the ideal required bed length if there was no spreading of the concentration front. The LES is then the length in the adsorption bed between the ideal concentration front and the inlet of the bed at breakthrough time. However, due to spreading, if the LES were employed as the actual bed length to be used, the bed would not achieve the same capacity as in the ideal case. The length of unused bed (LUB) is then the additional length needed in the bed to reach that same capacity. In

Figure 14, the LUB is the length in the adsorption bed between the ideal concentration front and the beginning of the actual concentration front at the breakthrough time[21, 22]. The LUB can be calculated with the following equation[23]:

$$LUB = \left(1 - \frac{t_b}{t_s}\right) L_b \tag{1.22}$$

where t_b is the breakthrough time, t_s is the stoichiometric time, and L_b is the actual length of the bed.

The stoichiometric time bisects the breakthrough curve in such a way that the areas above and below it are equal, as shown by[22]:

$$t_s = \int_0^{t_e} \left(1 - \frac{C}{C_F}\right) dt \tag{1.23}$$

where t_e is the equilibration time, and C and C_F are the effluent and feed concentrations respectively. A sharper concentration front will lead to a smaller LUB, such that the sorbent will be more efficiently used and actual bed lengths can be reduced. And as mentioned previously, reducing mass transfer resistances and any non-idealities in the bed will lead to a sharper breakthrough curve.

The side of the bed where the feed gas enters will adsorb the species first and become saturated with the adsorbate, therefore coming to equilibrium with the feed gas. The side of the bed where the product gas exits will contain only the residual adsorbate that did not desorb during the regeneration phase until the concentration front reaches it. The section of the bed where the amount adsorbed varies from the equilibrium concentration to the residual concentration (the moving concentration front) is called the mass transfer zone (MTZ), as shown in

Figure 14. This transition zone is where the adsorption is actively taking place, and moves forward through the bed until breakthrough occurs[24]. The length of the MTZ

is directly related to the overall mass transfer resistances and dispersion discussed in Section 2.3 and to the shape / spreading of the breakthrough curve.

2.4.2 Adsorption Isotherms

Equilibrium isotherms are used to describe the capacity of an adsorbent for a certain adsorbate as a function of pressure at a constant temperature. The general shapes of these isotherms determine how the concentration front or mass transfer zone will propagate through the bed. Figure 15 shows an example of the three general shapes of the equilibrium isotherm: favorable, linear, and unfavorable. Favorable (also known as Langmuir or type I) isotherms are characterized by a steep initial increase in capacity with increasing partial pressure (or adsorbate concentration), followed by a gradual increase to the saturation capacity of the sorbent at infinite pressure (with limitations). This type of isotherm is typical for gases adsorbed on zeolites and activated carbon. Favorable isotherms pertaining to the adsorption of gases can be predicted with the following equation[25]:

$$\left[\frac{\partial \ln P}{\partial (1/T)}\right]_n = -\frac{\Delta h}{R} \tag{1.24}$$

where P is the pressure, T is the temperature, n is the (constant) loading, Δh is the differential enthalpy of adsorption in kJ/mol (which can be measured by calorimetry), and R is the gas constant. In contrast, unfavorable isotherms are characterized by a slow initial capacity increase with partial pressure, followed by a sharp increase to the saturation capacity.

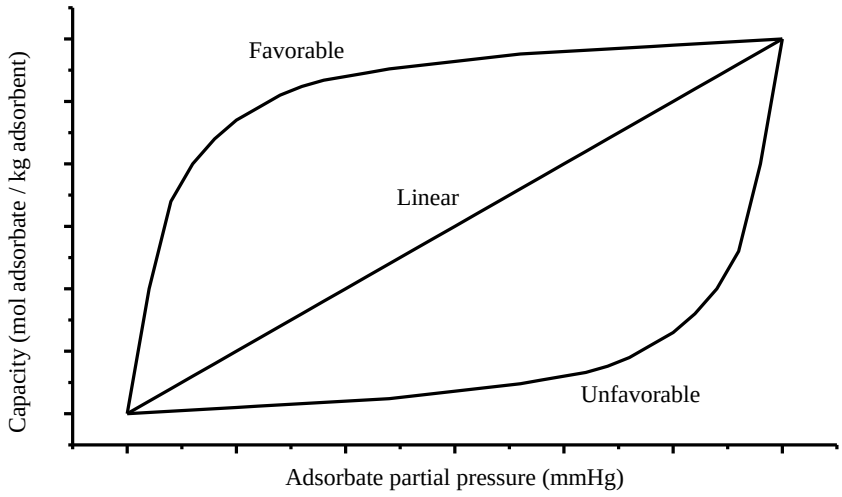

Figure 15: Equilibrium isotherm diagram showing a favorable, linear, and unfavorable isotherm. The capacity, or amount adsorbed shown on the y-axis is normalized by the mass of the adsorbent. Isotherms are plotted as a function of its partial pressure (or concentration) in the gas mixture. Adapted from Ruthven.

For beds giving favorable equilibrium isotherms, the mass transfer zone is initially broad, but sharpens as the concentration front moves forward, eventually giving a constant shape after some distance. This asymptotically approached profile, often called constant-pattern behavior, is reached for any combination of finite and negligible axial dispersion and mass transfer resistance provided that the bed is long enough to allow it[26]. The required bed length for constant-pattern behavior is typically short, and depends on the particular shape of the isotherm and sorption behavior. This close to ideal, constant-pattern shape is then retained until the concentration front reaches the end of the bed. In contract, in beds giving linear or unfavorable equilibrium isotherms, the mass transfer zone spreads continuously as the concentration front moves forward. The width of the MTZ in this case expands proportionally to the distance down the bed[13]. Isotherms that are favorable for adsorption are unfavorable for desorption, so the behavior patterns that occur in each of these adsorption isotherms are reversed for their ensuing desorption isotherms. However, increased temperatures tend to make adsorption

isotherms unfavorable due to the exothermic nature of adsorption, therefore making desorption isotherms favorable[23]. This phenomenon is exploited with temperature swing adsorption (TSA) for regenerating the bed, as will be discussed in Section 2.5.4.

2.4.3 Thermal Considerations

Because the adsorption process is usually exothermic, the temperature rise in the bed due to sorption may present a problem, as sorption capacity is generally inversely proportional to temperature[22]. As mentioned in Section 2.1, this problem generally only applies to systems with a high concentration of adsorbate, but will be briefly discussed here for completion. The heat generated by adsorption will be concentrated in the mass transfer zone. To determine whether the heat front will be ahead of or following behind the mass transfer zone, a crossover ratio can be defined by the equation[27]:

$$CR = \frac{C_{p,g}(X_i - X_r)}{C_{p,s}(Y_i - Y_o)} \tag{1.25}$$

where CR is the crossover ratio, $C_{p,g}$ and $C_{p,s}$ are the heat capacities of the gas (in Btu/mole°F) and of the solid sorbent (in Btu/lb°F) respectively, X_i and X_r are the inlet and residual adsorbent loadings respectively in mole/lb, and Y_i and Y_o are the molar ratios of the adsorbate to carrier (inert) gas at the gas inlet and outlet respectively in mole/mole. For crossover ratios greater than 1, the heat generated by adsorption is pushed forward ahead of the MTZ by the gas, resulting in a temperature front that leads the concentration front. Systems with large crossover ratios can be considered to be isothermal because the heat wave will not directly impact the active sorbing section of the bed. The reverse situation happens when the crossover ratio is less than 1, with the temperature front following the concentration front such that the temperature increase will affect the sorbing section of the bed.

When the thermal front leads the concentration front, as in the case of high pressure and / or low adsorbate concentration systems such as the current study, the temperature change in the bed and of the product gas can be predicted by[28]:

$$QG = (GC_{p,a} + mC_{p,s} + VC_v)(\Delta T) \tag{1.26}$$

where Q is the heat of adsorption (in Btu/lb), G is the weight of adsorbed adsorbate (lb), $C_{p,a}$ is the adsorbate heat capacity (Btu/lb°F), $C_{P,s}$ is the adsorbent heat capacity (Btu/lb°F), C_v is the carrier gas heat capacity (Btu/scf°F), m is the weight of adsorbent (lb), V is the volume of carrier gas processed (scf), and ΔT is the temperature rise of the bed (°F).

2.5 Fiber Module Design Considerations

In designing a fiber module adsorption system for odorant removal from pipeline natural gas, many essential parameters must be considered. Every aspect of the system geometry, fabrication, and set-up affects key optimization points and is discussed in this section. A cost effective, simple system with a low pressure drop and high heat and mass transfer rate is desired.

2.5.1 Fiber Sorbent Spinning

Organic-inorganic fiber sorbents are made using a dry-jet, wet-quench technique to incorporate zeolites into a polymer matrix with desired gas separation properties[29]. First a dope solution is made with precisely proportioned amounts of zeolite, polymer, solvent, and non-solvent. After mixing and sonicating to form a homogenous solution, the mixture is extruded into the fiber form and submerged in a quench bath of water. It is

important to note that this ‘spinning’ process itself has many adjustable parameters that may be modified to achieve desired fiber properties, but will not be elaborated upon here. The freshly spun fibers must then undergo a solvent exchange process in which solvent and high surface tension fluids (water) initially present in the fibers are exchanged with low surface tension fluids such that the fiber pore structure does not collapse when drying[2]. Once the solvent exchange is complete, the fibers can be dried under high temperatures under vacuum to remove the remaining fluid. The end product is a dry fiber consisting of sorbent particles suspended within a continuous porous polymer network.

2.5.2 Fiber Sorbent Module Design and Geometry

After fabrication, the fibers must be bundled together, potted, and sealed into a module with ports on either end for gas flow. Optimization of a fiber sorbent module system involves balancing various trade-offs in the design parameters. Different adjustable physical properties such fiber and module length, diameter, and porosity or packing fraction, and gas flow velocity (adjusted through the number of modules to be used), affect physical limits such as pressure drop and heat and mass transfer in conflicting ways. Table 3 shows the trade-offs of the parameters considered in this study.

Table 3: General trade-offs between the higher and lower limits of various design parameters. The gas flow velocity shown in the last row is related to the number of modules used but is considered its own parameter here for completeness.

Lower Bound / Constraint	Parameter	Higher Bound / Constraint
-Inefficient fibers	13X sorbent loading	-Poor fiber properties (flexibility, spinnability, etc)
-Heat of sorption high (non-negligible)	13X amount	-Expensive
-Increased pressure drop	Fiber diameter	-Slow heat & mass transfer
-Poor mass transfer	Fiber porosity	-Poor mechanical stability -Inefficient fibers
-Residence time too low (poor mass transfer)	Fiber / Module length	-Increased pressure drop
-Residence time too low (poor mass transfer)	Module diameter	-Bad aspect ratio
-Increased pressure drop -Poor mass transfer	Module void	-Channeling / bypass -Inefficient modules
-Heat of sorption high (non-negligible)	Number of modules	-Expensive
-Unable to continuously process large volumes of gas (or need excess beds)	Gas flow velocity (related to number of modules)	-Residence time too low (poor mass transfer) -Increased pressure drop

Because of these trade-offs, the module must be designed in such a way that a realistic compromise between these limits is achieved. Figure 16 shows the various parameters that may be considered in both fiber sorbent modules and pellet packed beds (for comparison). There may be several designs that fit within the specifications necessary for a project.

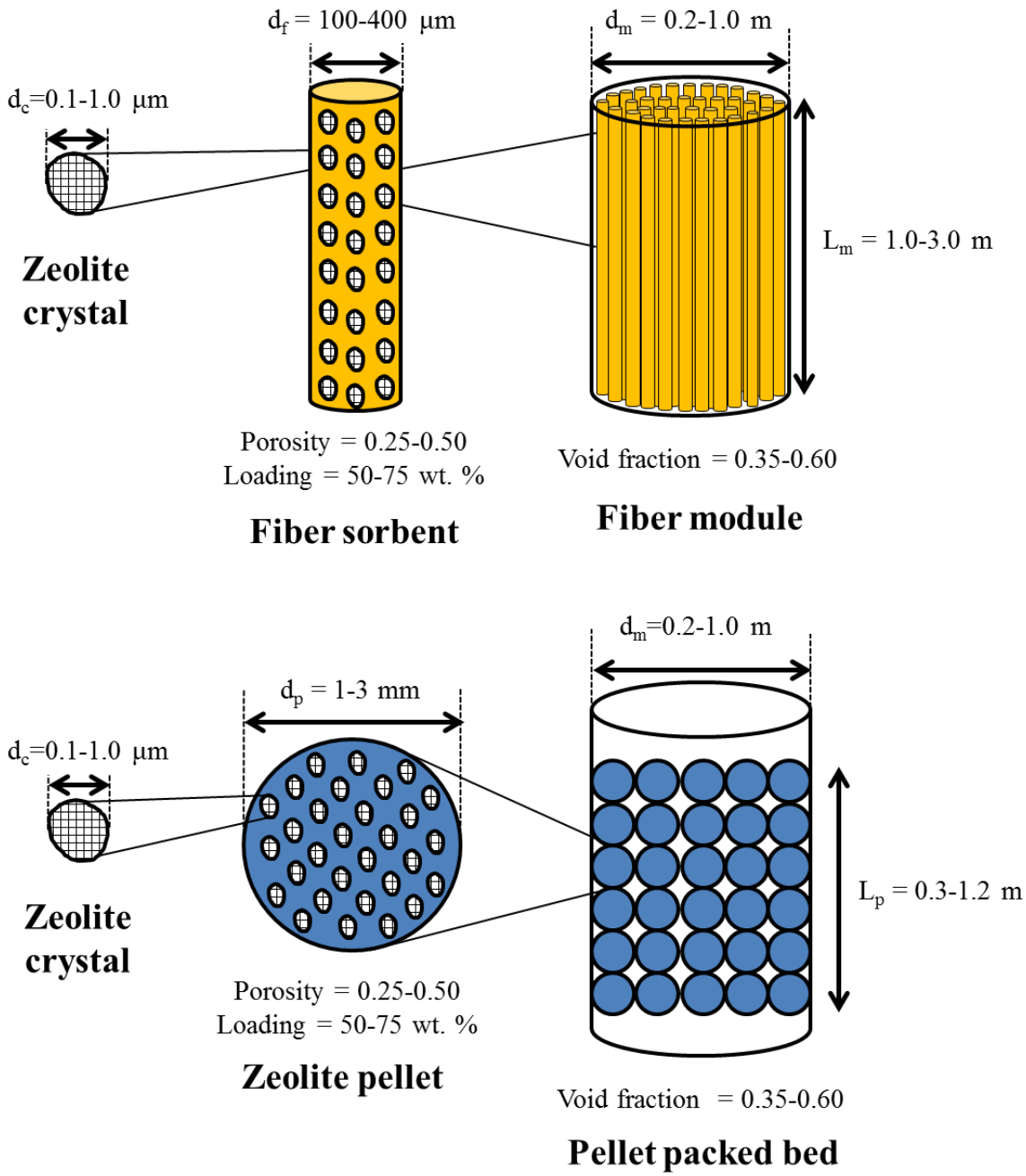

Figure 16: Schematic of a fiber module adsorber compared to a pellet packed bed adsorber for sulfur odorant removal from natural gas. The typical dimensions for each are indicated. (Note: Figure is not drawn to scale) Adapted from Bhandari et. al., 2010.

2.5.3 Gas Flow Configuration

The flow through a fiber sorbent module can be either parallel to the fibers or across them as shown in Figure 17. In addition to these different flows, the shape of the module itself can be cylindrical, conical, or rectangular[30], with each leading to different flow patterns within the bed. The parallel flow pattern in a similar adsorption system has been studied and shown to provide the low pressure drop and high mass transfer desired for the adsorptive desulfurization of natural gas[31]. For ease of design and future construction, a cylindrical module with a parallel gas flow was chosen for this study without optimization or consideration of other flow configurations.

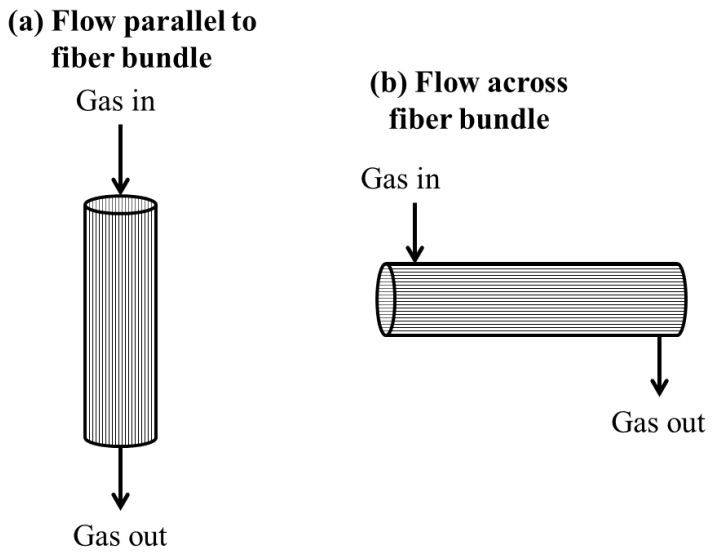

Figure 17. Examples of different gas flow configurations for fiber sorbent modules. Typically, the flow can be either a) parallel to or b) across the fiber bundle. The module itself can be cylindrical as shown here or rectangular or conical.

2.5.4 Sorbent Regeneration

As mentioned briefly in Chapter 1, the two most popular ways to regenerate solid sorbents is by either temperature swing adsorption (TSA) or pressure swing adsorption

(PSA). These two approaches take advantage of the differences in the affinity of the adsorbate for the adsorbent at different temperatures and pressures – for example, low capacities at low pressures and high temperatures[32]. In these two processes, the feed gas mixture is first contacted with the sorbent at one end of the bed and the species with greater affinity is adsorbed, resulting in a purified product gas at the outlet of the bed. In a subsequent regeneration step, the conditions of the bed (either temperature or pressure) are changed such that desorption of the species is favored, resulting in an outlet gas stream rich in the adsorbate[33]. For the separation process to operate continuously, two or more beds must be used in a staggered manner such that some beds may be in the adsorption phase while others are being regenerated for subsequent adsorption.

In PSA mode, the adsorbate is selectively adsorbed onto the adsorbent when contacted under high pressure. The product gas is then still pressurized at approximately the inlet pressure or even higher, making pressure drop less of a concern. The pressure of the bed is then lowered to desorb it from the sorbent and prepare the sorbent for the next cycle[34]. Since there is no heating involved and the bed temperature is kept relatively constant, heat degradation of the fiber materials and / or adsorbate is not a concern, and dangers of working with natural gas at high temperatures is avoided. However, PSA is expensive for processes with very high gas flows such as a large power plant[33], and since the zeolite can be saturated with odorant at very low partial pressures, the depressurization ratio is so high that a significant vacuum would be required for desorption[35].

In TSA mode, the adsorbate is selectively adsorbed in the bed when contacted under low temperatures. With a low adsorbate concentration, the product gas will come out at approximately the same temperature as the feed gas, but with a lower pressure due to pressure drop. The temperature of the bed is then raised for desorption and must be cooled again for a subsequent cycle[33]. This process is kept relatively isobaric so that no energy intensive compression or depressurization of gases is needed. Thermal

degradation of the polymer fibers may present a problem but may be mitigated by choosing a lower regeneration temperature. The TSA process is preferred for feed gases with low concentrations of adsorbate[36], and full regeneration of faujasite type zeolites (X and Y) is possible in various regeneration media. Air, an inert purge gas such as nitrogen, purified feed gas, and water / steam (with a barrier layer) have all been successfully used as the regeneration media in these studies[3, 37-41]. The choice of which to use depends on the specifications of each process, safety and simplicity considerations, available space, and the balance between capital and operating costs, as summarized in Table 4.

Table 4: The advantages and disadvantages of common regeneration media

Advantages	Regeneration Media	Disadvantages
-Simplifies process -Greater safety (closed system)	Purified Feed	-Wastes product (subject to change in product cost, so can be expensive)
-Greater safety (no risk of explosion)	Inert Gas (i.e. N_2)	-Expensive & complex (must add on-site nitrogen generator, requires space)
-Inexpensive -Simplifies process	Air	-Very dangerous
-Inexpensive -Higher heat than other gases	Water / Steam	-Complicates process (requires impermeable barrier layer to use)

2.5.5 Economic and Spatial Considerations

The economics and footprint of this process are critical to its success, especially in small or off-shore processes. To be realistically feasible and advantageous, the fiber module adsorption system must not significantly increase the cost of electricity or be

substantially greater than the cost of replacing a turbine due to corrosion. Additionally, the system should not take up a significant amount of space or be very complicated to start-up and run continuously.

The capital and operating costs associated with the construction and operation of the fiber sorbent system were estimated using various correlations based on the cost of the equipment items used, and their power requirements as a function of size, if applicable[42, 43]. A capital cost was also estimated for an 85 MW turbine for comparison. More details on the cost estimation process are presented in Appendix B. A process flow diagram was developed to aid in cost and space estimates for the system.

2.6 References

1. McKelvey, S.A., D.T. Clausi, and W.J. Koros, *A guide to establishing hollow fiber macroscopic properties for membrane applications.* Journal of membrane science, 1997. **124**(2): p. 223-232.
2. Lively, R.P., et al., *Hollow Fiber Adsorbents for CO2 Removal from Flue Gas.* Industrial & Engineering Chemistry Research, 2009. **48**(15): p. 7314-7324.
3. Bhandari, D.A., N. Bessho, and W.J. Koros, *Hollow Fiber Sorbents for Desulfurization of Natural Gas.* Industrial & Engineering Chemistry Research, 2010. **49**(23): p. 12038-12050.
4. Bhandari, D., et al., *Dual layer hollow fiber sorbents: Concept, fabrication and characterization.* Separation and Purification Technology, 2013. **104**: p. 68-80.
5. Gilleskie, G.L., J.L. Parker, and E.L. Cussler, *GAS SEPARATIONS IN HOLLOW-FIBER ADSORBERS.* Aiche Journal, 1995. **41**(6): p. 1413-1425.
6. Lively, R.P., *Hollow fiber sorbents for post-combustion CO_2 capture*. 2011, Georgia Institute of Technology: Atlanta, Ga.

7. Yang, M.C. and E.L. Cussler, *DESIGNING HOLLOW-FIBER CONTACTORS.* Aiche Journal, 1986. **32**(11): p. 1910-1916.
8. Levenspiel, O., *Chemical reaction engineering*. 3rd ed. ed. 1999, Wiley: New York.
9. Feng, X.S., et al., *Hollow-fiber-based adsorbers for gas separation by pressure-swing adsorption.* Aiche Journal, 1998. **44**(7): p. 1555-1562.
10. Davis, M.E. and R.J. Davis, *Fundamentals of chemical reaction engineering*. 2012: Courier Dover Publications.
11. Chiang, H.-L., et al., *Diffusion of hydrogen sulfide and methyl mercaptan onto microporous alkaline activated carbon.* Chemosphere, 2000. **41**(8): p. 1227-1232.
12. Hirschfelder, J.O., *Molecular theory of gases and liquids*. 2d printing, corr. with notes added. ed, ed. C.F. Curtiss and R.B. Bird. 1964, Wiley: New York.
13. Ruthven, D.M., *Principles of adsorption and adsorption processes*. 1984, Wiley: New York.
14. Baker, R.W., *Membrane technology and applications*. 2nd ed. ed. 2004, J. Wiley: Chichester ;.
15. Rawlings, J.B.E., J.G. , *Chemical reactor analysis and design fundamentals*. 2002, Madison, Wisconsin: Nob Hill Publishing.
16. Hines, A.L., *Mass transfer : fundamentals and applications*. Prentice-Hall international series in the physical and chemical engineering sciences, ed. R.N. Maddox. 1985, Prentice-Hall: Englewood Cliffs, N.J.
17. Do, D.D., *Adsorption analysis : equilibria and kinetics*. Series on chemical engineering ;. 1998, Imperial College Press: London.
18. Fogler, H.S., *Elements of chemical reaction engineering*. 3rd ed. ed. Prentice-Hall international series in the physical and chemical engineering sciences. 1999, Prentice Hall PTR: Upper Saddle River, N.J.

19. Welty, J.R., *Fundamentals of momentum, heat, and mass transfer*. 5th ed. ed. 2008, Wiley: Hoboken, N.J. ;.

20. Asimakopoulou, A. and A. Karabelas, *A study of mass transfer in hollow-fiber membrane contactors—The effect of fiber packing fraction.* Journal of membrane science, 2006. **282**(1): p. 430-441.

21. Seader, J.D., *Separation process principles*, ed. E.J. Henley. 1998, Wiley: New York.

22. Kohl, A.L., *Gas purification*. 5th ed. / ed, ed. R. Nielsen. 1997, Gulf Pub.: Houston, Tex.

23. Crittenden, B.T., W.J., *Adsorption Technology & Design*. 1998, Great Britain: Butterworth-Heinemann. 288.

24. Taty-Costodes, V.C., et al., *Removal of lead(II) ions from synthetic and real effluents using immobilized Pinus sylvestris sawdust: Adsorption on a fixed-bed column.* Journal of Hazardous Materials, 2005. **123**(1-3): p. 135-144.

25. Myers, A.L., *Thermodynamics of adsorption in porous materials.* Aiche Journal, 2002. **48**(1): p. 145-160.

26. Cooney, D.O. and Lightfoo.En, *EXISTENCE OF ASYMPTOTIC SOLUTIONS TO FIXED-BED SEPARATIONS AND EXCHANGE EQUATIONS.* Industrial & Engineering Chemistry Fundamentals, 1965. **4**(2): p. 233-&.

27. Keller, G.E.A., R.A.; Yon, C.M., *Handbook of separation process technology*, ed. R.W. Rousseau. 1987, J. Wiley: New York.

28. Kovach, J.L., *Handbook of separation techniques for chemical engineers*. 2nd ed. ed, ed. P.A. Schweitzer. 1988, McGraw-Hill: New York.

29. Husain, S. and W.J. Koros, *Mixed matrix hollow fiber membranes made with modified HSSZ-13 zeolite in polyetherimide polymer matrix for gas separation.* Journal of membrane science, 2007. **288**(1-2): p. 195-207.

30. Wickramasinghe, S.R., M.J. Semmens, and E.L. Cussler, *MASS-TRANSFER IN VARIOUS HOLLOW FIBER GEOMETRIES.* Journal of membrane science, 1992. **69**(3): p. 235-250.
31. Ruthven, D.M. and C. Thaeron, *Performance of a parallel passage adsorbent contactor.* Gas Separation & Purification, 1996. **10**(1): p. 63-73.
32. Harlick, P.J.E. and F.H. Tezel, *Equilibrium analysis of cyclic adsorption processes: CO2 working capacities with NaY.* Separation Science and Technology, 2005. **40**(13): p. 2569-2591.
33. Hedin, N., et al., *Adsorbents for the post-combustion capture of CO2 using rapid temperature swing or vacuum swing adsorption.* Applied Energy, 2013. **104**(0): p. 418-433.
34. Tagliabue, M., et al., *Regenerability of zeolites as adsorbents for natural gas sweetening: A case-study.* Fuel, 2012. **93**(0): p. 238-244.
35. Bhandari, D.A., *Hollow fiber sorbents for the desulfurization of pipeline natural gas*. 2010, Georgia Institute of Technology: Atlanta, Ga.
36. Yang, R.T., *Gas separation by adsorption processes*. 1987, Butterworths: Boston.
37. Merel, J., M. Clausse, and F. Meunier, *Carbon dioxide capture by indirect thermal swing adsorption using 13X zeolite.* Environmental Progress, 2006. **25**(4): p. 327-333.
38. Lee, D., et al., *Adsorptive removal of tetrahydrothiophene (THT) and tert-butylmercaptan (TBM) using Na-Y and AgNa-Y zeolites for fuel cell applications.* Applied Catalysis a-General, 2008. **334**(1-2): p. 129-136.
39. Satokawa, S., et al., *Adsorptive Removal of t-Butanethiol Using Metal Ion-exchange Y Type Zeolite under Ambient Conditions.* Journal of the Japan Petroleum Institute, 2010. **53**(2): p. 83-87.

40. Bezverkhyy, I., et al., *Adsorption of tetrahydrothiophene on faujasite type zeolites: Breakthrough curves and FTIR spectroscopy study.* Applied Catalysis B-Environmental, 2006. **62**(3-4): p. 299-305.

41. Clausse, M., J. Bonjour, and F. Meunier, *Influence of the presence of CO2 in the feed of an indirect heating TSA process for VOC removal.* Adsorption-Journal of the International Adsorption Society, 2003. **9**(1): p. 77-85.

42. Peters, M.S., *Plant design and economics for chemical engineers*. 4th ed. ed. McGraw-Hill chemical engineering series, ed. K.D. Timmerhaus. 1991, McGraw-Hill: New York.

43. Tedder, D.W., *Preliminary chemical process design and economics*. ill. ;: xxii, 396.

CHAPTER 3

FIBER ADSORBENT MODULE SYSTEM DESIGN, ECONOMIC ANALYSIS, AND COMPARISON

A fiber sorbent adsorption process for the removal of odorant t-butyl mercaptan (TBM) from pipeline natural gas (NG) was designed. Mass and energy balances and various adsorbent bed design equations were used with realistic system dimensions based on existing fiber sorbent technology. The capital and operating costs and footprint of the fiber system were estimated and compared to that of a pellet packed bed, another popular adsorption technology. This design will help to guide the future fabrication and testing of fiber sorbent modules for this purpose.

3.1 Final Fiber Adsorbent System Design

For this design, an 85 MW General Electric 7EA gas turbine was used as the basis for the TBM removal system. From the specifications and requirements of this particular turbine, the adsorption system is assumed to need to process 15,000 standard cubic feet per minute (SCFM) of pipeline natural gas[1]. The typical concentration of TBM in pipeline NG is <10 ppmv so for this analysis, the upper limit of 10 ppmv was used. With this TBM concentration at the specified NG flow rate, the system must process 11.2 moles per hour of TBM. Figure 18 shows the placement of such an adsorbent treatment system in relation to a gas turbine within a natural gas-fueled combined cycle power plant.

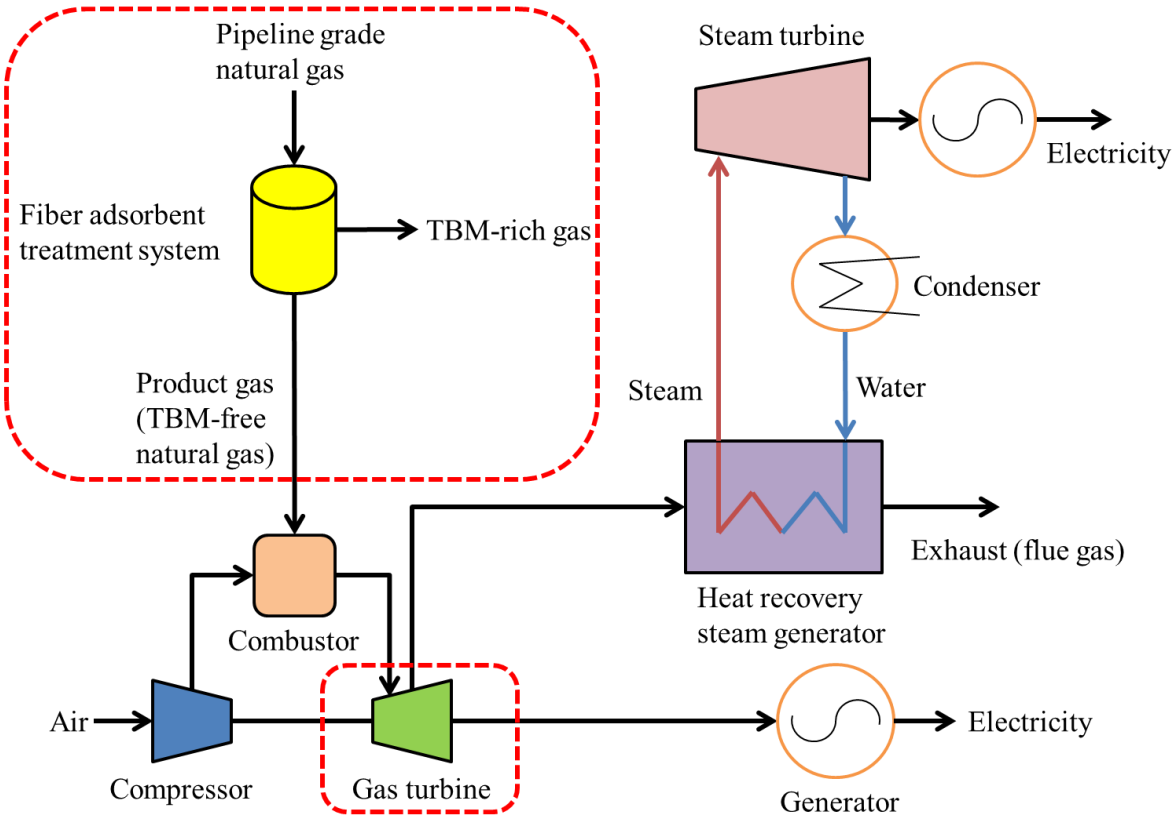

Figure 18: Illustration showing the placement of the fiber sorbent treatment system in a combined cycle power plant. The system is placed just before the inlet to the gas turbine such that only treated (TBM free) natural gas will reach the turbine.

The final fiber and module design dimensions are shown in Figure 19. The fiber is set at 75 wt. % loading of zeolite 13X with a porosity of 0.25 and a diameter of 300 microns. Its length is the same as the length of the module, set at 1.4 meters. Additionally, the module is set at diameter of 0.4 meters with a void fraction of 0.35. This constrains the number of fibers in one module to 1,155,556 fibers, the density of the fiber to 1134.6 kg/m^3, and the amount of zeolite 13X and cellulose acetate polymer in one module to 97.1 kg and 32.9 kg respectively. These dimensions were chosen to maximize heat and mass transfer and to minimize pressure drop (see Appendix A). As mentioned in Chapter 2, a parallel flow configuration is assumed in this study due to ease of construction and the pressure drop advantage it has over a cross flow configuration[2].

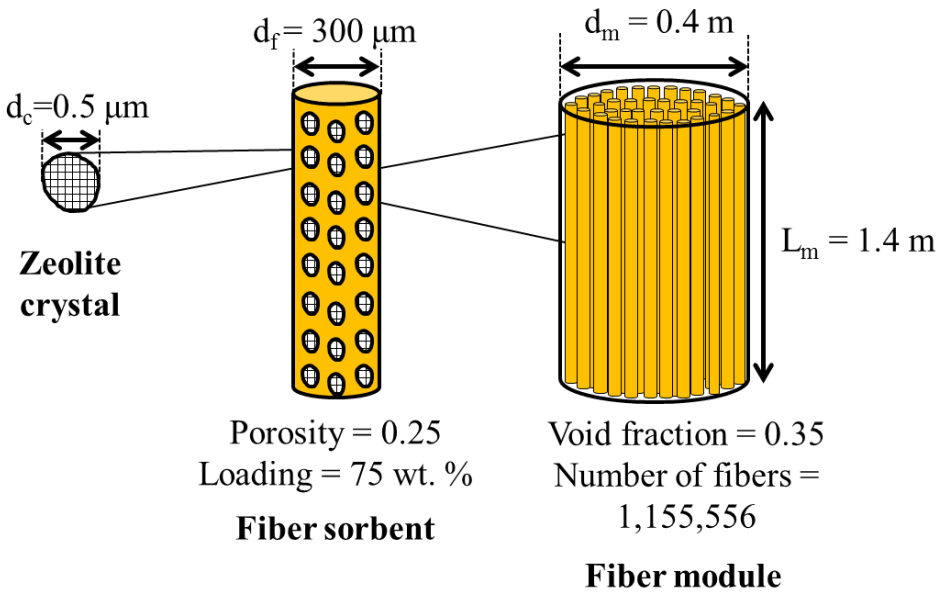

Figure 19: Illustration of the fiber sorbent design with the final dimensions specified. The 13X zeolite crystals with an average diameter of 0.5 microns will be embedded into the polymer fibers at a loading of 75 wt. %. The fibers themselves will have a diameter of 300 microns and a length of 1.4 meters with a porosity of 0.25. These fibers will be bundled into a module with a diameter of 0.4 meters and a void fraction of 0.35.

Adsorbent beds, whether they be bundled with fibers or packed with pellets, are meant to be used in either pressure swing adsorption (PSA) or temperature swing adsorption (TSA) to cyclically and selectively adsorb and desorb the species of interest from the feed gas. A TSA cycle was chosen for this study due to the high pressure of the pipeline natural gas feed requiring a large amount of decompression and possibly vacuum for the desorption step in the PSA cycle, and the subsequent large amount of recompression that would be needed to bring the beds back up to pipeline pressures[3].

In this TSA process, the first step is the adsorption step, in which the pipeline natural gas is fed through the inlet of the module while the treated TBM-free natural gas exits at the outlet. The second step and third steps together comprise the sorbent regeneration step. Hot product gas is chosen as the regeneration gas and is fed through the inlet while interstitial gas exits at the outlet. As the fibers heat up, the adsorbed TBM will desorb and exit at the outlet. This concentrated TBM gas stream will be burned as

waste, so any product gas used in this step is counted into a parasitic load value. The fourth step is the cooling step, in which cool product gas, chosen as the cooling gas, is fed through the inlet to cool the fibers back to the adsorption temperature. The product gas in this step will exit at the outlet at a higher temperature than at the inlet, but its composition will remain unchanged as any residual TBM is not expected to desorb further in this step. Therefore the product gas used in this step is not wasted and not counted into the parasitic load. Figure 20 illustrates these distinct cyclic steps.

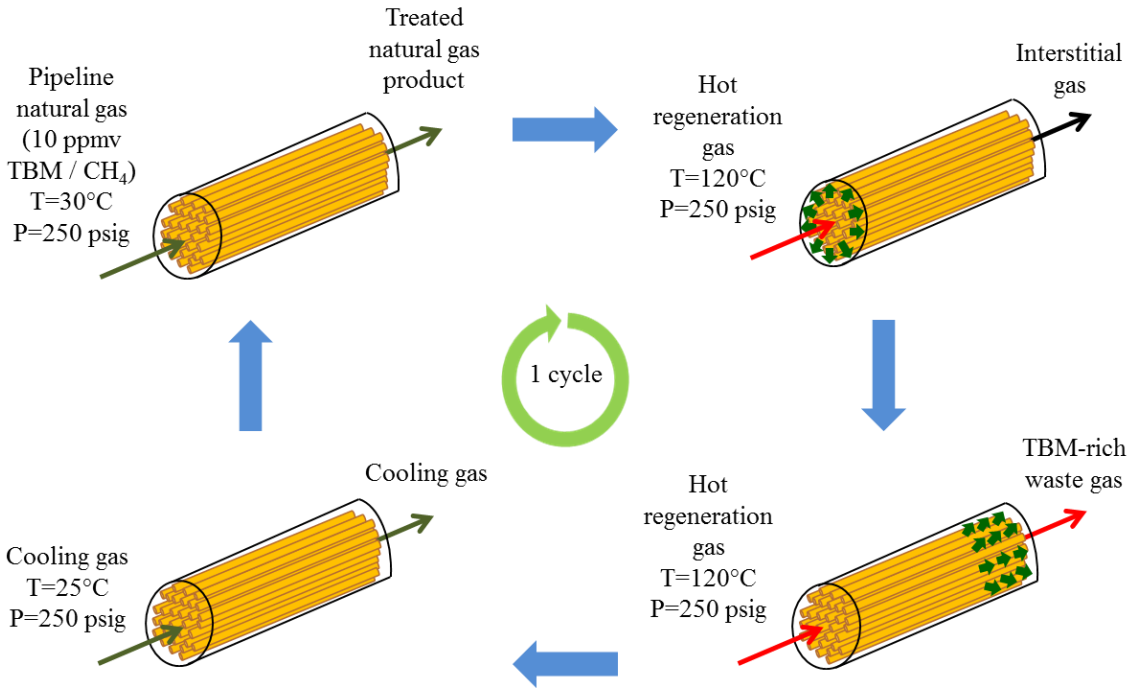

Figure 20: Schematic of a fiber bed cycling through the continuous steps of adsorption and desorption. The top left bed shows the first step, adsorption, where pipeline natural gas is fed at the inlet of the module while treated product gas exits on the opposite end. The top and bottom right beds show the second step, heating / desorption, where hot regeneration gas is fed at the inlet. Initially, the regeneration gas will push out the interstitial gas left over from the adsorption step. Finally, the fibers will be heated to the desorption temperature by the regeneration gas and TBM will be desorbed and carried out of the bed as a waste gas stream. The bottom left bed shows the third and last step, cooling, where cooling gas is fed at the inlet of the module and simply exits at a higher temperature.

Four beds are used in this process, with three beds always in adsorption mode while one bed is being regenerated and cooled. To control the feed gas velocity through

the beds, the pipeline natural gas will be evenly split into three streams running in parallel through the three modules in adsorption mode. A staggered start-up will ensure the process can be operated continuously in this fashion. Figure 21 shows the envisioned setup of the system of fiber modules for the treatment of enough pipeline natural gas to fuel one 85 MW turbine. Note that there are five modules shown in the figure, though only four of the beds are active and necessary for the process. An extra module is added for practical reasons as a backup in case one of the active modules needs to be repaired or replaced. A simple flipping of a few switches will put this extra module "online" and take an active module "offline."

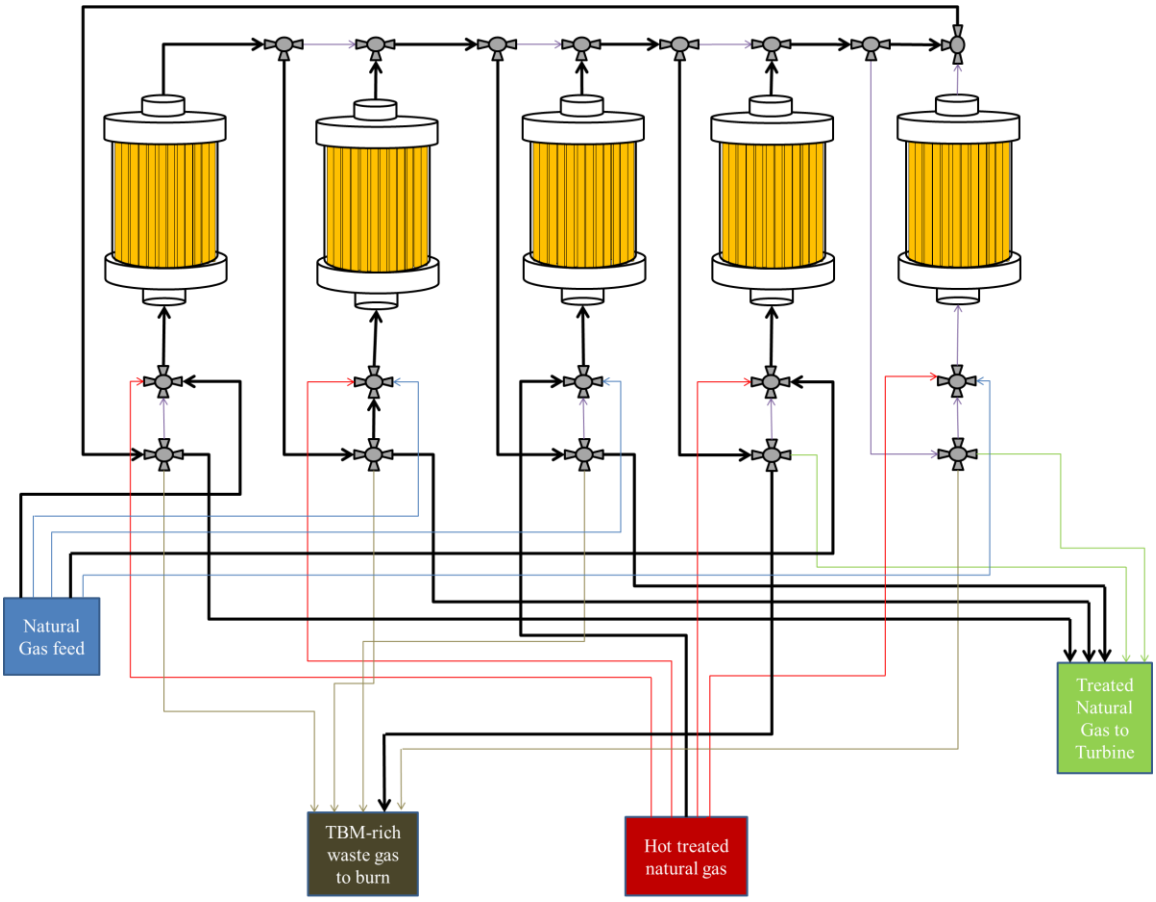

Figure 21: Illustration of how the fiber sorbent modules will be connected together with various multi-position automated switching valves. The thick lines indicate an example of how gas can flow through the system. The thin lines indicate which gas lines are connected, but closed. These valves will direct the inlet and outlet streams through each module appropriately. The inlet valve switches between pipeline natural gas feed, hot desorption gas, or cooling gas, while the outlet valve switches between product gas to the turbine, product gas to be re-routed for regeneration or cooling, or waste gas to be burned.

3.2 Mass & Energy Balances

Mass and energy balances were performed on the fiber module system as part of an iterative optimization process to minimize pressure drop and maximize mass transfer for the adsorption step, and minimize the amount of product gas needed for the regeneration and cooling steps (which also minimizes the cycle times of these "non-active" phases). The same sorts of calculations were performed for a pellet packed bed as a competing, existing technology. The pellet bed dimensions and void fractions were kept the same as in the fiber modules, as illustrated in Figure 22. The only major difference is the bed is filled with 1 mm diameter pellets loaded with zeolite instead of filled with fibers.

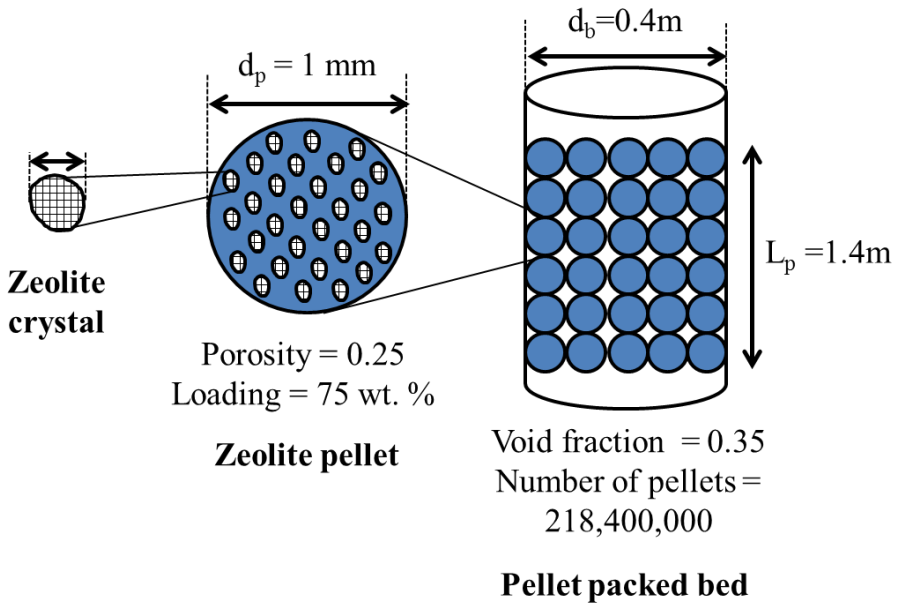

Figure 22: Illustration of the pellet packed bed design with the final dimensions specified for comparison. The 13X zeolite crystals are pressed into pellets with a binder material at a loading of 75 wt. %. The pellets will have a diameter of 1 mm and a porosity of 0.25. These pellets will be packed into a bed with a diameter of 0.4 meters, a length of 1.4 meters and a void fraction of 0.35. These dimensions were selected to match with that of the fiber sorbent modules.

3.2.1 Pressure drop

The modified Hagen-Poiseuille equation below was derived directly from Navier-Stokes equations in cylindrical coordinates, and was used to describe the pressure drop down the length of a fiber module as a function of the interstitial gas velocity, fiber radius, and packing fraction in the module[4]:

$$\frac{\Delta P}{L_m} = \frac{8\mu_{NG} v_i}{2r_a^{\,2}\ln r_a - 2r_a^{\,2}\ln r_f - r_a^{\,2} + r_f^{\,2}} \tag{1.27}$$

where r_a is a hypothetical annual radius of void space around each fiber defined by:

$$r_a = \sqrt{\frac{A_m}{\pi N_{fm}}} \tag{1.28}$$

Alternatively, the Ergun equation below was used to describe the pressure drop down the length of a pellet packed bed[5]:

$$\frac{\Delta P}{L_m} = \left(\frac{1}{150}\frac{(1-\varepsilon_m)\mu_{NG}}{d_p v_s \rho_{NG}} + 1.75\right) \times \left(\frac{1-\varepsilon_m}{\varepsilon_m^{\,3}}\right) \times \left(\frac{\rho_{NG} v_s^2}{d_p}\right) \tag{1.29}$$

Using these equations, the pressure drop down the fiber module at an interstitial gas velocity of 3.3 m/s is 1.53 atm/m. At the same bed packing fraction and gas velocity, the pressure drop down a bed packed with 1 mm diameter pellets is 4.34 atm/m. There are two main ways to reconcile this almost 3-fold pressure drop difference in terms of system design and economic analysis. The first way would be to allow for this high pressure drop in the pellet packed bed and pay for it by adding an extra compressor to the system to re-pressurize the product gas stream. However, for the case in which the product gas is to be used for both regeneration and cooling steps, this pressure drop will need to be accounted for twice. The second way would be to make the pellet beds match the pressure drop in the fiber modules by employing more beds and therefore reducing

the gas velocity through each bed. This method was initially chosen for this study to minimize system complexity and operating cost. In this way, it was found that the interstitial velocity needed in the pellet beds to keep the same pressure drop as in the fiber modules is 1.96 m/s. This corresponds to five pellet packed beds needed for the adsorption step, as compared to three fiber beds needed for the adsorption step. However, as will be discussed later, this gas velocity is still too high for the pellets to reach mass transfer equilibrium and must be slowed further to reach the same mass transfer equilibrium as in the fiber modules.

3.2.2 Mass and Heat Transfer

The mass transfer coefficients (MTC) for each of the three regions (external film layer, internal meso/macropore layer, and internal micropore layer) surrounding a fiber or pellet sorbent is presented below in Table 5. The calculations for these results are shown in Appendix A using Sherwood correlations to find the external MTCs[6, 7] and the linear driving force approximation to find the internal MTCs[8]. From a comparison of these MTCs, it can be seen that the fibers have better internal meso/macropore mass transfer than the pellets, which makes sense because the gas has a larger distance to penetrate in the pellets than in the fibers. Additionally, it can be seen that the pellets have better external mass transfer than the fibers, which also makes sense because the pellets have three dimensions in which the gas can penetrate while the fibers only have two. The internal micropore mass transfer is very high compared with the two other regions because of the small size of the 13X crystals, and is the same in both fiber and pellet cases because the crystals are the same in both. However, the Biot mass number[9], calculated to be >1 for both fiber and pellet beds (see Appendix A), shows that the internal meso/macropore resistance, which is proportional to the inverse of the MTC, is

the limiting resistance for both fiber and pellet beds. Meaning that overall, mass transfer in the fiber beds will be better than that of pellet beds for this system.

Table 5: Mass transfer coefficients associated with the three different regions within both a fiber sorbent module and a pellet packed bed. External mass transfer is greater in the pellet bed than in the fiber module, but internal meso/macropore mass transfer is greater in the fiber module than in the pellet bed. Sensibly, the internal micropore mass transfer is the same in both.

	External (Film) Mass Transfer Coefficient (cm/s)	Internal (Meso/macropore) Mass Transfer Coefficient (cm/s)	Internal (Micropore) 13X Mass Transfer Coefficient (cm/s)
Fiber Module	0.13	0.05	4.40
Pellet Bed	1.19	0.02	4.40

At an interstitial velocity of 3.30 m/s in a 1.4 meter long fiber bed, the residence time of a gas molecule inside the module is 0.42 seconds, while at an interstitial velocity of 1.96 m/s in a pellet packed bed (from pressure drop matching) of the same length, the residence time is 0.71 seconds. With an effective diffusion coefficient through the sorbent meso/macro pores of 2.5×10^{-4} cm^2/s, a residence time of 0.42 seconds in the fibers is enough time for the fibers to reach 95% mass equilibration. In other words, this contact time is enough for the fiber sorbents to reach 95% of its maximum capacity, which was considered acceptable for this analysis. However, a residence time of 0.71 seconds in the pellets is only enough time for the pellets to reach about 72% mass equilibration[10]. This demonstrates an inefficient use of sorbent in the pellet packed bed, such that the adsorption step time would be significantly lower than in the fiber module system and the unused zeolite in the bed would be essentially wasted. More beds would then be required to make up for this lost capacity in the pellets. Another option would be to reduce the gas velocity even further in order to lengthen the contact time such that the same 95% mass equilibration can be reached in the pellet bed. Either method of comparison, matching pressure drop or matching mass transfer, would lead to requiring a significantly larger

number of pellet packed beds than fiber beds to remove the required amount of TBM continuously. The method of matching the mass transfer rate was finally chosen for this study in order to use the sorbent as effectively as possible.

Heat transfer happens on a much shorter time scale than mass transfer in this system (on the order of ~0.01 seconds) such that thermal equilibration does not limit the system in the regeneration and cooling phases (see Appendix A calculations). In the regeneration (heating) step, hot product gas is assumed to flow over the fibers at 120°C, heating the center of the fiber or pellet to at least 90°C and desorbing most of the TBM. This desorbed TBM is carried out of the bed with the hot regeneration gas. In the cooling step, cool product gas is assumed to flow over the fibers at 30°C, cooling the center of the fiber to at least 35°C.

Using an energy balance on the system in the adsorption step, the temperature rise of the fibers due to the heat of adsorption was estimated to be about 1°C for the fiber sorbent system (see Appendix A) due to the very low concentration of TBM in the feed gas. This is small enough that the adsorption phase can be considered to be isothermal without needing a cooling agent to carry away the heat of adsorption, and no extra temperature control is used during this step. If the temperature rise were greater, hollow fibers or a cooling jacket around the module could be considered.

The cycle time for the adsorption step was calculated to be about 57 minutes from the total amount of TBM that will be sorbed in one module and the flow rate of TBM through the module.

3.2.3 Temperature Swing Adsorption Cycles

As mentioned in Chapter 2, various regeneration media can be used for heating the fibers in order to desorb the TBM, all with different advantages and disadvantages[11-13]. Three of the regeneration media mentioned in Chapter 2, compressed air, nitrogen,

and product gas, were explored further in this work. Water was not considered because it requires an impermeable barrier layer to be added to each fiber, which is unnecessary for this application. Table 6 quantifies the amount of each of these regeneration gases flowing at an interstitial velocity of 3.30 m/s (same as the feed gas velocity) that would be needed at a temperature of 120°C and a pressure of 250 psig (same as pipeline natural gas pressure) to heat the fibers to at least 90°C to desorb the TBM inside. These estimations were made using an energy balance on the system in the regeneration mode (see Appendix A). The regeneration cycle time associated with each of these gases is also listed, estimated from the amount needed and the flow rate of the gas. Further, the amount of regeneration gas needed per cycle is also defined in terms of bed volumes, or the total volume of void space inside one fiber module. Finally, the last column compares the volume of regeneration gas needed for this step to the volume amount of natural gas treated during the adsorption step in a percent value. For product gas as the regeneration gas, this last column is considered the parasitic load on the system because this gas is to be burned outside of the turbine. For the other regeneration gases, the value in the last column is only included for comparison, as this wasted gas is not taking away from the valuable product to be used in the turbine and adding to the operating cost of the system.

Table 6: Quantities and timing of the various possible regeneration gases that can be used for the heating / desorption step. When product gas is used as the regeneration media, the last column represents a parasitic load on the system. This value is also included for comparison purposes for compressed air and nitrogen regeneration gases, but does not represent a parasitic load.

Regeneration Gas	Amount of regen gas per cycle (kg)	Amount of regen gas per cycle (m^3)	Regen cycle time (min)	Bed volumes	Vol of regen gas / vol of natural gas treated (%)
Compressed Air	257	16	1.8	177	3.23
Compressed Nitrogen	250	16	1.9	178	3.25
Product Gas	104	12	1.3	127	2.31

Compressed air, considered initially, was eventually eliminated due to the safety issues that arise from feeding large quantities of hot compressed air next to highly combustible natural gas. To decrease the risk of explosion, it is desired to have a regeneration gas that is free of oxygen. Compressed nitrogen from an on-site generator was also considered, but eventually eliminated due to high cost, as will be discussed further in Section 3.3. Finally, a fraction of the product gas was chosen as the regeneration media due to its safety, low cost, simplicity, and smaller volume needed. From Table 6, it can be seen that the parasitic load on the system is 2.31% for using product gas for the regeneration step.

The concentration of TBM in the gas exiting after the regeneration step is about 0.31 moles/m^3, or about 514 ppm at pipeline regeneration conditions. This exiting TBM-rich gas stream is to be burned as waste, but as it still contains a large amount of methane, it is possible to use the heat from its combustion to generate steam. This extra steam can then be used to heat the product gas for the regeneration cycle (such that the regeneration cycle can become self-sustaining without requiring energy from outside the process) and / or in the steam turbine part of a natural gas-fueled combined cycle power plant (discussed in Chapter 1). For the cost analysis part of this study, these options were not examined, and the process is considered to be without heat integration or optimization around this point. However, it is worth noting that this presents an opportunity for future work to further bring down operating costs by integrating the heat created from this TBM-rich waste stream.

The combustion of this TBM-rich stream will create the poisonous gas SO_2 in the same molar concentration. There currently exists no SO_2 treatment system in natural gas power plants because the concentration normally created through its combustion is so low (only the trace amount of sulfur odorant present in the natural gas is converted to SO_2). However, through capturing the TBM and desorbing it in a concentrated stream, the SO_2 concentration also increases and must be dealt with. The first option would be to simply

re-dilute this combustion stream in the flue gas of the turbine, as this would not release any more SO_2 into the atmosphere than what would be released without the fiber adsorbent system. The second option, not considered for the purposes of this study, would be to add in an extra SO_2 treatment system to sequester it and prevent its release into the atmosphere. However, this option would greatly increase both the capital and operating cost of the fiber adsorbent system and was therefore not used in this analysis.

The product gas was chosen as the cooling gas without consideration of other gases, as it greatly simplifies the process, does not waste any product, and natural gas (composed mainly of methane) has a higher heat capacity than either air or nitrogen. Table 7 shows the amount, cycle time, and relative volume of product gas needed at a temperature of 30°C and a pressure of 250 psig to cool the fibers to at least 35°C using the same estimation methods as the regeneration gas.

Table 7: Quantity and timing of the product gas needed for the cooling step. The cycle time of this step is generally longer than the cycle time of the heating step because the temperature difference between the between the cooled product gas and the desired temperature of the fibers is not very large. If the long cycle time is a problem, the product gas can be cooled further to allow for a shorter time.

Cooling Gas	Amount of cooling gas per cycle (kg)	Amount of cooling gas per cycle (m^3)	Cooling cycle time (min)	Bed volumes	Vol of cooling gas / vol of natural gas treated (%)
Product gas	703	59	6.5	650	11.85

The only major disadvantage of using product gas is having to pay for the pressure drop down the fiber modules twice. Still, the amount of product gas that must be used for this cooling step is low, at approximately 11.85% of the total volumes of pipeline natural gas treated during the adsorption step. This amount is controlled by the temperature of the product gas. The cooler the product gas is, the faster it will cool the fibers, and the less the amount of gas that will be needed. However, the drawback of using a cooler stream is having to use more cooling water to cool it.

As mentioned in Section 3.2.1, the pellet packed beds were directly compared to the fiber beds by matching the mass transfer in both. It is desired to have the fiber or pellet sorbent reach at least 95% capacity. For this to happen, the residence time of the natural gas feed in the pellet bed must be a minimum of 2.5 seconds (see Appendix A). This is much longer than in the fiber beds because of the smaller critical length of the fibers (fiber radius of 150 microns versus pellet radius of 500 microns). While fibers may be easily spun with such small radii, pellets are not typically created with diameters less than 1 mm[3]. Even if smaller diameter pellets could be created, the pressure drop penalty would be much larger such that the gas velocity would again have to be slowed. This needed residence time of 2.5 seconds in the pellet bed translates to an interstitial velocity of 0.56 m/s in a 1.4 meter long bed, and a superficial velocity of 0.20 m/s for a bed void fraction of 0.35. Finally, to keep this velocity with the same bed dimensions, the number of pellet packed beds must be increased to about 18 beds for the adsorption step (see Appendix A for elaboration). The regeneration and cooling gases were again taken to be fractions of the product gas so that a direct comparison to the fiber modules could be made. However, the gas velocity was slowed to match the new NG feed velocity.

Table 8 summarizes the cycle times for each of the three phases and the number of beds needed in a fiber module system versus a pellet packed bed system.

Table 8: Step times and bed number comparison between fiber and pellet adsorbers. The cycle times are much longer for the pellet bed and the number of beds much higher because of the slower interstitial velocity required.

	Fiber Module System	Pellet Bed System
Adsorption Step Time (min)	57	340
Regeneration Step Time (min)	1.3	22
Cooling Step Time (min)	6.5	116
Total Cycle Time (min)	65	478
Number of Beds in Adsorption	3	18
Total Number of Active Beds	4	24

The times associated with each of the three steps are much longer in the pellet beds than in the fiber beds due to the much slower interstitial velocity required through the pellet beds. Also, the pellet bed system spends a larger fraction of its total cycle time in regeneration and cooling modes because of the difference in heat capacity between the kaolin clay used as the binder material in pellets and the cellulose acetate polymer used as the structure material in fibers. Six times more pellet packed beds are needed than fiber beds, again due to this slower gas velocity through the pellet beds. The difference between the total number of active beds and the number of beds in adsorption mode indicates the number of beds that will be in regeneration / cooling mode with proper staggered bed start-up and timing. One extra inactive bed will be included in the cost analysis of both designs to be on stand-by in case of an emergency. In other words, once steady state continuous operation is reached in the five-bed fiber module system, three of the active beds will always be in adsorption mode while the fourth active bed will be in regeneration / cooling mode or at rest. Similarly for the twenty-five-bed pellet packed bed system, eighteen of the active beds will always be in adsorption mode while the six other active beds will be in regeneration / cooling mode or at rest.

3.3 Economic Analysis

Once the designs of both the fiber module and pellet packed bed adsorber systems were finalized, an economic analysis was performed on both systems for a direct comparison of the two technologies. All cost estimates are reported in terms of 2011 U.S. dollars.

3.3.1 Capital Cost of Adsorption System

The capital costs of both fiber module and pellet packed bed systems were estimated using cost correlations and heuristics found in Tedder[14]. The capital cost of a single fiber module was first estimated based on the cost of the raw materials needed to create a module such as zeolite 13X, cellulose acetate polymer, solvents, and module materials. The module shell is assumed to be made of low cost carbon steel, which is considered acceptable for processes that are essentially free of water and don't involve halogens[14], both of which are true for this work. The total cost for one fiber module was then scaled up from the raw material cost using two different factoring methods (Guthrie and Page) that take into account labor, construction equipment, overhead, and other indirect costs. The base cost per module was taken to be the average between these two factoring methods (see Appendix B for details). The capital cost of a single pellet packed bed was estimated with a cost correlation of a packed bed based on reactor volume plus an estimation of the cost of the pellets to fill the bed.

The adsorbent system is assumed to operate at a constant pressure of 250 psig, the typical pressure of pipeline natural gas[15]. The piping and other equipment items needed for the whole skid are also assumed to be made of carbon steel for this application. To estimate the cost of the whole system, including piping and equipment for regeneration and cooling of the sorbent, a basic process flow diagram was first developed for the system. As mentioned previously, three types of regeneration media were considered for the heating / desorption step in the fiber modules, each requiring different equipment items to be added to the fiber modules to create a skid. A major equipment list can be developed from the process flow diagram and each equipment item can be sized based on the requirements of the fiber system (mass and energy balances). Finally, the cost of each equipment item can be estimated using cost correlations[14, 16]. Table 9 summarizes the

various equipment items needed and their respective costs for the heating / desorption step for each of the three regeneration media considered.

Table 9. Summary of the equipment items and costs associated with the three types of regeneration media considered – compressed air, nitrogen, and product gas. The purchased equipment cost takes into account the high operating pressure of the system, which will slightly raise the cost of each equipment item.

Desorption Equipment List	Purchased Equipment Cost
Compressed Air Desorption	
Air Compressor	**$89,000**
Nitrogen Desorption	
Air Compressor	$85,000
Air Dryer	$33,000
Air Filter	$9,000
Air Tank	$6,000
Nitrogen PSA Generator	$34,000
Nitrogen Tank	$7,000
High Pressure Compressor	$95,000
Total	**$269,000**
Product Gas Desorption	
Heat Exchanger	**$22,000**

Using compressed air for desorption would only require an air compressor and using product gas for desorption would only require a heat exchanger, making the capital costs associated with these two regeneration gases low. However, using nitrogen for desorption would require an on-site nitrogen generation system composed of many components, complicating the process and significantly increasing the capital cost of the system. From Table 9 it can be seen that the capital cost of a fiber module system that uses product gas for the regeneration step will be lower than a system which uses either compressed air or nitrogen. Therefore, product gas was chosen as the regeneration media for system simplicity and lower cost.

After choosing product gas as the regeneration media, the capital costs for the whole fiber module and pellet packed bed systems were estimated using Guthrie and

Page cost correlations. Both of these methods give system capital cost estimates as percentages of the base and purchased equipment costs (see Appendix B for details). In addition to the heat exchanger used to heat the product gas with steam, the other equipment items are the adsorber beds themselves (5 fiber modules versus 25 pellet packed beds) and a second heat exchanger used to cool the product gas with cooling water. Both Guthrie and Page methods take into account the size / capacity of each equipment item needed, the high operating pressure of the system, and other direct and indirect costs such as piping, labor, materials for construction, safety, taxes, delivery, overhead, and engineering. Table 10 compiles the various capital costs associated with both fiber and pellet adsorber beds. The pellet packed bed system costs about three times more than the fiber module system. Example calculations, as well as a list of possible sources of error in this estimation are detailed in Appendix B.

Table 10: Summary of the major capital costs associated with fiber module and pellet packed bed systems. The cost per bed is the cost of one fiber module or one pellet packed bed (raw material costs and other indirect costs) while the total cost of beds is the cost per bed multiplied by the number of beds needed in the system and a pressure factor to account for the high pressure of the system. The total capital investment is the cost of the whole adsorber system including piping and equipment to support regeneration and cooling of the sorbent, as well as other direct and indirect costs.

	Fiber Module System	Pellet Bed System
Cost per Bed	$19,000	$19,000
Total Cost of Beds	$112,000	$475,000
Cost of Hot Heat Exchanger	$22,000	$8,000
Cost of Cold Heat Exchanger	$19,000	$6,000
Total Capital Investment	$857,000	$2,792,000

3.3.2 Operating Cost of Adsorption System

The operating costs of both fiber module and pellet packed bed systems without heat integration include two major contributing costs: utilities and the parasitic load incurred by using the product gas to do heating and desorption. Labor costs were

considered with operating costs in an initial estimate, but finally omitted due to reasoning that the fiber sorbent system is easily automated and no extra workers need specifically be hired to operate it[17]. Instead, it is assumed that the employees already working at the plant can be given the extra responsibility of checking on the adsorption system intermittently, and that the system does not need continuous supervision once it has been started up. Other costs that were also considered but finally omitted from the final operating cost are the cost of purchasing the pipeline natural gas feed because this is a cost that would be incurred even without the sorbent system, the cost of compressing the final product for introduction into the turbine based on similar reasoning that this is a cost that would be incurred anyway, and finally, the cost of waste gas disposal (SO_2 gas scrubbing) because the amount of SO_2 produced will be relatively small and can simply be disposed of with the flue gas.

Different equipment items are needed for each of the three regeneration media considered for the fiber module system, and as such, different utilities are also needed for each system. After sizing the equipment items for the capital cost estimate, the energy requirements of the various systems were estimated with an energy balance and the costs were extrapolated using the cost of the utilities required. For regeneration with compressed air, the air compressor requires electricity as the major utility[16]. Similarly, regeneration with nitrogen requires electricity to power the on-site nitrogen generation system, specifically the two compressors and the air dryer. With both air and nitrogen, the gas is naturally heated through compression, and does not require further heating. Regeneration with product gas requires steam as a utility for heating the product gas. Additionally, the parasitic load incurred by mixing this product natural gas with TBM and wasting it must be accounted for. Table 11 presents the operating costs associated with a fiber module adsorber system using each of the three regeneration gases considered.

Table 11: Annual operating costs associated with different regeneration gases considered for the regeneration step in the fiber module system only. The compressed air desorption shows the lowest cost, but was eliminated from consideration due to safety issues. The sum of the operating costs associated with product gas desorption is higher than the operating cost of compressed nitrogen desorption.

Regeneration Gas	Utility	Price	Unit	Amount Needed	Units	Annual Cost
Compressed Air	Electricity	$0.04	per kWh	81,775	kWh/year	$3,000
Compressed Nitrogen	Nitrogen	$0.04	per Nm^3	489,746	kWh/year	$19,000
Product Gas	Steam	$0.02	per kg	226,050	kg/year	$4,000
	Product NG*	$0.16	per m^3	317,815	m^3/year	$51,000
* Parasitic load						

Though using compressed air for the regeneration step would give the lowest operating cost, again, it was eliminated due to safety reasons. Using compressed nitrogen for the regeneration step would present the next lowest annual operating cost, but compared with the capital costs given in Table 9 over the 5 year lifetime of the fiber adsorption system, the product gas would still be less expensive overall, and also simplifies the system by not having to introduce the on-site nitrogen generation system.

For the system in general, the adsorption step does not require a compressor or pump because the feed gas is already at a high pressure of 250 psig, and can be fed directly into the adsorber beds. Product gas was chosen as the cooling media for the cooling step as mentioned in Section 3.2.3, and requires cooling water as a utility for cooling the product gas. An estimate for the annual operating cost of this cooling step was done in the same way as the regeneration step. Table 12 compiles the various operating costs associated with both fiber and pellet adsorber beds using product gas for both regeneration and cooling. The total annual operating cost for the pellet packed bed system is about 3.5 times greater than the operating cost for the fiber module system.

Table 12: Summary of the major annual operating costs associated with fiber module and pellet packed bed systems. The product gas parasitic load is the amount of product gas that is required for the regeneration step each year multipled by the cost of natural gas.

	Fiber Module System	Pellet Bed System
Steam for Regeneration Step	$4,000	$27,000
Product Gas Parasitic Load	$51,000	$150,000
Cooling Water for Cooling Step	$6,000	$34,000
Total Annual Operating Cost	**$61,000**	**$211,000**

If heat integration is considered, the total operating cost for the fiber system can be lowered significantly. With heat integration, a fraction of the heat generated from the combustion of the TBM-rich waste gas stream can be used to create steam, which can be used to heat the product gas in the regeneration step. This would eliminate the cost of purchasing steam as a separate utility and lower the amount of product gas wasted, which in turn lowers the cost of paying for this parasitic load. Additional water would then have to be purchased in order to create the steam, but this presents a lower cost increase than the savings gained from lowering the parasitic load and not purchasing steam. The second column in Table 13 lists the new operating costs associated with the fiber system if only enough steam is created this way for use in the regeneration step of the process.

Table 13: Summary of the major annual operating costs associated with the fiber module when two heat integration options are considered. The second column lists the new operating costs when only enough steam is created from waste gas combustion heat to use in the regeneration cycle. The third column lists the new opearating costs when all of the waste gas conbustion heat is used to create steam, and the excess steam created is subsequently used to generate electricity with a steam turbine. Both of these heat integration options eliminates the cost of steam and lowers or eliminates the parasitic load cost, but increases the cost of water. The total annual operating cost with heat integration is lower than that without heat integration.

	Steam Created for Regen Cycle Only	Steam Created using all Waste Stream
Steam Cost for Regeneration Step	$0	$0
Product Gas Parasitic Load Cost	$50,000	$0
Cooling Water for Cooling Step Cost	$6,000	$79,000
Product Electricity Profit	$0	-$88,000
Total Annual Operating Cost	**$56,000**	**-$9,000**

Another option for heat integration is to use all of the energy from the waste stream combustion to create steam. Because the amount of steam needed for the regeneration step is only a small fraction of the total amount of steam that could be created from all of the waste gas heat, there would be a large amount of excess steam left over. This excess steam can be used in a separate steam turbine to generate electricity in a similar fashion to that of a combined cycle power plant. With this option, the parasitic load on the system would be eliminated in addition to eliminating the cost of purchasing steam for the regeneration cycle. The annual cost of water would increase significantly due to having to purchase extra water to create the steam; however, this is counterbalanced by now having electricity as a useful end product. The third column in Table 13 list the new operating costs associated with the fiber system if all of the energy from waste stream combustion is used to create steam, with the excess steam being used to generate electricity for profit. The negative sign present in product electricity cost and total annual operating cost columns indicates an annual net profit instead of a net cost. In other words, heat integration has the potential to not only lower the operating cost, but create enough useful product that the profit gain is greater than the utilities cost.

A third option that was not explored in detail for heat integration would be to again use all of the heat from waste gas combustion to create steam, but instead of using the excess steam to create electricity as the end product, sell the steam directly as the end product. This option would eliminate the complication of having to integrate the gas turbine with the steam turbine and potentially be more profitable due to being able to sell the steam product directly instead of converting it to electricity first. However, this option may not be feasible unless there is a customer available who would be willing to purchase the steam.

3.3.3 Capital Cost of a Turbine

The capital cost of an 85 MW gas turbine was estimated to analyze the relative cost of implementing a fiber adsorbent system. A cost correlation was created using data available on the capital costs of four turbines of various capacities[18]. As shown in Figure 23, a curve was fitted to the data, and the cost for an 85 MW turbine was extrapolated to be $945/kW. The capital cost of the turbine was then estimated to be approximately $89.54 million.

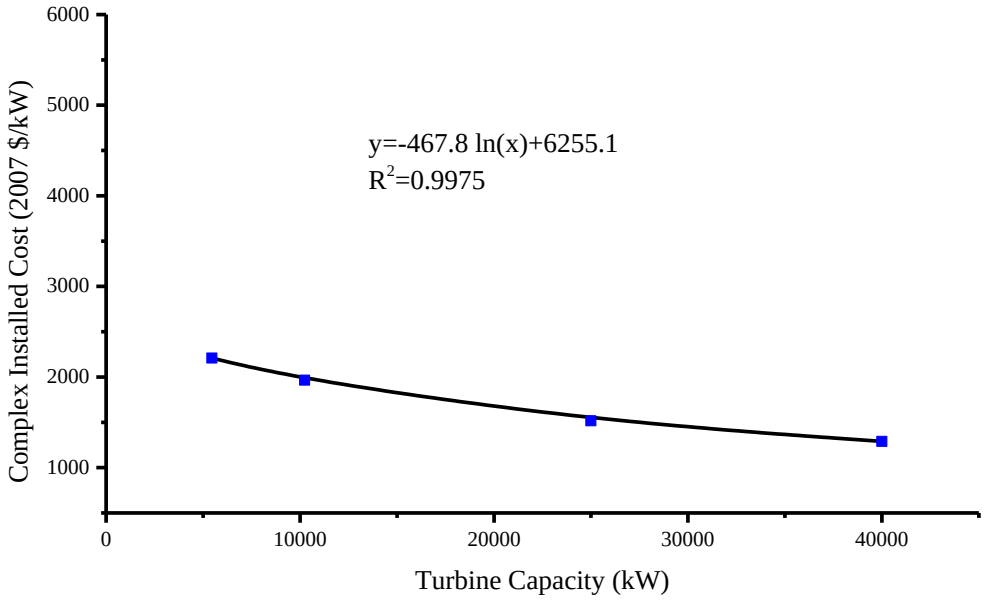

Figure 23: Correlation between capital cost of a gas turbine and turbine capacity. The blue squares represent actual data points while the black curve is an empirical fit to the data used to extrapolate the capital cost of the 85 MW turbine used as the basis of this study.

3.3.4 Cost and Savings by Removing TBM

The cost per million Btu can be estimated to determine the economic feasibility of implementing such a fiber sorbent system. First a yearly cost of the system is estimated,

taking into account both the total capital investment over the lifetime of the fiber adsorbent system (assumed to be 5 years) and the annual operating cost. This yearly cost is converted to cost per MMBtu by taking into account the flow rate of natural gas through a single turbine. It was found that implementing the fiber module adsorber system would cost about $0.03 per MMBtu without heat integration and $0.02 per MMBtu with heat integration, while implementing the pellet bed adsorber system without heat integration would cost about $0.08 per MMBtu. Additionally, not considering turbine or fiber system lifetimes, the capital cost of the fiber sorbent system was found to be about 1% of the capital cost of the 85 MW turbine, which is not prohibitively high (see Appendix B for calculations). Figure 24 illustrates the comparative cost of the fiber sorbent system versus the turbine as a function of original turbine lifetime without the adsorption system.

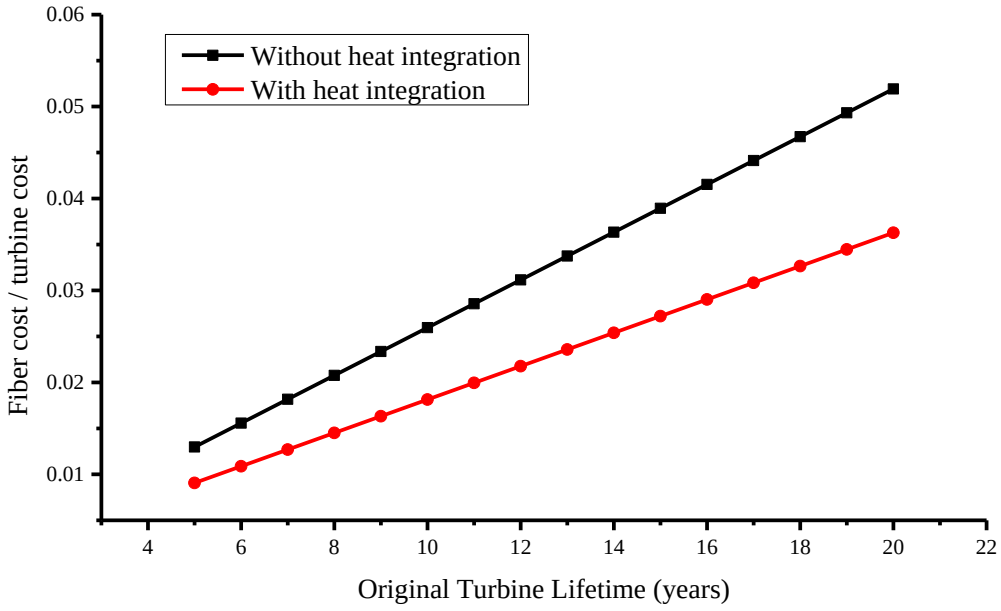

Figure 24: Ratio of the cost of the fiber sorbent system to the cost of an 85 MW turbine as a function of original turbine lifetime with and without heat integration. The heat integration option shown here is a "best case scenario" encompassing using all of the waste gas combustion heat for steam generation and using the excess steam to create electricity for profit. As the original turbine lifetime decreases, the cost of the fiber sorbent also decreases, as it will be balanced by the savings of increasing the turbine life. As the total fiber system cost is lower for a system with heat integration than without, the cost ratio is accordingly lower for the heat integrated system.

In contrast, the potential savings incurred by implementing the TBM removal system can be significant, as shown in Figure 25. The top graph shows the potential savings without heat integration while the bottom graph shows the potential savings with the more cost effective of the two heat integration methods considered. Savings are greatest when the original turbine lifetime (without implementing the TBM removal system) is short and the life extension with TBM removal system implementation is long. Without heat integration, the "worst case scenario" with an original turbine lifetime of 20 years and a life extension of only 1 year with fiber system implementation, the fiber system is not viable due to costing more than it will save. However, all other scenarios without heat integration show savings ranging from about $3,000 to $8,722,000 per year. With heat integration, the same "worst case scenario" would still have a savings of about $51,000 per year with system implementation. Then, over 20 years, the total amount saved would be $1.02 million. All other scenarios with heat integration show savings ranging from about $73,000 to $8,792,000 per year. While the fiber adsorbent system both with and without heat integration can offer significant savings on the cost of the gas turbine by extending its lifetime, it is clear that heat integration will offer greater savings in all scenarios and is a practical way to lower the environmental impact of the system.

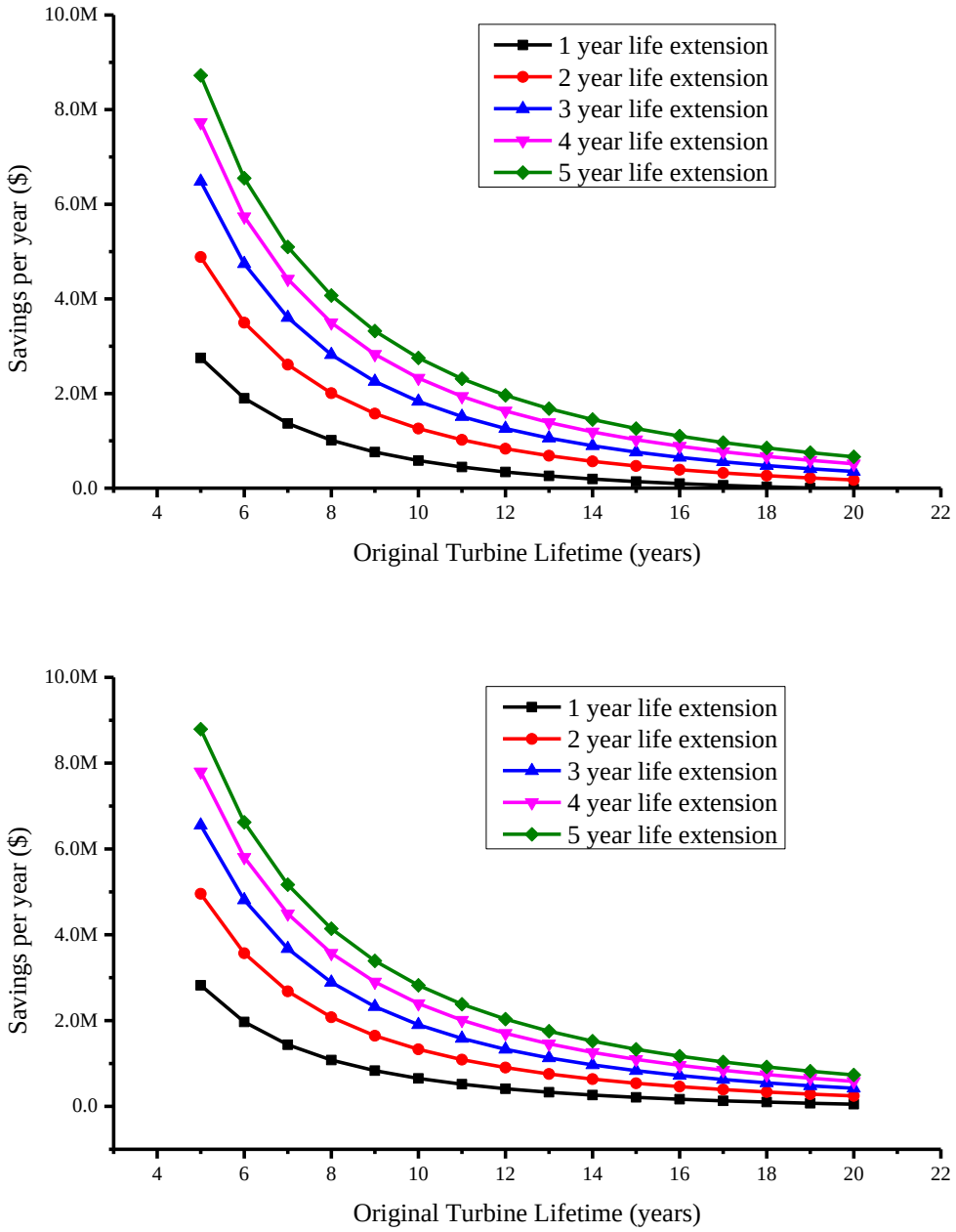

Figure 25: Potential savings per year by implementing the fiber sorbent system as a function of original turbine lifetime and length of turbine life extension. The top graph shows the savings without heat integration while the bottom graph shows the savings with heat integration. Savings per year are greatest when the original turbine lifetime is low and life extension with system implementation is high, and savings are greater with heat integration than without.

In summary, the capital cost of the fiber adsorbent system using product gas as the regeneration media is about $857,000, which is small compared with the $2,792,000 capital cost of a traditional pellet packed bed adsorbent system designed to process the equivalent amount of natural gas feed. It is also significantly smaller than the capital cost of the 85 MW gas turbine, which was estimated to be close to $90 million. Product gas was chosen as the regeneration media because of its low cost, simplicity, and safety. The capital cost estimates take into account the major equipment items in each system, sizing, materials of construction, and high pressure requirements, as well as other direct and indirect costs.

The highest possible operating cost that can be associated with such an adsorbent system using product gas as the regeneration media without heat integration is about $61,000 per year for the fibers and $211,000 per year for the pellet packed bed. However, these operating costs can be significantly lowered when heat integration options using the heat generated from waste gas combustion to create steam are considered. This extra steam can be used directly in the regeneration cycle to heat the product gas such that the steam required will not have to be purchased. With this kind of heat integration, the operating cost of the fiber sorbent system can be lowered to about $56,000 per year. If the extra steam is also used to power a steam turbine to generate electricity as a product in addition to heating the product gas, the profit becomes greater than the cost and the system earns about $9,000 per year. The operating cost estimates take into account the utilities such as steam, water, and electricity required to continuously run the system.

Compared with the cost of replacing the turbine due to corrosion associated with sulfur odorants in natural gas, the combined capital and operating costs of the fiber sorbent system are low enough to offer an attractive method of removing the odorant to increase turbine lifetime and save money. The fiber sorbent system is also requires less space and is economically advantageous to that of an equivalent pellet packed bed system.

3.4 References

1. *7EA Heavy Duty Gas Turbine*, 2013, General Electric Company.
2. Lively, R.P., *Hollow fiber sorbents for post-combustion CO_2 capture*. 2011, Georgia Institute of Technology: Atlanta, Ga.
3. Bhandari, D.A., *Hollow fiber sorbents for the desulfurization of pipeline natural gas*. 2010, Georgia Institute of Technology: Atlanta, Ga.
4. Welty, J.R., *Fundamentals of momentum, heat, and mass transfer*. 5th ed. ed. 2008, Wiley: Hoboken, N.J. ;.
5. Feng, X.S., et al., *Hollow-fiber-based adsorbers for gas separation by pressure-swing adsorption.* Aiche Journal, 1998. **44**(7): p. 1555-1562.
6. Asimakopoulou, A. and A. Karabelas, *A study of mass transfer in hollow-fiber membrane contactors—The effect of fiber packing fraction.* Journal of membrane science, 2006. **282**(1): p. 430-441.
7. Chiang, H.-L., et al., *Diffusion of hydrogen sulfide and methyl mercaptan onto microporous alkaline activated carbon.* Chemosphere, 2000. **41**(8): p. 1227-1232.
8. Patton, A., B.D. Crittenden, and S.P. Perera, *Use of the linear driving force approximation to guide the design of monolithic adsorbents.* Chemical Engineering Research & Design, 2004. **82**(A8): p. 999-1009.
9. Incropera, F.P., *Fundamentals of heat and mass transfer*. 5th ed. ed, ed. D.P. DeWitt. 2002, J. Wiley: New York.
10. Hines, A.L., *Mass transfer : fundamentals and applications*. Prentice-Hall international series in the physical and chemical engineering sciences, ed. R.N. Maddox. 1985, Prentice-Hall: Englewood Cliffs, N.J.
11. Clausse, M., J. Bonjour, and F. Meunier, *Influence of the presence of CO2 in the feed of an indirect heating TSA process for VOC removal.* Adsorption-Journal of the International Adsorption Society, 2003. **9**(1): p. 77-85.

12. Merel, J., M. Clausse, and F. Meunier, *Carbon dioxide capture by indirect thermal swing adsorption using 13X zeolite.* Environmental Progress, 2006. **25**(4): p. 327-333.
13. Satokawa, S., et al., *Adsorptive Removal of t-Butanethiol Using Metal Ion-exchange Y Type Zeolite under Ambient Conditions.* Journal of the Japan Petroleum Institute, 2010. **53**(2): p. 83-87.
14. Tedder, D.W., *Preliminary chemical process design and economics*. 2005, ill. ;: xxii, 396.
15. *About Natural Gas: Consumer Information*, 2013, American Gas Association.
16. Peters, M.S., *Plant design and economics for chemical engineers*. 4th ed. ed. McGraw-Hill chemical engineering series, ed. K.D. Timmerhaus. 1991, McGraw-Hill: New York.
17. Realff, M.J., *Personal communication*, 2013.
18. *Technology Characterization: Gas Turbines*, 2008, Energy and Environmental Analysis: Arlington, VA.

CHAPTER 4

CONCLUSIONS AND RECOMMENDATIONS

4.1 Summary and Conclusions

Chapter 1 of this thesis discusses need for sulfur odorant removal from pipeline grade natural gas for turbine lifetime extension. Odorants in natural gas, added for safety reasons, combust inside gas turbines to form corrosive products that destroy turbine blades, vanes, and other components. This corrosion leads to a decreased turbine efficiency and lifetime, so there is a desire to remove the sulfur components to prevent corrosion. The goal of this project was to assess the feasibility of using a novel fiber sorbent for t-butyl mercaptan removal from pipeline natural gas, and compare this technology to that of a traditional pellet packed bed adsorber.

Chapter 2 discusses the fiber sorbent concept and their potential advantages over pellet packed beds in terms of reduced pressure drop and increase mass transfer. Three regions of transport associated with the fiber sorbent were identified, as well as each region's mass transfer resistance and impact on sorption kinetics and the shape of breakthrough curves. Some key equations guiding the design, optimization, and feasibility assessment of the fiber sorbent system versus the pellet packed bed system were presented here. Fiber module design considerations were also discussed and the tunable variables and their upper and lower limits identified. Additionally, gas flow configuration, sorbent regeneration options, and economic and spatial considerations were also briefly touched upon.

Chapter 3 discusses the results of the fiber sorbent system design, optimization, economic analysis, and comparison to the fixed bed. The final parameters of the system design and its envisioned incorporation into a power plant were presented. The results of pressure drop and mass transfer calculations on the fiber sorbent system were compared with those calculated for an equivalently designed pellet packed bed system. Additionally, for both fiber and pellet bed designs, the amounts of regeneration and cooling gases, as well as the step times for each of the three cycles (adsorption, regeneration, and cooling) were calculated and presented here. Finally, an economic analysis was performed on the two systems to compare their relative capital and operating costs. A capital cost was then estimated for an 85 MW turbine (used as the basis for these designs) so that the costs and savings of adding in the fiber sorbent system could be quantified.

In conclusion, a fiber adsorbent system was designed to remove the odorant t-butyl mercaptan from pipeline grade natural gas for the purpose of delaying or preventing corrosion in gas turbines. The system was found to be economically feasible in terms of its relatively low capital and operating cost, low spatial requirement, and its potential to provide significant savings by increasing the normal lifetime and efficiency of the turbine.

This novel fiber adsorbent system was compared to a traditional pellet packed bed adsorber system, which suffers from high pressure drop and low mass transfer rate. It was found that the fiber module configuration could offer significantly greater mass transfer with the same amount of sorbent. To reconcile this difference, the pellet packed bed system was matched with the fiber sorbent system on mass transfer rate (more limiting than pressure drop in this case) while keeping the general bed dimensions the same. It was found that about six times more pellet beds are needed than fiber beds for treating the same amount of natural gas. This translates to six times more space and raw material needed than the fiber bed system. This is reflected in the higher capital and operating cost for the pellet beds than the fiber beds. Therefore, the fiber sorbent system has the potential to provide a low cost and spatially efficient alternative to a traditional pellet packed bed system.

4.2 Recommendations and Future Directions

More research in this area is still needed before such a fiber sorbent system can be fabricated and implemented into existing power plants. Some recommendations for future work are detailed below.

4.2.1 Experimental Work to Validate Fiber Sorbent System Design

A major flaw in this project is the absence of experimental data to validate some of the figures and numbers presented in the system design. The next step in this work would be to conduct breakthrough and pressure drop experiments on both fiber and pellet sorbents to verify that the values reported here using design equations and mass balances are valid.

4.2.2 New Materials for Selective Adsorption of Sulfur Compounds

Another major area for further exploration is that of new materials for the adsorption of sulfur-containing odorant compounds. The development of new water-stable materials with a high capacity for sulfur is highly desired due to the likely presence of small amounts of water in pipeline natural gas. Zeolite 13X, the material chosen for this work, is a standard because of its high capacity and commercial availability, but its hydrophilicity makes it difficult to work with outside of very dry environments. Even trace amounts of water present in the atmosphere could significantly (though not irreversibly) hinder its capacity.

Another aspect of new material development is its selectivity. Not only must a material for such an application be water-stable and have a high / competitive capacity, but it also must be selective towards the odorant. Both CO_2 and methane are present in significant quantities in pipeline natural gas, and have a potential to co-adsorb onto the sorbent, therefore decreasing the number of adsorption sites available to the odorant. MOFs may be considered in this portion of future work.

APPENDIX A

SYSTEM DESIGN EXAMPLE CALCULATIONS

A.1 System Design Basis and Assumptions

In order to assess the feasibility of using fiber sorbents to remove odorants from pipeline grade natural gas (NG), design calculations were performed to optimize such a system and give some rough estimates about its performance in comparison to a pellet packed bed system. This design assumes a dehydrated natural gas feed containing methane and the typical upper limit of 10 ppmv of t-butyl mercaptan (TBM) as the odorant. Other impurities commonly present in the natural gas were not considered for this study. Zeolite 13X was selected as the model adsorbent due to its high sorption capacity for mercaptans, its commercial availability, and its ease of incorporation into both fibers and pellets[1, 2]. A parallel flow configuration was chosen for the system. In terms of capacity / scaling, the sorbent system was considered on both a per turbine and a per power plant basis. For the turbine basis, specifications provided by General Electric for their 7EA heavy duty gas turbine were used. This turbine has a thermal efficiency of 32.7% for a simple cycle and requires an input of approximately 15,000 SCFM of natural gas with an output of approximately 85 MW[3]. This gas requirement is easily verified:

$$85MW \times \frac{1MW}{0.327} \times \frac{1000kW}{1MW} \times \frac{1hr}{60\,\text{min}} \times \frac{9.486 \times 10^{-4} Btu}{2.78 \times 10^{-7} kWh} \times \frac{1SCF}{1000Btu} \approx 15,000SFCM \qquad (1.30)$$

For the power plant basis, a single 840 MW power unit such as the one located at Plant McDonough-Atkinson in Smyrna, GA was considered. The flow rate requirement for the 7EA turbine is taken as the basis for the amount of natural gas that must be treated by a sorbent system.

A.2 Natural Gas Specifications

The inlet natural gas conditions are taken to be at T_0=30°C or 303.15K and P_0=250 psig or 18.01 atm. The molecular weight of natural gas is taken to be 17.14 g/mol, the weighted average of the various components listed in Chapter 1. At these conditions, using the EES software, the density and specific heat capacity of the natural gas is approximately ρ_{NG}=12.42 kg/m^3 and C_p=2226 J/kg-K respectively.

The actual natural gas flow rate (CFM) was calculated by converting the standard temperature and pressure flow rate (SFCM) to the actual temperature and pressure conditions.

$$\dot{V}_{NG,actual} = \dot{V}_{NG,standard} \times \left(\frac{P_{standard}}{P_{actual}} \right) \times \left(\frac{T_{actual}}{T_{standard}} \right) \tag{1.31}$$

$$\dot{V}_{NG,actual} = 15,000 \frac{STP\ ft^3}{min} \times \left(\frac{14.696\ psi}{264.7\ psi} \right) \times \left(\frac{303 K}{273.15 K} \right) = 923.8 CFM$$

Converting this value to metric units:

$$\dot{V}_{NG,actual} = 923.8 \frac{ft^3\ NG}{min} \times \left(\frac{60\ min}{1 hour} \right) \times \left(\frac{1 m^3}{35.315\ ft^3} \right) \approx 1570 \frac{m^3 NG}{hr}$$

The concentration of TBM is taken to be 10 ppm by volume. For 1 square meter of natural gas, the volume of TBM is 10x10^{-6}m^3. The ideal gas law is used to convert this volume to the moles and weight of TBM in 1 square meter of NG at pipeline conditions (at temperature 30°C and pressure 250 psig):

$$n_{TBM} = \frac{PV_{10\ ppm}}{RT} \tag{1.32}$$

$$n_{TBM} = \frac{\left(1.8 \times 10^6\ Pa\right) \times \left(10 \times 10^{-6} m^3\right)}{\left(8.314 \frac{m^3 Pa}{K\ mol}\right) \times \left(303 K\right)} = 0.00715 moles TBM\ in 1 m^3\ NG$$

Converting to moles to mass:

$$m_{TBM} = n_{TBM} MW_{TBM} = 0.00715 moles \times \left(90.19 \frac{g}{mol} \right) = 0.643 grams TBM in 1 m^3 NG$$

Therefore, the concentration of TBM in natural gas is:

$$c_{TBM} = 0.643 \frac{g\,TBM}{m^3\,NG}$$

Now to get the total mass and molar flow rates of TBM:

$$\dot{m}_{TBM,tot} = \dot{V}_{NG,actual} \times c_{TBM} = 1570 \frac{m^3 NG}{hr} \times 0.643 \frac{g\,TBM}{m^3\,NG} = 1.01 \frac{kg}{hr} TBM \tag{1.33}$$

$$\dot{n}_{TBM,tot} = \frac{\dot{m}_{TBM}}{MW_{TBM}} = \frac{1.01 \frac{kg}{hr} TBM}{90.19 \frac{kg}{kmole} TBM} = 11.2 \frac{moles}{hr} TBM \tag{1.34}$$

A.3 Fiber Sorbent Module Design

The dimensions of the fiber sorbent module were first fixed at reasonably achievable values, and physical parameters such as pressure drop and mass transfer coefficients were calculated based on these set dimensions. The desired values of the physical parameters as well as real physical limits drive the optimization of the fiber sorbent module dimensions. For example, several optimization points include: low pressure drop through the module, high mass transfer coefficients, low temperature rise of fibers due to sorption, and using as few modules as possible. Real physical limits include those listed in Table 3. One end result of this optimization process is presented here, with each of the optimization points and reality check calculations described in detail in later sections.

Module Dimensions

First, the dimensions of the module are set at reasonable values of:

Module length, L_m = 1.4 meters

Module diameter, d_m = 0.4 meters

As mentioned in Section 2.5.3, the module was chosen to be cylindrical in shape with the fibers bundled parallel to the module. The cross-sectional area of module is then:

$$A_m = \frac{\pi}{4} \times (d_m)^2 = \frac{\pi}{4} \times (0.4m)^2 = 0.126m^2 \tag{1.35}$$

Assuming 3 modules are to be used in the adsorption phase ($N_{m,ads}$ = 3), the superficial velocity through one module can be calculated as:

$$v_s = \frac{\dot{V}_{NG,actual}}{A_m \times N_{m,ads}} = \frac{1570 \frac{m^3}{hr}}{0.126m^2 \times 3} = 4{,}153 \frac{m}{hr} = 1.15 \frac{m}{s} \tag{1.36}$$

Setting the void fraction in the module as ε_m=0.35, the interstitial velocity through one module can be calculated from the superficial velocity:

$$v_i = \frac{v_s}{\varepsilon_m} = \frac{1.15m/s}{0.35} = 3.30 \frac{m}{s} \tag{1.37}$$

The volume of this module is:

$$V_m = \frac{\pi}{4} \times (d_m)^2 \times L_m = \frac{\pi}{4} \times (0.4m)^2 \times 1.4m = 0.176m^3 \tag{1.38}$$

And the volume occupied by fibers in one module is:

$$V_{fm} = (1 - \varepsilon_m) \times V_m = (1 - 0.35) \times 0.176 = 0.114m^3 \tag{1.39}$$

Fiber Dimensions

Next, the dimensions of the fibers are set at reasonably achievable values of:

Fiber length = module length, L_f = 1.4 meters

Fiber diameter, d_f = 300μm

Fiber porosity, ε_f = 0.25

With these dimensions, assuming cylindrical fibers, the volume of one fiber is:

$$V_{fo} = \frac{\pi}{4} \times (d_f)^2 \times L_f = \frac{\pi}{4} \times (0.0003m)^2 \times 1.4m = 9.9 \times 10^{-8} m^3 \quad (1.40)$$

The number of fibers in one module can then be calculated:

$$N_{fm} = \frac{V_{fm}}{V_{fo}} = \frac{0.114m^3}{9.9 \times 10^{-8} m^3} = 1{,}155{,}556\ fibers \quad (1.41)$$

With the total number of fibers for the whole system being simply this N_{fm} multiplied by the total number of modules ($N_{m,tot}$) used in the whole system:

$$N_{f,tot} = N_{fm} \times N_{m,tot} \quad (1.42)$$

A.4 Material Requirements

A fiber sorbent consists of sorbent crystals suspended within a polymer matrix. In this study, zeolite 13X and cellulose acetate are used as the sorbent and polymer respectively. Assuming a zeolite loading in the fiber of 75 wt. % and knowing the densities of zeolite 13X and cellulose acetate, the volume fraction of each material in the fiber can be calculated:

Weight fraction of zeolite 13X, w_{13X} = 0.75

Weight fraction of cellulose acetate, w_{CA} = (1 - w_{13X}) = 0.25

Density of cellulose acetate polymer, ρ_{CA} = 1300 kg/m^3

Density of zeolite 13X, ρ_{13X} = 1600 kg/m^3

Volume fraction of zeolite 13X:

$$\varphi_{13X} = \frac{\left(\frac{w_{13X}}{\rho_{13X}}\right) \times \left(1 - \varepsilon_f\right)}{\left(\frac{w_{13X}}{\rho_{13X}}\right) + \left(\frac{w_{CA}}{\rho_{CA}}\right)} = \frac{\left(\frac{0.75}{1600kg/m^3}\right) \times (1 - 0.25)}{\left(\frac{0.75}{1600kg/m^3}\right) + \left(\frac{0.25}{1300kg/m^3}\right)} = 0.53 \quad (1.43)$$

Volume fraction of cellulose acetate polymer:

$$\varphi_{CA} = \frac{\left(\frac{w_{CA}}{\rho_{CA}}\right)\times\left(1-\varepsilon_f\right)}{\left(\frac{w_{13X}}{\rho_{13X}}\right)+\left(\frac{w_{CA}}{\rho_{CA}}\right)} = \frac{\left(\frac{0.25}{1300kg/m^3}\right)\times\left(1-0.25\right)}{\left(\frac{0.75}{1600kg/m^3}\right)+\left(\frac{0.25}{1300kg/m^3}\right)} = 0.22 \tag{1.44}$$

From these material volume fractions and the porosity of the fiber, the fiber density can be calculated from:

$$\rho_f = \rho_{13X}\varphi_{13X} + \rho_{CA}\varphi_{CA} + \rho_{void}\varphi_{void} \tag{1.45}$$

$$\rho_f = 1600\frac{kg}{m^3}\times 0.53 + 1300\frac{kg}{m^3}\times 0.22 + 0\frac{kg}{m^3}\times 0.25 = 1134.6\frac{kg}{m^3}$$

Using the previous dimensions / specifications, the volume amount of 13X and cellulose acetate needed for the adsorption phase can be calculated:

$$V_{13X,ads} = V_{fo}\varphi_{13X}N_{fm}N_{m,ads} = 9.9\times10^{-8}m^3\times 0.53\times 1{,}155{,}556\times 3 = 0.182m^3 \tag{1.46}$$

$$V_{CA,ads} = V_{fo}\varphi_{CA}N_{fm}N_{m,ads} = 9.9\times10^{-8}m^3\times 0.22\times 1{,}155{,}556\times 3 = 0.076m^3 \tag{1.47}$$

These can be converted to mass amounts needed for the adsorption phase:

$$m_{13X,ads} = \rho_{13X,ads}V_{13X,ads} = 1600\frac{kg}{m^3}\times 0.182m^3 = 291.2kg \tag{1.48}$$

$$m_{CA,ads} = \rho_{CA}V_{CA,ads} = 1300\frac{kg}{m^3}\times 0.076m^3 = 98.8kg \tag{1.49}$$

The mass amount of fiber needed for the adsorption phase is calculated using the loading of 13X into the fiber:

$$m_{fiber,ads} = \frac{m_{13X,ads}}{w_{13X}} = \frac{291.2\,kg\,13X}{0.75} = 388.3kg \tag{1.50}$$

This can be converted to a volume amount using the fiber density:

$$V_{fiber,ads} = \frac{m_{fiber,ads}}{\rho_{fiber}} = \frac{388.3 kg\ fiber}{1134.6 \frac{kg}{m^3}\ fiber} = 0.342 m^3 \quad (1.51)$$

These mass and volume amounts can also be given on a per module basis by dividing the amount by the number of modules needed for the adsorption phase. An example for the mass of 13X:

$$m_{13X,\mathrm{m}} = \frac{m_{13X,ads}}{N_{m,ads}} = \frac{291.2 kg}{3} = 97.1 kg \quad (1.52)$$

A.5 Pressure Drop Considerations for Fiber and Pellet Beds

As mentioned in previous chapters, a low pressure drop is desired for adsorber beds such that the high pressure of the incoming natural gas feed can be maintained and excess recompression of the product stream will not be required. The pressure drop is considerably lower in a fiber module than in a packed bed, and is calculated using different equations for each.

A.5.1 Fiber Module Adsorber

Because there is no consensus currently in the literature on a single equation to estimate pressure drop across a fiber module such as the one used in this study, two approximations were used and are discussed here.

As a first approximation for pressure drop across the fiber module, a center channel analysis was used. The fibers are first assumed to be perfectly spaced and packed in the pattern shown in Figure 26.

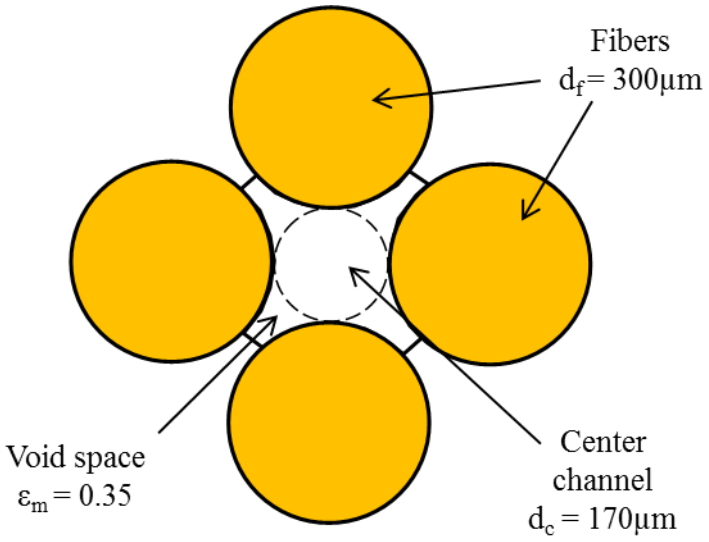

Figure 26: Fiber arrangement for center channel analysis of pressure drop. The fibers shown here are 300 microns in diameter and packed in this 4-fiber pattern. A "center channel" of void space then exists between the four fibers that is 170 microns in diameter at a module void fraction of 0.35.

With such a packing pattern, there will be a center channel of void space, itself with a well-defined diameter. Assuming the fiber diameter is fixed, moving the fibers closer or farther apart from each other will decrease or increase the total void space in the module respectively. This in turn will either decrease or increase the diameter of this hypothetical center channel, as shown in Table 14.

Table 14: Relationship between module void fraction and the diameter of the center channel of void space in between the fibers for a fixed fiber diameter. The diameter of the center channel was measured directly from images made in AutoCad. The numbers for the module void fraction were obtained by using Image J software to calculate the area of the void space in between the fibers in comparison to the total area occupied.

Module void fraction	Center channel diameter (µm)
0.21	124
0.36	170
0.41	191
0.56	267
0.66	340
0.71	405

Finally, the Hagen-Poiseuille equation for calculating pressure drop in a fluid flowing in the laminar region (Re < 2100) down a long cylindrical pipe was applied to the center channel[4]. That is, the center channel with its theoretical diameter of 170 μm (for 300 μm diameter fibers spaced with 0.35 void) was considered as the cylindrical pipe. With this consideration, the pressure drop per unit length was estimated as:

$$\frac{\Delta P}{L_m} = \frac{32\mu_{NG}v_i}{d_c^{\,2}} = \frac{32\times\left(1.67\times10^{-5}\,Pa\cdot s\right)\times\left(3.30\,m/s\right)}{(0.00017m)^2} = 61021\frac{Pa}{m} = 0.60\frac{atm}{m} \qquad (1.53)$$

With a fiber / module length of 1.4 meters, the total pressure drop across the module using this approximation is:

$$\Delta P = 0.60\frac{atm}{m}\times 1.4m = 0.84atm \qquad (1.54)$$

The second pressure drop estimate uses a modified form of the Hagen-Poiseuille equation, and should provide a more exact solution or at least a place an upper bound on the pressure drop. With this approximation, each fiber is envisioned to be evenly spaced and surrounded by a hypothetical annual void space of a particular radius (determined by the specifications of the fibers and module) as shown in Figure 27.

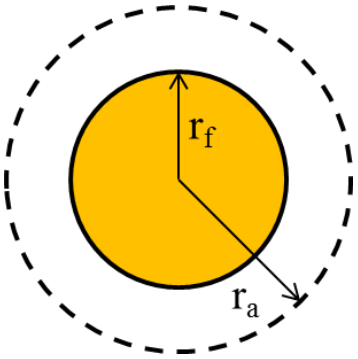

Figure 27: Schematic showing the hypothetical annular void space around each fiber of radius r_a.

The radius r_a of this annular space can be calculated using the specifications of the design, assuming the fibers are evenly spaced such that the void space of the module is evenly distributed between all fibers[5]:

$$r_a = \sqrt{\frac{A_m}{\pi N_{fm}}} = \sqrt{\frac{0.126 m^2}{\pi \times 1{,}155{,}556}} = 1.86 \times 10^{-4} m = 186 \mu m \tag{1.55}$$

Similar to the Hagen-Poiseuille equation, the Navier-Stokes equation in cylindrical coordinates can be solved using the same assumptions of steady-state, fully developed flow with only axial velocity components[6]. The only thing that changes is the symmetry boundary condition, which is taken at the center of the pipe in Hagen-Poiseuille, but is instead taken at r_a for this case. The same no-slip boundary condition is taken at the surface r_f of the fiber. The resulting equation is referred to as the modified Hagen-Poiseuille equation and also calculates pressure drop per unit length:

$$\frac{\Delta P}{L_m} = \frac{8 \mu_{NG} v_i}{2 r_a^{\,2} \ln r_a - 2 r_a^{\,2} \ln r_f - r_a^{\,2} + r_f^{\,2}} \tag{1.56}$$

$$\frac{\Delta P}{L_m} = \frac{8 \times \left(1.67 \times 10^{-5}\, Pa \cdot s\right) \times \left(3.30\, {}^{m}\!/\!_{s}\right)}{2(1.86 \times 10^{-4} m)^2 \ln(1.86 \times 10^{-4} m) - 2(1.86 \times 10^{-4} m)^2 \ln(1.5 \times 10^{-4} m) - (1.86 \times 10^{-4} m)^2 + (1.5 \times 10^{-4} m)^2}$$

$$\frac{\Delta P}{L_m} = 115440 \frac{Pa}{m} = 1.53 \frac{atm}{m}$$

With a fiber / module length of 1.4 meters, the total pressure drop across the module using this approximation is:

$$\Delta P = 1.53 \frac{atm}{m} \times 1.4 m = 2.15 atm \tag{1.57}$$

A.5.2 Packed Bed Adsorber

The pressure drop through a packed bed adsorption can be calculated with the well-known Ergun equation[4]. Keeping all parameters including superficial velocity the same as in the fiber module case (note that the superficial velocity of 1.16 m/s used here is equivalent to the interstitial velocity of 3.30 m/s used in equations (1.53) and (1.56) assuming the same bed void fraction of 0.35), the pressure drop per unit length for a typical 1 mm pellet is calculated as:

$$\frac{\Delta P}{L_m} = \left(\frac{1}{150} \frac{(1-\varepsilon_m)\mu_{NG}}{d_p v_s \rho_{NG}} + 1.75 \right) \times \left(\frac{1-\varepsilon_m}{\varepsilon_m{}^3} \right) \times \left(\frac{\rho_{NG} v_s^2}{d_p} \right) \tag{1.58}$$

$$\frac{\Delta P}{L_m} = \left(\frac{1}{150} \times \frac{(1-0.35) \times \left(1.67 \times 10^{-5}\, Pa \cdot s\right)}{(0.001m) \times \left(1.16\, {}^{m}\!/_{s}\right) \times \left(12.42\, {}^{kg}\!/_{m^3}\right)} + 1.75 \right) \times \left(\frac{1-0.35}{(0.35)^3} \right) \times \left(\frac{\left(1.67 \times 10^{-5}\, Pa \cdot s\right) \times \left(1.16\, {}^{m}\!/_{s}\right)^2}{0.001m} \right)$$

$$\frac{\Delta P}{L_m} = 439{,}580 \frac{Pa}{m} = 4.34 \frac{atm}{m}$$

Here, the pressure drop is a quadratic function of the gas velocity through the bed and therefore the pressure drop is about thrice as much as for the fiber modules. In order to decrease the pressure drop for a packed bed, the gas velocity should be kept low or the particle size increased, as shown in Figure 28.

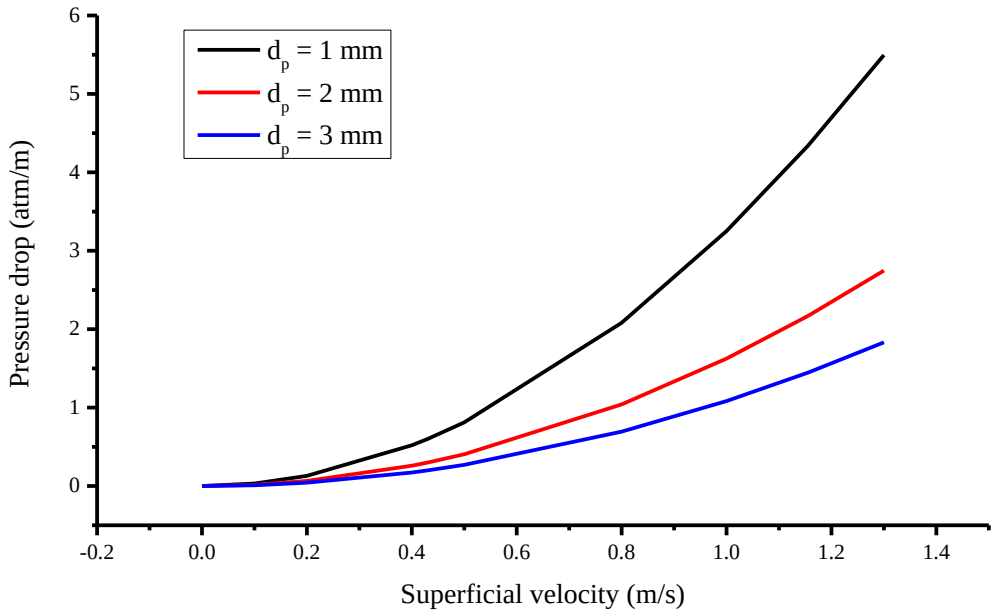

Figure 28: Pressure drop per unit length in pellet packed beds as a function of superficial velocity through the bed at various pellet diameters.

However, increasing the particle size will lead to greater mass transfer resistance, which is undesirable. Therefore, to compare fiber modules to pellet packed beds, the gas velocity was decreased for the packed bed case until the pressure drop matched that of the fiber module. Again, bed void fraction and natural gas density and viscosity were kept at the same values as for the fiber module case. The Goal Seek function in Excel was used on the Ergun equation to set the value of pressure drop to be either 0.60 atm/m (pressure drop for fibers using center channel analysis) or 1.53 atm/m (pressure drop for fibers using modified Hagen-Poiseuille) by changing the velocity. In this way, it was found that the interstitial velocity needed to keep the same pressure drop is 1.23 m/s or 1.96 m/s for the two fiber ΔP equations respectively. Then, from equations (1.36) and (1.37), the number of beds needed for the adsorption phase at these velocities can be back calculated. Using the center channel analysis approximation for fiber ΔP, the number of pellet packed beds needed is 5, and using the modified Hagen-Poiseuille for fiber ΔP, the

number of pellet packed beds needed is and 8. Figure 29 shows a comparison of the different pressure drops calculated from each method, as well as a pellet comparison.

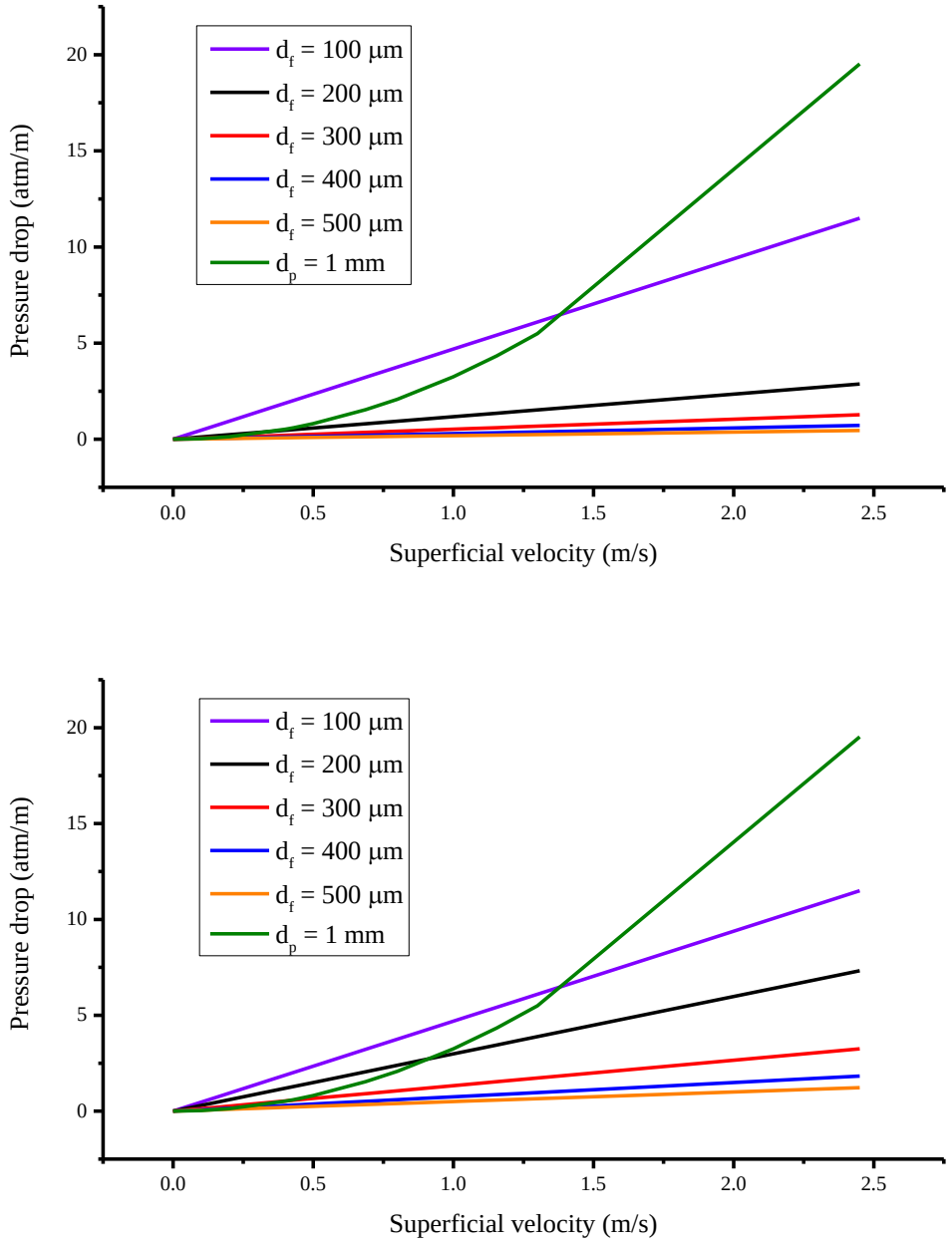

Figure 29: Pressure drop per unit length in fiber modules as a function of superficial velocity through the bed at various fiber diameters. The pressure drop in the top graph is calculated using the center channel analysis and the pressure drop in the bottom graph is calculated using the modified Hagen-Poiseulle equation. The pressure drop curve of a 1 mm pellet is overlaid over both plots for comparison purposes.

A.6 Mass Transfer Considerations

This section mainly deals with the determination of the mass transfer coefficients for each of the three regions mentioned in Chapter 2.

A.6.1 Residence Time

The residence time of gas flowing through a fiber module can be calculated from knowing the interstitial velocity and the length of the module:

$$t_{residence} = \frac{L_m}{v_i} = \frac{1.4m}{3.30\,m/s} = 0.42s \tag{1.59}$$

This is the average amount of time that a gas molecule will spend inside the module. The residence time must be long enough for heat and mass equilibration to happen. This will be checked in later sections.

A.6.2 Binary Diffusion Coefficient

$D_{TBM\text{-}CH4}$ is the molecular diffusivity, or diffusion coefficient, which can be estimated from the Chapman-Enskog equation for gaseous systems[7]. For a binary gas mixture such as the one between TBM and CH_4 (assumed to be the only two species in this design study):

$$D_{TBM-CH4} = \frac{1.858\times10^{-23}\times T^{\frac{3}{2}}}{P\sigma^2_{TBM-CH4}\Omega}\times\left(\frac{1}{MW_{TBM}}+\frac{1}{MW_{CH4}}\right)^{\frac{1}{2}} \tag{1.60}$$

Where MW_{TBM} and MW_{CH4} are the molecular weights, P is the total pressure in atmospheres, T is temperature in Kelvins, Ω is the temperature-dependent dimensionless

collision integral of order 1, and $\sigma_{TBM\text{-}CH4}$ is the average collision diameter, calculated as $\sigma_{TBM\text{-}CH4}=0.5(\sigma_{TBM}+\sigma_{CH4})$.

With the following specifications of M_{TBM} =90.19 g/mol, M_{CH4} =16.04 g/mol, σ_{CH4} =3.89 Å, $\sigma_{TBM} \approx 5.6$ Å, ($\sigma_{TBM\text{-}CH4}$ = 4.75 Å), T=303 K, P=18 atm, the diffusivity is:

$$D_{TBM-CH4} = \frac{1.858\times10^{-23}\times(303K)^{\frac{3}{2}}}{(18.01atm)\times\left(4.75\times10^{-10}m\right)^2\times(1.667)}\times\left(\frac{1}{90.19g/mol}+\frac{1}{16.04g/mol}\right)^{\frac{1}{2}} \approx 0.003\frac{cm^2}{s}$$

This diffusion coefficient is valid for the external film layer that surrounds a fiber or pellet. However, it must be modified to account for the sorbent and / or polymer when calculating the mass transfer inside of the fiber or pellet.

A.6.3 External Mass Transfer Coefficient (Film Layer)

Determination of the external mass transfer coefficient, k_{ext} is easiest using Sherwood correlations that accurately describe the situation of interest. The Sherwood number is first estimated from the correlation, and then the definition of Sherwood number is applied to find the external mass transfer coefficient using the following definition:

$$Sh \equiv \frac{d\cdot k_{ext}}{D} \tag{1.61}$$

The diffusion coefficient in this region is simply the binary diffusion coefficient as there are no hindrances in this external region. The gas molecules only interact with each other.

The dimensionless Schmidt number, present in the Sherwood correlations, is calculated below and applies to both fibers and pellets:

$$Sc = \frac{\mu_{NG}}{D_{TBM-CH4}\rho_{NG}} = \frac{1.67\times10^{-5}\ Pa\cdot s}{\left(3.0\times10^{-7}\ m^2/s\right)\times\left(12.42\frac{kg}{m^3}\right)} = 4.48 \quad (1.62)$$

Fiber module adsorber

First, the dimensionless Reynolds number must be calculated for the fiber sorbent module:

$$Re = \frac{d_f v_i \rho_{NG}}{\mu_{NG}} = \frac{(0.0003m)\times\left(3.30\frac{m}{s}\right)\times\left(12.42\frac{kg}{m^3}\right)}{1.67\times10^{-5}\ Pa\cdot s} = 736.28 \quad (1.63)$$

For flow outside and parallel to a bundle of fibers, the Sherwood number can be correlated from the Reynolds and Schmidt numbers as[5]:

$$Sh = 1.45\left[ReSc\frac{d_f}{L_b}\right]^{0.33} = 1.45\left[736.28\times4.48\times\frac{0.03cm}{140cm}\right]^{0.33} = 1.29 \quad (1.64)$$

Rearranging and solving equation (1.61) for the external mass transfer coefficient:

$$(k_{ext})_f = \frac{Sh\cdot D_{TBM-CH4}}{d_f} = \frac{1.29\times0.003\ cm^2/s}{0.03cm} = 0.129\frac{cm}{s} \quad (1.65)$$

Packed bed adsorber

Following the same steps as above for the pellet packed bed adsorber:

$$Re = \frac{d_p v_i \rho_{NG}}{\mu_{NG}} = \frac{(0.001m)\times\left(1.96\frac{m}{s}\right)\times\left(12.42\frac{kg}{m^3}\right)}{1.67\times10^{-5}\ Pa\cdot s} = 1457.68 \quad (1.66)$$

Using the Ranz-Marshall Sherwood correlation for external mass transfer coefficient in a packed-bed adsorber when axial dispersion is negligible and Schmidt number is less than 160[8]:

$$Sh = 2.0 + 0.6\,Re^{0.5}\,Sc^{0.33} = 2.0 + 0.6\times(1457.65)^{0.5}\times(4.48)^{0.33} = 39.58 \quad (1.67)$$

$$(k_{ext})_p = \frac{Sh \cdot D_{TBM-CH4}}{d_p} = \frac{39.58 \times 0.003 \, cm^2/s}{0.1 cm} = 1.187 \frac{cm}{s} \quad (1.68)$$

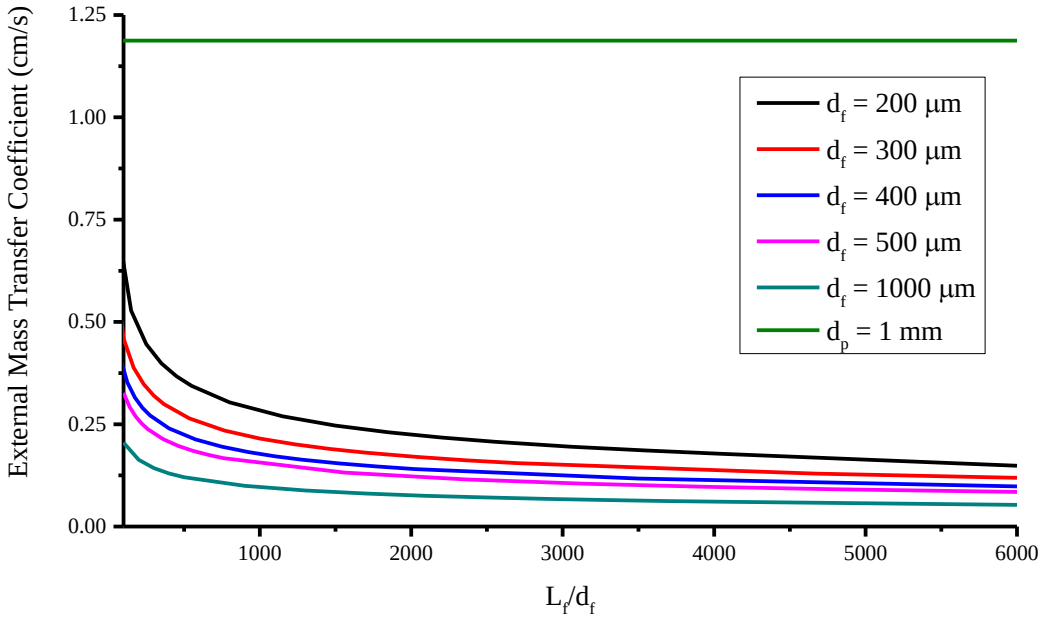

Figure 30: External mass transfer coefficient plotted as a function of the aspect ratio of the fibers for various fiber diameters. The external MTC of a 1 mm pellet is also shown for comparison purposes (no aspect ratio factor for the pellet).

A.6.4 Internal Mass Transfer Coefficient (Fiber or Pellet Layer)

As mentioned in Chapter 2, the diffusion of a gas through the meso and macropores of a fiber or pellet is hindered by the sorbent such that the effective diffusivity, D_e, is lower than the binary diffusion coefficient found in Section A.6.2. First, the mean free path of the molecules must be determined. An example of the mean free path of a TBM molecule at the feed temperature of 30°C is shown:

$$\lambda_{TBM} = \frac{k_B T}{\sqrt{2}\pi d_A^2 P} = \frac{\left(1.38 \times 10^{-23} \frac{m^2 kg}{s^2}\right) \times (303.15K)}{\sqrt{2}\pi \left(5.6 \times 10^{-10} m\right)^2 \times (1{,}825{,}042 Pa)} = 1.65 \times 10^{-9} m \quad (1.69)$$

Similarly, the mean free path can be calculated for the TBM molecule at the regeneration temperature of 120°C, and also for the methane molecules. These various mean free paths are shown in Table 15.

Table 15: Mean free path for TBM and methane molecules at feed and regeneration temperatures

Temperature	TBM Mean Free Path (m)	Methane Mean Free Path (m)
30°C	1.65×10^{-9}	3.39×10^{-9}
120°C	2.13×10^{-9}	4.40×10^{-9}

The average pore diameter of a fiber sorbent containing zeolite 13X ranges from 1 to 2 microns, with the most typical diameter being 1 micron, or 10^{-6} meters[9]. The mean free paths of both molecules at both temperatures are well below an order of magnitude below the pore radius, indicating that only molecular diffusion will be important in this region. That is, the collisions between diffusing molecules provide the main diffusional resistance to flow.

The effective diffusivity is then:

$$D_{eff} = \frac{\varepsilon_f D_{TBM-CH4}}{\tau} \approx \frac{0.25 \times 0.003 \frac{cm^2}{s}}{3} = 0.00025 \frac{cm^2}{s} \tag{1.70}$$

The tortuosity factor, τ, accounts for the effect of the random orientation of the pores and the variation in the pore diameter, and varies inversely with porosity. For straight, randomly oriented cylindrical pores, it was shown that $\tau = 3$, and experimental tortuosity factors generally fall within the range of 2-6[10]. For the purposes of this design study, the tortuosity factor is taken to be 3.

Fiber module adsorber

The shape factor (SF) for catalysts or adsorbers is generally defined as the volume of the sorbent over the surface area of the sorbent, such that for solid cylinders, the shape factor simplifies to r/2. However, for porous materials consisting of sorbent and inert

binder material, a new shape factor must be defined to account for both the porosity and how that affects the effective surface area, and the fact that the sorbent is only a fraction of the total fiber volume:

$$SF_f = \frac{\pi r_f{}^2 L_f \varphi_{13X}}{2\pi r_f L_f (1-\varepsilon_f)} = \frac{r_f \varphi_{13X}}{2(1-\varepsilon_f)} \tag{1.71}$$

Applying this shape factor to Liaw et al.'s method for internal mass transfer coefficient in a solid cylinder (long enough for end effects to be negligible)[11], we get:

$$(k_{int})_f = \frac{8D_{eff}}{r_f{}^2} \times \frac{r_f \varphi_{13X}}{2(1-\varepsilon_f)} = \frac{8\left(0.00025\frac{cm^2}{s}\right)}{(0.015cm)^2} \times \frac{0.015cm \times 0.53}{2(1-0.25)} = 0.047\frac{cm}{s} \tag{1.72}$$

Packed bed adsorber

Following the same steps as above for the pellet packed bed adsorber:

$$SF_p = \frac{\frac{4}{3}\pi r_p{}^3 \varphi_{13X}}{4\pi r_p{}^2 (1-\varepsilon_p)} = \frac{r_p \varphi_{13X}}{3(1-\varepsilon_p)} \tag{1.73}$$

Applying Glueckauf's equation for internal mass transfer coefficient in a spherical pellet for $D_{eff}t/R^2 > 0.1$, we get[11]:

$$(k_{int})_p = \frac{15D_{eff}}{r_p{}^2} \times \frac{r_p \varphi_{13X}}{3(1-\varepsilon_p)} = \frac{15\left(0.00025\frac{cm^2}{s}\right)}{(0.05cm)^2} \times \frac{0.05cm \times 0.53}{3(1-0.25)} = 0.018\frac{cm}{s} \tag{1.74}$$

Figure 31 shows the internal mass transfer coefficient for fibers as a function of fiber diameter, as well as the internal MTC of a 1 mm pellet for comparison (diameter unchanging). The effective diffusivity, 13X volume fraction, and internal porosity was held at the same values for both fibers and pellets for the purposes of this figure.

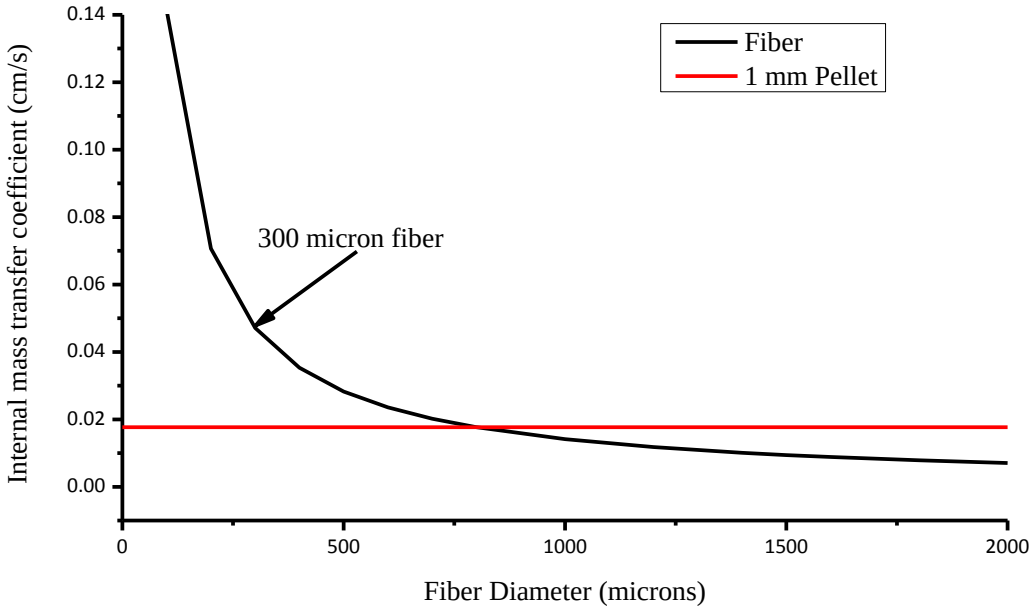

Figure 31: Internal mass transfer coefficient plotted as a function fiber diameter. The internal MTC of a 1 mm pellet is also shown for comparison purposes (no diameter change for the pellet).

A.6.5 Limiting Mass Transfer Resistance / Equilibration Time

To check if external or internal resistance is limiting, a Biot mass number can be calculated. The Biot mass number is used to estimate the ratio of external to internal mass transfer resistance as[12]:

$$Bi_m = \frac{(k_{ext})r}{D_{eff}} \tag{1.75}$$

Fiber module adsorber

For the fiber module adsorber, the Biot mass number is:

$$Bi_{m,f} = \frac{(k_{ext})_f r_f}{D_{eff}} = \frac{\left(0.129\frac{cm}{s}\right)\times\left(0.015cm\right)}{\left(0.00025\frac{cm^2}{s}\right)} = 7.74 \tag{1.76}$$

This Bi_m on the order of 1 indicates the relative importance of both external and internal mass transfer resistances. However, when $Bi_m>1$ as in this case, the internal meso/macropore mass transfer resistance is the limiting resistance.

With this known, it is desired to estimate the extent of mass equilibration in the fiber in this region. How much mass transfer will occur in the set residence time of the gas can be estimated for a fiber from Hines & Maddox Figure 4-15 for unsteady state mass transfer in an infinitely long cylinder[7]. The value of α is taken to be ∞ for constant surface concentration and the x-axis value of the figure can be derived with the residence time calculated above:

$$\sqrt{\frac{D_{eff}\,t_{res}}{(r_f)^2}} = \sqrt{\frac{\left(0.00025\frac{cm^2}{s}\right)\times\left(0.42s\right)}{(0.015cm)^2}} = 0.68 \qquad (1.77)$$

Reading off the value of M_t/M_∞ from the y-axis with this value for the x-axis then gives $M_t/M_\infty \approx 0.95$. That means the residence time of 0.42 seconds is enough for the fibers to reach 95% capacity, an acceptable value.

Packed bed adsorber

For the pellet packed bed adsorber, the Biot mass number is:

$$Bi_{m,p} = \frac{(k_{ext})_p\, r_p}{D_{eff}} = \frac{\left(1.187\frac{cm}{s}\right)\times\left(0.05cm\right)}{\left(0.00025\frac{cm^2}{s}\right)} = 237.4 \qquad (1.78)$$

As in the case of the fiber beds, $Bi_m>1$ here also, indicating that the internal meso/macropore mass transfer resistance is the limiting resistance.

Again, the extent of mass equilibration in a pellet in this region is estimated. How much mass transfer will occur in the set residence time of the gas can be estimated for a pellet from Hines & Maddox Figure 4-17 for unsteady state mass transfer in a sphere.

The value of α is taken to be ∞ again for constant surface concentration. As an initial comparison between fiber and pellet bed adsorbers, the pressure drop in the pellet bed was matched with that in the fiber bed (using the modified Hagen-Poiseuille equation) by changing the gas velocity through the pellet bed. In order to match the pressure drop of 1.53 atm/m, the interstitial velocity through a pellet bed of the same dimensions and porosity would have to be 1.96 m/s. With this velocity, the residence time through a 1.4 meter long bed is 0.71 seconds, and the x-axis value of the Hines & Maddox figure can be derived as:

$$\sqrt{\frac{D_{eff}\,t_{res}}{(r_p)^2}} = \sqrt{\frac{\left(0.00025\frac{cm^2}{s}\right)\times\left(0.71s\right)}{(0.05cm)^2}} = 0.27 \tag{1.79}$$

Reading off the value of M_t/M_∞ from the y-axis with this value for the x-axis then gives $M_t/M_\infty \approx 0.72$. That means the residence time of 0.71 seconds is only enough for the pellets to reach about 72% capacity, which is not optimal.

Redoing this analysis such that the same mass transfer equilibration of 95% can be reached in both fiber and pellet beds would mean setting M_t/M_∞ to be equal to 0.95 in Hines & Maddox Figure 4-17 and reading the y-axis value to be about 0.5. Rearranging to find the residence time (contact time) needed for this situation:

$$t_{residence,\,p} = \frac{\left(0.5\right)^2\times(r_p)^2}{D_{eff}} = \frac{\left(0.5\right)^2\times(0.05cm)^2}{\left(0.00025\frac{cm^2}{s}\right)} = 2.5seconds \tag{1.80}$$

This needed residence time translates to an interstitial velocity of 0.56 m/s in a 1.4 meter long bed, and a superficial velocity of 0.20 m/s for a bed void fraction of 0.35 from equations (1.59) and (1.37). Finally, to keep this velocity with the same bed dimensions, the number of pellet packed beds must be increased to about 18 beds for the adsorption step, from equation (1.36).

A.6.6 Internal Mass Transfer Coefficient (Sorbent 13X Crystals)

As mentioned previously, the internal mass transfer resistance in the sorbent crystals should be negligible compared to the internal meso/macropore resistance and the external film layer resistance. However, for completeness, this assumption will be checked here. The pore diameter of a zeolite 13X crystal is approximately 10 Angstroms, or 10^{-9} meters. The mean free paths of both TBM and methane molecules at both feed and regeneration temperatures are within an order of magnitude of this pore radius, indicating that diffusion through the zeolite pores are in the transition region. That is, collisions between diffusing molecules and with the sorbent wall are equally important and both will add to the diffusional resistance to flow. Assuming a 13X crystal diameter of 1 micron with a void fraction of 0.48, and a diffusivity in the sorbent $D_{TBM\text{-}13X}$ of $2.2*10^{-5}$ cm^2/s (the diffusivity of butane through 13X[13]), Glueckauf's equation for internal mass transfer coefficient in a sphere can again be used[11]:

$$(k_{int})_s = \frac{15 D_{TBM-13X}}{r_s^{\,2}} \times \frac{r_p \varphi_{13X}}{3(1-\varepsilon_s)} = \frac{15\left(2.2\times10^{-5}\,\frac{cm^2}{s}\right)}{(0.00005cm)^2} \times \frac{0.0001cm \times 0.52}{3(1-0.48)} = 4.4\frac{cm}{s} \qquad (1.81)$$

It can be seen that this internal micropore mass transfer coefficient is much higher than the external or internal macro/mesopore mass transfer coefficients, indicating that this region contributes insignificantly to the overall mass transfer resistance.

Another way to check this assumption of negligible sorbent mass transfer resistance is to calculate the time for the micropores to reach mass equilibration. From Hines & Maddox Figure 4-17 for unsteady mass transfer in a sphere, the value of α is taken to be ∞ for constant surface concentration and Mt/M∞ is taken to be 1.0 for a fully loaded crystal. From the figure, read:

$$0.75 = \sqrt{\frac{D_{TBM-13X}\,(t_{int})_{sorbent}}{(d_{13X}/2)^2}}$$

Rearranging this equation, the internal mass equilibration time can be extracted:

$$(t_{int})_{sorbent} = \frac{(0.75)^2 \times (d_{13X}/2)^2}{D_{TBM-13X}} = \frac{(0.75)^2 \times (0.0001cm/2)^2}{\left(2.2\times10^{-5}\,\frac{cm^2}{s}\right)} = 6.4\times10^{-5}\,seconds \qquad (1.82)$$

This is much shorter than the residence time of the gas in the module, indicating that there is more than enough time for mass equilibration to happen in the sorbent and it is indeed not the limiting resistance.

A.7 Heat Transfer Considerations

It is also important to make sure the fibers in this system are able to reach thermal equilibrium given the specifications stated previously. This can be done by estimating the minimum residence time needed for heat equilibration in the fiber during both the heating/desorption and cooling phases, and comparing that to the actual residence time of the heating or cooling media. First, some intrinsic properties of the fiber must be calculated.

Heat capacity of fiber:

$$C_{p,\ fiber} = C_{p,13X}\varphi_{13X} + C_{p,CA}\varphi_{CA} + C_{p,void}\varphi_{void} \qquad (1.83)$$

$$C_{p,\ fiber} = 800\frac{J}{kg\cdot K}\times0.532 + 1600\frac{J}{kg\cdot K}\times0.218 + 1000\frac{J}{kg\cdot K}\times0.25 = 1024.4\frac{J}{kg\cdot K}$$

Thermal conductivity of fiber:

$$\kappa_{fiber} = \kappa_{13X}\varphi_{13X} + \kappa_{CA}\varphi_{CA} + \kappa_{void}\varphi_{void} \qquad (1.84)$$

$$\kappa_{fiber} = 0.8\frac{W}{m\cdot K}\times0.532 + 0.5\frac{W}{m\cdot K}\times0.218 + 0.024\frac{W}{m\cdot K}\times0.25 = 0.54\frac{W}{m\cdot K}$$

Thermal diffusivity of fiber:

$$\alpha_{fiber} = \frac{\kappa_{fiber}}{\rho_{fiber} C_{p,\,fiber}} = \frac{\left(0.54 \frac{W}{m \cdot K}\right)}{\left(1134.6 \frac{kg}{m^3}\right) \times \left(1024.4 \frac{J}{kg \cdot K}\right)} = 4.65 \times 10^{-7} \frac{m^2}{s} \tag{1.85}$$

A.7.1 Thermal Equilibration Time for Heating Phase

For the heating phase, a hot regeneration gas (air, nitrogen, and product gas were considered for this study) was assumed to flow over the fibers at 120°C, heating the center of the fiber to at least 90°C. The time to reach thermal equilibrium can be calculated for a fiber from Figure 24 in for temperature distribution in a cylinder. In the figure, the value of r/α (radial position to cylinder radius) is taken to be 0 for temperature at the center of the cylinder and v/V (desired temperature to surface temperature) is taken to be 0.92 for a center to surface temperature ratio of 363K / 393K. The surface temperature is taken to be the same as the bulk hot air temperature since the surface of the fibers are in direct contact with the hot air. From the figure (κ is thermal diffusivity in the figure), read that the curve number should be approximately 0.5. The heat equilibration time (or minimum residence time needed) can then be extracted from this curve equation:

$$(t_{eq,heating})_f = \frac{0.5 \times (r_f)^2}{\alpha_{fiber}} = \frac{0.5 \times (150 \times 10^{-6} m)^2}{4.65 \times 10^{-7} \frac{m^2}{s}} = 0.02\, seconds \tag{1.86}$$

From equation (1.59), the residence time of the gas in the module is 0.42 seconds, which is more than enough time to reach thermal equilibrium.

A.7.2 Thermal Equilibration Time for Cooling Phase

For the cooling phase, a cool regeneration gas (only product gas was considered for this study) was assumed to flow over the fibers at 30°C, cooling the center of the fiber to at least 35°C. Figure 24 is again used to aid in this equilibrium check, with the value of r/α again taken to be 0 for temperature at the center of the cylinder. The desired temperature to surface temperature ratio v/V is taken to be 0.98 for a center to surface temperature ratio of 303K / 308K (notice the surface and center temperatures are actually flipped because heat is being transferred from the fibers to the treated natural gas, but the ratio should be the same). The surface temperature is taken to be the same as the treated natural gas temperature since the surface of the fibers are in direct contact with the treated natural gas. From the figure, read that the curve number should be approximately 0.8. The heat equilibration time can then be extracted from this equation:

$$(t_{eq,cooling})_f = \frac{0.8\times(r_f)^2}{\alpha_{fiber}} = \frac{0.8\times(150\times10^{-6}m)^2}{4.65\times10^{-7}\,\frac{m^2}{s}} = 0.04\,seconds \qquad (1.87)$$

Again this is more than enough time to reach thermal equilibrium.

A.8 Bed Cycling and Timing of the Phases

Another important parameter of this system is the cycle time, that is, the time it takes for one module to complete the steps of adsorption, heating/desorption, and cooling. The time to complete each of these phases is estimated in this section.

A.8.1 Adsorption Phase Time

The adsorption phase time was estimated by calculating how long it would take for all the fibers in a module to become saturated with TBM assuming a known capacity of the fibers for TBM, all of the TBM flowing through the module gets adsorbed, and 95% mass equilibration in the fibers themselves. First, the partial pressure of 10 ppmv TBM in the natural gas is calculated as follows:

$$p_{TBM} = ppmv \times P_{total} = \left(10 \times 10^{-6}\right) \times 18.01 atm \times \frac{760\, mm\, Hg}{1 atm} = 0.1368\, mmHg\, TBM \qquad (1.88)$$

A TBM adsorption isotherm on cellulose acetate fibers spun with Zeolite NaY was used to estimate the capacity of the fibers in this system for TBM[14]. The isotherm shows 0.4 millimoles of TBM sorbed per gram of fiber sorbent at a particle pressure of about 2 mmHg TBM at 35°C, and will be used to estimate the capacity of the current system:

$$x_f = 0.0002 \frac{moles\, TBM}{mmHg - g\ fiber} \times 0.1368\, mmHg\, TBM = 0.000028 \frac{moles\, TBM}{g\ fiber} \qquad (1.89)$$

This capacity value can be put in terms of the weight of 13X by dividing by the weight loading of 13X into the fiber:

$$x_{13X} = 0.000028 \frac{moles\, TMB}{g\ fiber} \times \frac{1}{0.75} \times \frac{1000\, g}{1 kg} = 0.0384 \frac{moles\, TBM}{kg 13X} \qquad (1.90)$$

The next step is to find the moles of TBM sorbed in one module, $n_{TBM,m}$, at the end of the adsorption phase (breakthrough time) using the capacity, mass of sorbent, and M_t/M_∞ (fraction of sorbent that is active) from equation (1.77) in lieu of experimental breakthrough data:

$$n_{TBM,\mathrm{m}} = \mathrm{x}_{13X} \mathrm{m}_{13X,\mathrm{m}} \frac{M_t}{M_\infty} = 0.0384 \frac{moles TBM}{kg 13X} \times \frac{291.2 kg 13X}{3} \times 0.95 = 3.54 moles TBM \qquad (1.91)$$

Finally, to get the adsorption cycle time:

$$t_{ads} = \frac{n_{TBM,\mathrm{m}}}{\dot{n}_{TBM,\mathrm{tot}} / N_{m,ads}} = \frac{3.54 moles TBM}{\left(11.2 \frac{moles}{hr} TBM\right) / 3} = 0.95 hr \cong 57 mins \quad (1.92)$$

A.8.2 Heating / Desorption Phase Time

To get the heating / desorption phase time, the amount of regeneration media needed per module must first be calculated as shown in Section A.9.1. This amount is then divided by its volumetric flow rate through the module, calculated by setting its interstitial velocity to 3.30 m/s, the same velocity as the feed gas:

$$t_{des} = \frac{V_{RegenMedia}}{\dot{V}_{RegenMedia}} = \frac{V_{RegenMedia}}{A_m \varepsilon_m (v_i)_{RegenMedia}} \quad (1.93)$$

For heating / desorption with a fraction of the product gas as the regeneration media, the phase time is:

$$t_{des} = \frac{11.45\ m^3}{0.126 m^2 \times 0.35 \times 3.3 \frac{m}{s} \times 60 \frac{s}{min}} \approx 1.3 minutes$$

A.8.3 Cooling Phase Time

Finally, to get the cooling phase time, the same procedure as the heating phase time calculation is followed, starting by first finding the amount of cooling media needed per module as shown in Section A.9.2:

$$t_{cool} = \frac{V_{CoolMedia}}{\dot{V}_{CoolMedia}} = \frac{V_{CoolMedia}}{A_m \varepsilon_m (v_i)_{CoolMedia}} \quad (1.94)$$

For cooling with a fraction of the product gas as the cooling media, the phase time is:

$$t_{cool} = \frac{58.7\ m^3}{0.126 m^2 \times 0.35 \times 3.3 \frac{m}{s} \times 60 \frac{s}{min}} \approx 6.5 minutes \quad (1.95)$$

A.9 Energy Balances for Heating and Cooling Fibers

To determine how much regeneration gas will be needed for the heating / desorption phase and how much cooling gas will be needed for the cooling phase, energy balances were performed around a fiber module. First, one bed volume was defined as the total void volume in one module. That is, the void space in the module plus the fiber porosity:

$$V_b = A_m \varepsilon_m L_f + \frac{\pi}{4} d_f^2 L_f \varepsilon_f N_{fm} \tag{1.96}$$

$$V_b = 0.126 m^2 \times 0.35 \times 1.4 m + \frac{\pi}{4} \times \left(0.0003 m\right)^2 \times 1.4 m \times 0.25 \times 1{,}155{,}556 \; fibers = 0.090 m^3$$

Using this, the bed volumes of pipeline natural gas treated during one adsorption cycle is:

$$N_{b,product} = \frac{v_i A_m \varepsilon_m t_{ads}}{V_b} = \frac{3.30 \frac{m}{s} \times 0.126 m^2 \times 0.35 \times 57 mins \times 60 \frac{s}{min}}{0.090 m^3} \cong 5{,}490 \tag{1.97}$$

A.9.1 Amount of Regeneration Media Needed for Heating / Desorption Phase

For the heating / desorption step, the regeneration media must both heat the fibers to the desired temperature and desorb the TBM (accounted for by the sorption enthalpy). Since there is no barrier layer needed in this system, all of the heat from the regeneration media goes into heating and desorbing the fibers directly:

$$Q_{removed \; from \; regen \; media} = Q_{gained \; by \; fibers} + Q_{desorption} \tag{1.98}$$

$$m_{RegenMedia} C_{p,RegenMedia} \Delta T_{RegenMedia} = m_{13X} C_{p,13X} \Delta T_{13X} + m_{CA} C_{p,CA} \Delta T_{CA} + \Delta H_{sorption} n_{TBM} \tag{1.99}$$

The heat of adsorption of TBM on zeolite 13X was assumed to be 37,500 J/mol with ΔT_{13X} and ΔT_{CA} = 60°C for a change from 30°C to 90°C and ΔT_{media} =30°C for a change from 120°C to 90°C. The split fraction of product gas to be used for heating will be heated from an assumed initial temperature of 30°C to 120°C with by heat exchange with steam, which should be readily available at a power plant. The total moles of TBM adsorbed per cycle per module, n_{TBM}, were calculated in equation (1.91) as 3.54 moles. The following calculations are done using heated product gas as the regeneration media, but other gases (calculations not shown here) may be used. Rearranging equation (1.99) to calculate the amount of heated product gas needed for this heating phase:

$$m_{p,heating} = \frac{97.1kg\,13X \times 800\frac{J}{kg\cdot K}\times 60\,K + 32.9\,kg\,CA\times 1600\frac{J}{kg\cdot K}\times 60\,K + 37500\frac{J}{mol}\times 3.54\,moles\,TBM}{2{,}561\frac{J}{kg\cdot K}\times 30\,K}$$

$$m_{p,heating} = 103.5kg$$

This corresponds to:

$$V_{p,heating} = \frac{m_{p,heating}}{\rho_{\text{p@120}C\ and\ 250\ psig}} = \frac{103.5\ kg}{9.04\frac{kg}{m^3}} = 11.45\ m^3 \qquad (1.100)$$

Which corresponds to:

$$N_{b,heating} = \frac{V_{p,heating}}{V_b} = \frac{11.45\ m^3}{0.090\,m^3} \approx 127\ bed\ volumes\ of\ product\ gas \qquad (1.101)$$

This calculation was repeated for the other two regeneration gases considered, nitrogen and air (both compressed to the feed pressure of 250 psig), using their respective specific heat capacities.

The fraction of product gas (treated NG) needed for this heating/desorption step is estimated as:

$$\frac{N_{b,heating}}{N_{b,product}} = \frac{127}{5,490} \approx 0.0231 \tag{1.102}$$

Therefore, about 2.31% of the total amount of treated natural gas produced will need to be used for heating and desorption, getting remixed with the TBM odorant. In other words 2.31% of the treated natural gas product will be burned with the unwanted TBM. This "wasted product" must be counted into the parasitic load of the process.

A.9.2 Amount of Cooling Media Needed for Cooling Phase

For the cooling step, the cooling media only needs to cool the fibers down to the desired temperature. Again, since there is no barrier layer, all of the heat from the fibers goes into the cooling media directly:

$$Q_{to\ be\ removed\ \ from\ \ fibers} = Q_{gained\ by\ cooling\ media} \tag{1.103}$$

$$m_{13X} C_{p,13X} \Delta T_{13X} + m_{CA} C_{p,\ CA} \Delta T_{CA} = m_{CoolMedia} C_{p,CoolMedia} \Delta T_{CoolMedia} \tag{1.104}$$

The following calculations are done using ambient temperature product gas as the regeneration media, but other gases may be used as well. Assuming ΔT_{13X} and ΔT_{CA} = 60°C for a change from 90°C to the adsorption temperature of 30°C and $\Delta T_{CoolMedia}$ =5°C for a change from 25°C to 30°C. The split fraction of product gas to be used for cooling will be cooled from an assumed initial temperature of 30°C to 25°C with a cooling heat exchanger. Rearranging equation (1.104) to calculate the amount of cooled product gas needed for this cooling phase:

$$m_{p,cooling} = \frac{97.1kg\,13X \times 800\frac{J}{kg \cdot K} \times 60\,K + 32.9\,kg\,CA \times 1600\frac{J}{kg \cdot K} \times 60\,K}{2,226\frac{J}{kg \cdot K} \times 5\,K} = 702.7\,kg$$

This corresponds to:

$$V_{p,cooling} = \frac{m_{p,cooling}}{\rho_{\text{p@25C and 250 psig}}} = \frac{702.5\ kg}{11.97\frac{kg}{m^3}} = 58.7\ m^3 \tag{1.105}$$

Which corresponds to:

$$N_{b,cooling} = \frac{V_{p,cooling}}{V_b} = \frac{58.7\ m^3}{0.090 m^3} \approx 650 bed\ volumes\ of\ \ product\ gas \tag{1.106}$$

The fraction of product gas (treated NG) needed for this cooling step is estimated as:

$$\frac{N_{b,cooling}}{N_{b,product}} = \frac{650}{5,490} \approx 0.1185 \tag{1.107}$$

That means about 11.85% of the total amount of treated natural gas produced will need to be used for cooling. In other words 11.85% of the treated natural gas will pass through the system twice before being used in the turbines. However, as this split is only used for cooling (so only the temperature of the stream will change), it will not be wasted and is not counted into the parasitic load of the process.

Another option for the cooling step to keep the overall process as simple as possible is to simply have adsorption take place at the ambient atmospheric temperature, which will vary seasonally. Therefore, without a temperature controlled adsorption, the capacity of the beds will fluctuate according to the time of year and day based on fluctuations in ambient temperature. The same gas streams would still be used for heating and cooling, but the product stream for cooling would not have an additional cooler attached. This option would deconvolute the added complication of needing to control the temperature of the feed and cooling streams, but would add complexity to the bed cycling process, as the length of each phase would constantly change depending on ambient temperature.

A.9.3 Temperature Rise in Fibers Due to Heat of Adsorption

From the beginning, it was assumed that the temperature rise of the fibers due to the heat of adsorption would be negligible due to the very low concentration of TBM in the pipeline natural gas, such that the fibers stay relatively isothermal during the adsorption step without cooling. This assumption must be checked because if there is a large temperature rise, the capacity of the fiber sorbent may decrease. To check this assumption, an energy balance is again performed around a module, but without considering a cooling media:

$$Q_{released\ during\ sorption} = Q_{gained\ by\ fibers} \tag{1.108}$$

$$\dot{n}_{TBM} t_{ads} \Delta H_s = \left(m_{13X} C_{p,13X} + m_{CA} C_{p,CA} \right) \Delta T_{sorption} \tag{1.109}$$

Rearranging and solving for the temperature rise:

$$\Delta T_{sorption} = \frac{3.73 \frac{moles}{hr} TBM \times 0.95 hrs \times 37500 \frac{J}{mol}}{\left(97.1 kg 13X \times 800 \frac{J}{kg \cdot K} + 32.9 kg CA \times 1600 \frac{J}{kg \cdot K} \right)} \approx 1K$$

This temperature rise is small enough that the adsorption phase can be considered to be isothermal without needing a cooling agent to carry away the heat of adsorption. If the temperature rise were greater, hollow fibers or a cooling jacket around the module could be considered.

A.10 References

1. Bhandari, D.A., N. Bessho, and W.J. Koros, *Hollow Fiber Sorbents for Desulfurization of Natural Gas.* Industrial & Engineering Chemistry Research, 2010. **49**(23): p. 12038-12050.
2. Lively, R.P., R.R. Chance, and W.J. Koros, *Enabling Low-Cost CO2 Capture via Heat Integration.* Industrial & Engineering Chemistry Research, 2010. **49**(16): p. 7550-7562.
3. *7EA Heavy Duty Gas Turbine*, 2013, General Electric Company.
4. Feng, X.S., et al., *Hollow-fiber-based adsorbers for gas separation by pressure-swing adsorption.* Aiche Journal, 1998. **44**(7): p. 1555-1562.
5. Asimakopoulou, A. and A. Karabelas, *A study of mass transfer in hollow-fiber membrane contactors—The effect of fiber packing fraction.* Journal of membrane science, 2006. **282**(1): p. 430-441.
6. Welty, J.R., *Fundamentals of momentum, heat, and mass transfer*. 5th ed. ed. 2008, Wiley: Hoboken, N.J. ;.
7. Hines, A.L., *Mass transfer : fundamentals and applications*. Prentice-Hall international series in the physical and chemical engineering sciences, ed. R.N. Maddox. 1985, Prentice-Hall: Englewood Cliffs, N.J.
8. Chiang, H.-L., et al., *Diffusion of hydrogen sulfide and methyl mercaptan onto microporous alkaline activated carbon.* Chemosphere, 2000. **41**(8): p. 1227-1232.
9. Lively, R.P., *Hollow fiber sorbents for post-combustion CO_2 capture*. 2011, Georgia Institute of Technology: Atlanta, Ga.
10. Ruthven, D.M., *Principles of adsorption and adsorption processes*. 1984, Wiley: New York.

11. Patton, A., B.D. Crittenden, and S.P. Perera, *Use of the linear driving force approximation to guide the design of monolithic adsorbents.* Chemical Engineering Research & Design, 2004. **82**(A8): p. 999-1009.
12. Incropera, F.P., *Fundamentals of heat and mass transfer*. 5th ed. ed, ed. D.P. DeWitt. 2002, J. Wiley: New York.
13. Adem, Z., et al., *PFG NMR investigation of hydrocarbon diffusion in large NaX zeolite crystals: Effect of internal field gradients on diffusion data.* Microporous and Mesoporous Materials, 2008. **114**(1-3): p. 337-342.
14. Bhandari, D.A., *Hollow fiber sorbents for the desulfurization of pipeline natural gas*. 2010, Georgia Institute of Technology: Atlanta, Ga.

APPENDIX B

ECONOMIC ANALYSIS EXAMPLE CALCULATIONS

B.1 Final System Design and Assumptions

The final fiber sorbent design for TBM removal from natural gas is shown in Figure 21. The design has five modules connected together with a series of multi-position switching valves for controlling the timing of different gas flows in a fashion similar to that of a simulated moving bed. As stated in Chapter 3, low cost carbon steel was assumed as the material of construction for the modules and skid.

At start-up, the modules will first be pretreated to desorb any water or residual impurities from the sorbent. Then the feed of pipeline natural gas will be passed through a module until TBM breakthrough on the outlet side, at which point, the valve will be switched to feed in hot regeneration gas until the fibers have reached the desired temperature and most of the TBM has been desorbed. Once the desorption is complete, the valve will be switched to feed in the cooling gas until the fibers have reached the adsorption temperature, and then the valve will again be switched to feed in pipeline natural gas once again, as shown in Figure 32.

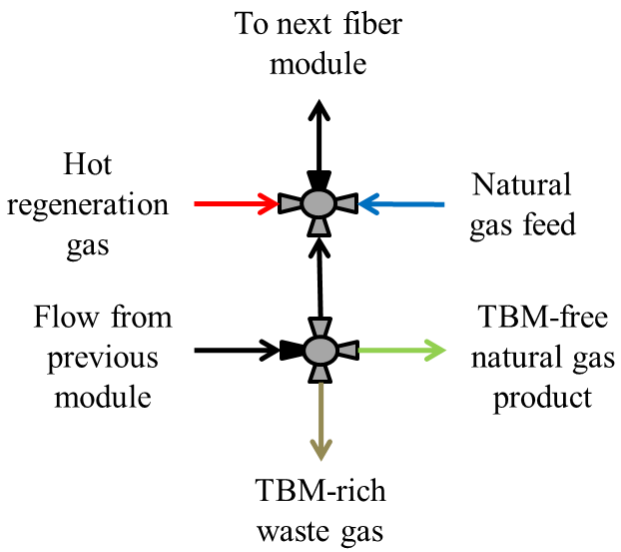

Figure 32: Schematic of the various inlet and outlet streams of the multi-position switching valves shown in Figure 21. The top valve is always open towards the next module in line, while the inlet gas can be switched between hot regeneration gas, the natural gas feed, or the outlet flow from the previous module. The bottom valve always receives flow from the previous module in line, while its outlet can be switched between the top valve, the turbine, or the waste gas disposal.

Three modules will always be in adsorption mode with pipeline natural gas being fed into the modules in parallel while one module will be in regeneration mode about three-fifths of the time (with the other two-fifths of the time in resting mode with no gas flow). A fifth module will be connected into the skid, but will only serve as a backup and will not be in operation unless one of the working modules needs to be replaced. Both the regenerating and cooling media chosen for this design are simply a fraction of the product gas. The product gas is heated with steam and cooled with cooling water using a heat exchanger to do the regeneration and cooling respectively. Other regenerations gases considered were compressed air and nitrogen, requiring the installation of an on-site nitrogen generation system. However, employing nitrogen was found to be more expensive (capital and operating cost-wise) than the product gas, and using hot air with a natural gas system, though cheap, was considered too dangerous to be practical. The TBM-rich waste gas stream is assumed to be burned as waste gas such that there are no purity or recovery requirements for the TBM. The heat generated from the combustion of

this waste gas stream can be used to create steam, which can then be used to heat the product gas for the regeneration step. Any excess steam created in this way can be further used in a separate steam turbine to generate more electricity for product. The fiber system was considered both with and without this heat integration step.

With this general idea of how the system will look and operate, the economic analysis can be completed as detailed below, starting first with an estimate of capital and operating cost, and finishing with an analysis of the savings gained by implementing this system. Cost correlations and heuristics from Tedder[1] were mainly used to guide this part of the project, though some cost estimations from Peters and Timmerhaus[2] were also used. All cost estimates are reported in terms of 2011 U.S. dollars.

B.2 Capital Investment – Cost to build a fiber module

The capital cost of a fiber module was first estimated based on the cost of the raw materials and the cost of construction and delivery, recognizing that fiber modules typically cost between $10 to $20 per m^2. To get the raw material cost of everything needed to build a module, the following equation was used to convert from lab prices to industrial bulk prices for bulk chemical prices that are not easily available[1]:

$$P_b = P_l \left(\frac{Q_b}{Q_l} \right)^{-0.75} \tag{1.110}$$

where P_b is the estimated bulk price in $/kg for purchases of the bulk amount in 60 lb lots, P_l is the laboratory selling price in $/kg, Q_b=60lbs=27,216 g, is a representative bulk amount (i.e. purchase lot), and Q_l is the laboratory quantity purchased in grams. This estimation was used for zeolite 13X, CA polymer, and NMP. Direct market price estimates for 2012 were used for water, methanol, hexane, epoxy, and steel. The amount

of each of these raw materials needed was then estimated to get a total raw materials cost. With this, labor and other indirect costs were estimated with correlations based on material cost. Two correlations, one from Guthrie[3, 4] and one from Page[5], were used for this portion to get a final cost per module.

B.2.1 Fiber Materials

The amount of zeolite 13X and CA polymer needed per module are determined from the module and fiber design (fiber and module lengths and diameters, module void, fiber porosity, zeolite loading). For a 1.4 meter long, 0.4 diameter module with a void of 0.35, and 300 micron diameter fibers with porosity of 0.25 and 13X loading of 75 wt. %, the amount of 13X needed is 97.1 kg and the amount of CA needed is 32.9 kg per module.

B.2.2 Solvents

Four liquid solvents are needed to produce fibers: NMP, hexane, methanol, and water. The amount of NMP needed is found from a ratio of mass of the fibers in one module:

$$m_{NMP} = \frac{\pi}{4}(1-\varepsilon_m)\left(d_m\right)^2 L_m \rho_f \left(\frac{0.481}{0.434}\right) \tag{1.111}$$

$$m_{NMP} = \frac{\pi}{4}\left(1-0.35\right)\left(0.4m\right)^2\left(1.4m\right)\times\left(1134.6\frac{kg}{m^3}\right)\times\left(\frac{0.481}{0.434}\right) = 143.8kg$$

The amount of water needed is estimated as 10 m^3.

The amount of methanol and hexane needed is found by assuming we need 3 times the bed volume (see Appendix A) of a module per wash and three separate washes to complete the solvent exchange for one module's worth of fibers:

$$V_{solvent} = 3V_b \times 3washes = 3 \times 0.090\,m^3 \times 3 = 0.81m^3 \quad (1.112)$$

B.2.3 Module Materials

The fibers are assumed to be bundled together with 6 centimeters of epoxy on both ends of the module. Therefore, the amount of epoxy needed is:

$$V_{epoxy} = L_{epoxy}\frac{\pi}{4}\left(d_m\right)^2 = (0.12m) \times \frac{\pi}{4} \times \left(0.4m\right)^2 = 0.0151m^3 \quad (1.113)$$

The amount of steel needed for one module is found by assuming a shell wall thickness of 1 centimeter, with the inner diameter of this shell being what we have been calling module diameter d_m throughout this work:

$$V_{steel} = \frac{\pi}{4}\left(d_{mo}^2 - d_m^2\right)L_m == \frac{\pi}{4} \times \left(\left(0.41m\right)^2 - \left(0.40m\right)^2\right) \times 1.4m = 0.0089\,m^3 \quad (1.114)$$

Convert this amount to mass of carbon steel needed:

$$m_{CS} = V_{steel} \times \rho_{CS} = 0.0089\,m^3 \times 7840\frac{kg}{m^3} = 69.8kg \quad (1.115)$$

B.2.4 Surface area of fibers in one module

To get a cost per area for the module, the surface area of all the fibers in one module must be calculated:

$$SA_{fm} = \pi d_f L_f N_{fm} = \pi \times \left(300 \times 10^{-6} m\right) \times 1.4m \times 1{,}155{,}556 = 1524.7\,m^2 \quad (1.116)$$

B.2.5 Total cost of one module

Based on just the raw materials alone (cost of materials times how much of each material is needed), the cost for one module is about $4,600. This translates to about \$3.00 / m^2. See Table 16 for more details.

Table 16: Module raw material cost summary listing the materials needed, the bulk price of each material, the amount of each material needed to fabricate one module, the individual costs of these materials, and finally, the total cost of one module on an absolute and per sorbent area basis.

Material	Price	Units	Amount Needed	Units	Cost	Cost per m^2
Zeolite 13X	$8.44	kg	97.1	kg	$820	
CA polymer	$7.44	kg	32.9	kg	$250	
NMP	$13.15	kg	143.8	kg	$1,890	
Water	$1.13	m^3	10	m^3	$10	
Methanol	$383.05	m^3	0.81	m^3	$310	
Hexane	$739.92	m^3	0.81	m^3	$600	
Epoxy	$41,137.00	m^3	0.0151	m^3	$620	
Carbon steel	$0.90	kg	70	kg	$60	
Total					**$4,560**	**$3.00**

However, besides the raw materials, there are other costs associated with constructing a module, such as labor, equipment, and other indirect costs. Using two different factoring methods (Guthrie and Page methods from Tedder, discussed later in section on cost per skid) to estimate the rest of these costs from the raw materials cost, and taking the average of the two estimates, the final cost for one module is about $19,000. This translates to about $12.25 / m^2. See Table 17 for more details. This value is used as the base equipment cost (E) in subsequent skid calculations.

Table 17. Total module cost summary with Guthrie and Page factoring methods.

Method	Base Cost	Direct Costs	Indirect Costs	Total Cost	Cost per m^2
Guthrie	$4,560	$9,100	$5,200	$18,900	$12.38
Page	$4,560	$8,700	$5,200	$18,500	$12.12
Average	$4,560	$8,900	$5,200	**$18,700**	**$12.25**

B.3 Capital Investment – Cost to build a skid

The basic procedure to cost a skid is to complete a process flow diagram (PFD), size all major equipment items, and develop a major equipment cost list, followed by

using cost correlations to extrapolate the total cost of the skid. From the PFD in Figure 21, the only two major equipment items are:

1) The fiber sorbent modules
2) Heat exchangers (one for heating and one for cooling the natural gas product)

Others equipment items considered but not included in the final calculations include:

3) Multi-position valves and their control systems, which are indeed an important part of the design, but are instead factored into the "piping" costs.
4) Pumps, which should not be necessary due to the high pressures used throughout the system.
5) Compressors, which are generally needed to bring pipeline natural gas up to a pressure necessary for use in turbines. However, because this would be needed even no fiber sorbent system was implemented, it is not an additional cost of this system.
6) SO_2 scrubber system for the SO_2 produced during burning of TBM in the waste gas stream, because the amount produced will be very low compared to total amount of flue gas produced from burning the product stream, and should be within government regulations on SO_2 emission levels.
7) Storage tank for treated natural gas product, assumed to be unnecessary because the fiber system was designed specifically to meet the flow rate requirements of one GE turbine.

Two methods, Guthrie method and Page method, are used to estimate the cost per skid. They give slightly different answers, and the average between the two was taken.

B.3.1 Equipment Sizing

Figure 33 shows the inlet and outlet streams for the heat exchanger (U tube) used for the heating step. Steam enters one end of the heat exchanger at 185°C and is condensed, exiting at a reduced temperature of 120°C. Natural gas product enters from the other end at 30°C and is heated by the steam to 120°C.

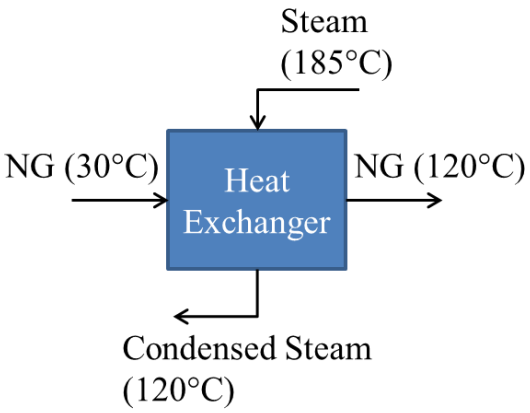

Figure 33. Schematic of the heat exchanger used for heating the natural gas product with steam to be used during the heating / desorption step.

To size this heat exchanger, first calculate the log mean temperature difference to determine the temperature driving force for this heat transfer:

$$\Delta T_{lm} = \frac{\Delta T_{steam} - \Delta T_{NG}}{\ln\left(\frac{\Delta T_{steam}}{\Delta T_{NG}}\right)} = \frac{60-90}{\ln\left(\frac{60}{90}\right)} = 74K \tag{1.117}$$

Then calculate the heat transfer rate:

$$\dot{Q} = \frac{Q_{req'd\ by\ natural\ gas}}{t_{des}} = \frac{m_{NG} C_{p,NG} \Delta T_{NG}}{t_{des}} = \frac{(103.5 kgNG) \times \left(2226 \frac{J}{kg \cdot K}\right) \times (90K)}{80s} = 2.6 \times 10^5 \frac{J}{s} \tag{1.118}$$

Assuming an overall heat transfer coefficient U of 100 W/m^{2}K for high pressure gases for both streams of the heat exchanger, a heat exchange area can be estimated by[6]:

$$A_{HE} = \frac{\dot{Q}}{U \Delta T_{lm}} = \frac{2.6 \times 10^5 \frac{J}{s}}{100 \frac{W}{m^2 K} \times 74K} = 35 m^2 \cong 377\ ft^2 \tag{1.119}$$

These same sort of equipment sizing steps were followed for the heat exchanger used for the cooling step, as well as the equipment items needed for the alternative regeneration medias of compressed air and nitrogen that were considered. A brief description of the sizing process for the items needed for the alternative regeneration media is included in Section B.5 but detailed calculations are not shown.

B.3.2 Base Equipment Cost and Time Factoring

The base equipment cost is for equipment made of carbon steel and operating at low (atmospheric) pressures, and is estimated using the following cost correlation:

$$E = E_0\left(\frac{S}{S_0}\right)^a \tag{1.120}$$

where E is the base equipment cost, E_0 is a reference cost associated with a unit of size S_0, S is a size parameter such as volume, transfer area, or power requirement, S_0 is the reference size, and a is the power dependency factor for the equipment item. Values for E_0, S_0, and a are given for various equipment items in mid-1968 dollars by Guthrie[3].

Because the costs given in the Tedder book are in mid-1968 dollars, they must be modified to reflect current costs (in 2011 dollars in this project). The capital estimates given are factored from one time period to another by:

$$\frac{C(t_2)}{C(t_1)} = \left[\frac{Index(t_2)}{Index(t_1)}\right] \tag{1.121}$$

where $C(t_i)$ is the estimated cost at time t_i, and $Index(t_i)$ is the *Chemical Engineering*'s Plant Cost Index (CEPCI) time t_i. The CE index in 1968 is 113.6 and the CE index in 2011 is 585.7. These index values will be used throughout the following example calculations.

Combining equations (1.120) and (1.121), the base equipment cost for any item in 2011 dollars is:

$$E = E_0 \left(\frac{S}{S_0} \right)^a \left[\frac{Index(t_2)}{Index(t_1)} \right] \tag{1.122}$$

For the heat exchanger sized in equation (1.119), read values from Table 4.9 in Tedder to cost a U tube heat exchanger in the 100 to 10,000 ft^2 range:

$$E_{heat\ exchanger} = \$1,700 \left(\frac{377\ ft^2}{100\ ft^2} \right)^{0.65} \left[\frac{585.7}{113.6} \right] \cong \$20,800 \tag{1.123}$$

For the fiber sorbent modules, this type of correlation is not used. Instead, the base equipment cost is taken to be the per module capital cost calculated in Section B.2 multiplied by the number of modules to be used in the process:

$$E_{m,tot} = E_m \times N_{m,tot} = \$18,675 \times 5 \cong \$93,400 \tag{1.124}$$

B.3.3 Purchased Equipment Costs

The purchased equipment cost accounts for special materials of construction and / or high pressure operation. The base and purchased equipment costs may be the same if the equipment purchased does not require special materials or need to handle high pressures. The purchased equipment cost is estimated from the base equipment cost:

$$E' = EF_m F_p \tag{1.125}$$

where E is the low-pressure, carbon steel cost (base cost), E' is the adjusted unit cost (purchased cost), F_m is the materials adjustment factor, and F_p is the pressure adjustment factor.

No extra materials factors are used in this analysis because of the previously stated assumption that everything will be made of carbon steel, the default material used in Tedder (F_m=1 for everything). The pressure factor F_p is correlated with:

$$F_p = \begin{cases} 1 & for\ P \le P^* \\ 1 + d\left(P - P^*\right) & for\ P > P^* \end{cases} \tag{1.126}$$

where P is the pressure the equipment item will be operated at, P* is a reference pressure at which costs begin to increase significantly, and d is an empirical parameter that measures the incremental effects of pressure on cost.

For the heat exchanger costed in equation (1.123), read values from Tedder Table 4.16 for a shell & tube heat exchanger and calculate the subsequent purchased equipment cost:

$$F_{p,heat\ exchanger} = 1 + d\left(P - P^*\right) = 1 + 0.0007\left(264.7\ psia - 150\ psia\right) = 1.08 \tag{1.127}$$

$$E'_{heat\ exchanger} = \$20,800 \times 1 \times 1.08 \cong \$22,400 \tag{1.128}$$

For the fiber sorbent modules, read values from Tedder Table 4.16 for a generic pressurized process vessel and calculate the subsequent purchased equipment cost:

$$F_{p,m} = 1 + d\left(P - P^*\right) = 1 + 0.001\left(250\ psia - 50\ psia\right) = 1.2 \tag{1.129}$$

$$E'_{m,tot} = \$93,400 \times 1 \times 1.2 \cong \$112,050 \tag{1.130}$$

B.3.4 Guthrie Method for Total Cost of One Skid

Besides the purchased cost of the equipment itself, there are two other direct costs: the other direct materials costs and the direct labor costs. Together, these other direct costs account for piping, concrete, steel (for foundations), instrumentation, electrical connections, insulation, paint, safety devices, and installation labor. These

direct costs are estimated as percentages of the base equipment cost E with factors from Tedder's tables:

$$Guthrie\,Total\,Direct\,Costs = TDC_G = E' + M + L = (E') + \left[0.7\,f_t E' + \left(f^{mat} - 0.7\,f_t\right)E\right] + \left(f^{lab}E\right) \quad (1.131)$$

where M is the direct field materials cost not including E, L is the field labor cost for installing the equipment item, f_t is the piping factor for the equipment item, f^{mat} is the materials factor for the base equipment cost, and f^{lab} is the labor cost factor for the base equipment cost.

The direct field materials cost M is separated into two terms because 70% of the piping costs contained within it are affected by special materials of construction and high pressures. In other words, 70% of the total piping costs for an equipment item are for process piping costs and are therefore affected by the higher purchased equipment cost (using the first term 0.7ftE'). The rest of the 30% of the total piping costs for an equipment item are for non-process piping costs that do not require special materials and are not affected by high operating pressure in the process. All other non-piping direct field materials costs are also not affected by pressures or special materials and should be factored based on the base equipment cost alone (using the second term (f^{mat}-0.7f_t)E. To account for the many multi-position valves and control systems needed for this design that is more complex than normal, the piping factor given in Tedder is multiplied by 1.33 in the subsequent calculations.

For the heat exchanger, read values from Tedder Table 4.17 for shell & tube heat exchangers:

$$M_{heat\ exchanger} = \left[0.7 \times 0.595 \times \$22,400 + (0.699 - 0.7 \times 0.595) \times \$20,800\right] \cong \$15,200 \quad (1.132)$$

$$TDC_{G,heat\ exchanger} = \$22,400 + \$15,200 + 0.604 \times \$20,800 \cong \$50,190 \quad (1.133)$$

For the fiber sorbent modules, read values from Tedder Table 4.18 (for a vertical process vessel, assumed to apply to the vertical fiber modules):

$$M_{m,tot} = \left[0.7 \times 0.791 \times \$112,050 + (1.027 - 0.7 \times 0.791) \times \$93,400\right] \cong \$106,240 \quad (1.134)$$

$$TDC_{G,m\,tot} = \$112,050 + \$106,240 + 0.972\left(\$93,400\right) \cong \$309,060 \quad (1.135)$$

Besides the direct costs, there are indirect costs that include taxes, freight, insurance, overhead, and engineering. These indirect costs are accounted for with an indirect cost factor as a percentage of the base equipment cost:

$$Guthrie Total\ Indirect\ Costs = TNC_G = Ef^{\,ind} \quad (1.136)$$

where f^{ind} is the indirect cost factor for the base equipment cost.

For the heat exchanger, again read values from Tedder Table 4.17:

$$TNC_{G,heat\ exchanger} = \$20,800 \times 0.875 \cong \$18,170 \quad (1.137)$$

For the fiber sorbent modules, again read values from Tedder Table 4.18:

$$TNC_{G,m\,tot} = \$93,400 \times 1.14 \cong \$106,450 \quad (1.138)$$

The bare module cost (BMC) of any equipment item is a sum of the total direct costs and total indirect costs:

$$Guthrie\ BMC = BMC_G = TDC_G + TNC_G = (E^{'} + M + L) + Ef^{\,ind} \quad (1.139)$$

For the heat exchanger:

$$BMC_{G,heat\ exchanger} = \$50,190 + \$18,170 = \$68,360 \quad (1.140)$$

For the fiber modules:

$$BMC_{G,m\,tot} = \$309,060 + \$106,450 = \$415,510 \quad (1.141)$$

The total installed cost (TIC) for the battery limits (skid limits) is the sum of all costs to completely construct the facility so that it can be operated. It does not include

start-up costs or working capital. Instead, it is the cost to purchase and install the equipment items, calculated as the sum of the total bare module cost plus contingency and fees. Tedder assumes an average contingency of 15% and an average A/E fee of 3% of the bare module cost for the entire battery limits of the plant site (the chemical process area only, not including storage & handling, utilities, and service areas), such that the TIC can be approximated as:

$$Guthrie TIC_b = TIC_{b,G} = 1.18 \sum_{i=1}^{N} BMC_i \tag{1.142}$$

where BMC_i is the bare module cost of the i^{th} item in the purchased equipment list and N is the number of items in the purchased equipment list.

For the fiber module system then:

$$TIC_{b,G,\ systsem} = 1.18\ (BMC_{G,heating\ heat\ exchanger} + BMC_{G,cooling\ heat\ exchanger} + BMC_{G,m\,tot}) \tag{1.143}$$

$$TIC_{b,G,system} = 1.18(\$68,360 + \$58,920 + \$415,510) \cong \$640,490$$

Note that the previous example calculations do not include the estimates for the cooling heat exchanger. The calculations for the cooling heat exchanger follow the same steps as that of the heating heat exchanger, except that it uses water to cool the natural gas product instead of steam to heat it.

B.3.5 Page Method for Total Cost of One Skid

Similar calculations are repeated now for comparison using Page's factoring method for a refinery process system that operates at low to moderate pressures and have equipment mostly made of carbon steel. The Page factors are applied directly to the purchased equipment costs, not to the base low pressure carbon steel equipment cost. The total purchased equipment cost is:

$$E'_{total} = E'_{heating\ heat\ exchanger} + E'_{cooling\ heat\ exchanger} + E'_{m,tot} \quad (1.144)$$

$$E'_{total} = \$22,400 + \$19,340 + \$112,050 \cong \$153,830 \quad (1.145)$$

The E'total is now used with Page direct and indirect cost factors. Page takes the direct costs to be for materials and field labor (same definitions as Guthrie), as well as subcontracts:

$$Page\,Total\ Direct\ Costs = TDC_P = E'_{total}\left(f_{materials} + f_{labor} + f_{subcontracts}\right) \quad (1.146)$$

where $f_{materials}$, f_{labor}, and $f_{subcontracts}$ are Page factors for materials, labor, and subcontracts respectively. From the average values in Tedder Table 4.25 for the various factors:

$$TDC_{P,system} = \$153,830 \times (1.801 + 0.7835 + 0.479) \cong \$471,240 \quad (1.147)$$

Page takes the indirect costs to be for construction equipment costs, overhead and indirects (as ratios of direct field labor), and home office service costs as a ratio of the total:

$$Page\,Total\ Indirect\ Costs = TNC_P = E'_{total}\,f_{lab}\left(f_{cons} + f_{ind}\right) + \left[E'_{total}\,f_{lab}\left(f_{cons} + f_{ind}\right) + TDC_P\right] f_{off} \quad (1.148)$$

where f_{lab}, f_{cons}, f_{ind}, and f_{off} are Page factors for labor, construction, overhead & indirects, and home office services respectively. From the average values in Tedder Table 4.31 and 4.32 for the various factors:

$$E'_{total}\,f_{lab}\left(f_{cons} + f_{ind}\right) = \$153,830 \times 0.7835 \times (0.31 + 0.85) \cong \$139,800 \quad (1.149)$$

$$TNC_{P,system} = \$139,800 + (\$139,800 + \$471,240) \times 0.133 \cong \$221,070 \quad (1.150)$$

B.4 Total Capital Investment

The total capital investment for the adsorption system was estimated using Guthrie and Pages methods. The average of these two estimates was taken to be the total capital investment as detailed below.

B.4.1 Guthrie Method for Total Installed Cost for the Whole Chemical Plant

To take into account other major areas of the whole chemical plant besides the battery limit (the storage and handling areas, the utilities area, and the other support services area), Heuristic 9 was used from Tedder, which states that the total installed cost for an expansion to an existing plant is roughly 133% of the total installed cost of the battery limits. The fiber module system is much closer to an expansion on an existing plant rather than a grass-roots plant, so the 133% approximation was used to estimate the total installed cost for the whole chemical plant:

$$GuthrieTIC_p = TIC_{p,G} = 1.33TIC_{b,G} \tag{1.151}$$

$$TIC_{\mathrm{p},G,\ system} = 1.33 \times \$640,490 \cong \$851,860 \tag{1.152}$$

B.4.2 Page Method for Total Installed Cost for the Whole Chemical Plant

The total installed cost for the whole chemical plant using Page factors is simply the sum of the direct and indirect costs:

$$PageTIC_p = TIC_{p,P} = TDC_P + TNC_P \tag{1.153}$$

$$TIC_{p,P} = \$471,240 + \$221,070 = \$692,320 \tag{1.154}$$

B.4.3 Total Capital Investment - Comparison and Average of Guthrie and Page Methods

The total capital investment for a chemical plant is the sum of the total installed cost for the whole plant, the working capital, and any start-up costs:

$$TCI = TIC_p + I_W + I_s \tag{1.155}$$

where I_w and I_s are the working capital and start-up costs respectively. From Table 3.5 in Tedder, the working capital is often 11-25% of the total installed cost. The lower end of this, 11% is used for this work to account for both working capital and start-up costs because there should not be much working capital associated with this process, and the system is relatively simple and small so start-up costs should not be significant. The total capital investment is then:

$$TCI = 1.11 TIC_p \tag{1.156}$$

For the TIC_p estimated from Guthrie's method, the TCI is:

$$TCI_G = 1.11 \times \$851,860 \cong \$945,560 \tag{1.157}$$

For the TIC_p estimated from Page's method, the TCI is:

$$TCI_P = 1.11 \times \$692,320 \cong \$768,470 \tag{1.158}$$

There is approximately a 20% difference between these two estimates. The total capital investment using the average of these two methods is $857,020.

B.4.4 Uncertainties / Possible Sources of Error

There are several uncertainties and possible sources of error in this capital investment estimate. Some major ones are listed below.

1) The major equipment list – any missing or overlooked items will lead to an underestimation of capital cost
2) The cost of the fiber sorbent module – Guthrie and Page methods were developed for the construction and installation of a chemical system or plant, and may not apply for a single equipment item
3) Materials of construction – assuming carbon steel is suitable for all system components

B.5 Operating Cost

As mentioned in Chapter 3, the operating costs of the adsorber system only include utilities and any parasitic load. The utilities needed for the fiber system with product gas regeneration are steam for the heating heat exchanger and water for the cooling heat exchanger, two of the three major equipment items needed for the system, based on the process flow diagram. If the equipment items list changes, it will change both the capital and operating cost of the system. Only the calculations for the steam are shown in this section. Similar calculations were done for the cooling water. For operation, the plant is assumed to operate 365 days per year, 24 hours per day, for nominal design basis of ~8765 operating hours (525,949 minutes) per year.

First, an energy balance is performed to estimate the mass of steam required for one heating / desorption cycle:

$$Q_{required\ by\ natural\ gas} = Q_{supplied\ by\ steam} \tag{1.159}$$

$$m_{NG} C_{p,NG} \Delta T_{NG} = m_{steam} (\Delta H_{vap,steam} + C_{p,\ steam} \Delta T_{steam}) \tag{1.160}$$

The heating/desorption step is approximately 1.3 minutes long, while the total time for a whole cycle (adsorption, heating / desorption, and cooling) is approximately 70 minutes.

If the timing of the beds is staggered for continuous operation, it is seen that steam is only needed for 3 cycles for every 60 minutes of operation. Rearranging equation (1.160), plugging in values, and factoring for one year of operation, the mass of steam per year needed is:

$$m_{steam} = \frac{(103.5 kgNG) \times \left(2226 \frac{J}{kg \cdot K}\right) \times (90K)}{\left(2{,}260{,}000 \frac{J}{kg}\right) + \left(2537 \frac{J}{kg \cdot K}\right) \times (60K)} \times \frac{3 cycles}{60 mins} \times \frac{525{,}949 mins}{year} = 2.26 \times 10^5 \frac{kg}{year}$$

B.5.1 Operating Cost without Heat Integration

The cost of steam as a direct purchased utility is about \$0.02/kg[1], so the operating cost (OC) for the heating heat exchanger is:

$$OC_{steam} = 2.26 \times 10^5 \frac{kg}{year} \times \frac{\$0.02}{kg} = \$4{,}430 / year \tag{1.161}$$

The parasitic load (PL) on the system is 2.31%, as this is the percent of natural gas product needed for the regeneration step that will be lost as waste. To translate this parasitic load into an operating cost, find the flow rate of natural gas lost this way and convert to the flow rate at the temperature and pressure of operation:

$$PL_{NG} = 0.0231 \times 15{,}000 SCFM = 347 SCFM \cong 3.18 \times 10^5 \frac{m^3}{year} \tag{1.162}$$

Then, using the price of natural gas for industrial applications, \$0.16/m^3, calculate the cost[7]:

$$OC_{NG} = 3.18 \times 10^5 \frac{m^3}{year} \times \frac{\$0.16}{m^3} \cong \$50{,}850 \tag{1.163}$$

The total operating cost on a per year basis is then simply the sum of the annual utilities cost (calculation for annual cost of cooling water not shown here):

$$OC_{total} = OC_{steam} + OC_{water} + OC_{NG} \tag{1.164}$$

$$OC_{total} = \$4,430/\,year + \$5,550/\,year + \$50,850/\,year \cong \$60,840/\,\text{year} \tag{1.165}$$

The power requirements for the equipment items needed for compressed air and nitrogen regeneration were also estimated for comparison. The cost of electricity to run both these systems was taken to be $0.04/kWh for electricity produced and used on site. This estimation will be described briefly here but detailed calculations are not shown. First an air compressor (for regeneration with air) was sized to 380 cfm according to the compressed air requirements calculated from energy balances. Once the capacity requirement is known, Figure 14-47 in Peters and Timmerhaus[2], showing horsepower requirement as a function of compressor flow rate, was used to extrapolate the power requirement in hp. This can then be converted to the power needed (in kWh) per year. For compressed air desorption, this value is about 81,800 kWh/year, which will cost about $3,000 per year. The two compressors needed for on-site nitrogen generation were sized in the same way to estimate the capacity requirement in Nm^3 of nitrogen per year. The requirement was found to be about 489,700 Nm^3/year. For operating cost estimation, a cost of $0.11 per hundred standard cubic feet of nitrogen generated (or about $0.04 per Nm^3 of nitrogen) was assumed[8], such that the cost for a fiber module system with nitrogen regeneration is about $19,000 per year.

B.5.2 Operating Cost with Heat Integration Considerations

Heat integration presents the opportunity to reduce the operating costs of the fiber adsorbent system. This can be done by using the heat generated from burning the TBM-

rich waste gas stream to create steam to be used in the regeneration cycle. An energy balance is done to determine the amount of energy required to create steam from water, assuming an initial water temperature of 15°C and a final steam temperature of 185°C, for a ΔT value of 170°C. The mass of water is taken to be the mass of steam needed. The energy balance is shown below:

$$Q_{required\ by\ waste\ gas\ combustion} = m_{water,regen}\Delta H_{vap} + m_{water,regen}C_{p,water}\Delta T \tag{1.166}$$

$$Q_{required\ by\ waste\ gas\ combustion} = 226,050\,kg \times 2,260,000\frac{J}{kg} + 226,050\,kg \times 4,187\frac{J}{kgK} \times 170K$$

$$Q_{required\ by\ waste\ gas\ combustion} = 6.711\times10^{11}\,J\ per\ year$$

The amount of waste gas needed to create enough steam for the regeneration step can then be found by knowing the amount of energy needed:

$$Amount\ of\ waste\ gas = \left(6.711\times10^{11}\,J\right)\times\frac{1GJ}{10^{9}\,J}\times\frac{1MMBtu}{1.0546GJ}\times\frac{1m^3}{35.315\,ft^3}\times\frac{61.58\,ft^3}{1MMBtu} \tag{1.167}$$

$$Amount\ of\ waste\ gas = 1,110\,m^3\ per\ year\ needed\ to\ create\ steam\ for\ regen$$

This amount is subtracted from the parasitic load to get a new cost, assuming only enough steam is created for the regeneration step:

$$PL_{NG} = 3.18\times10^{3}\frac{m^3}{year} - 1,110\frac{m^3}{year} = 3.17\times10^{5}\frac{m^3}{year} \tag{1.168}$$

$$OC_{NG} = 3.17\times10^{5}\frac{m^3}{year}\times\frac{\$0.16}{m^3} \cong \$50,670 \tag{1.169}$$

With this heat integration, the cost of steam is eliminated and transferred to the cost of purchasing enough water to create the amount of steam instead. An example calculation of the increase in water cost is provided in the second method of heat integration.

A second method of heat integration involves using the total amount of energy from waste gas combustion to create steam. The amount of energy produced per year can be found from the parasitic load amount and the heating value of natural gas, which is 1 MMBtu / 1000 SCF, or 1 MMBtu / 61.58 ft^3 at pipeline conditions:

$$Energy\ produced = PL_{NG} \times NG\ Heating\ Value \tag{1.170}$$

$$Energy\ produced = 3.18 \times 10^3 \frac{m^3}{year} \times \frac{1 MMBtu}{61.58\ ft^3} \times \frac{35.315\ ft^3}{1 m^3} \times \frac{1.0546 GJ}{1 MMBtu}$$

$$Energy\ produced = 1.92 \times 10^{14}\ J\ per\ year$$

The amount of water that can be converted to steam using this amount of energy produced can be found through an energy balance:

$$Q_{produced\ \ from\ burning\ waste\ gas} = Q_{received\ by\ water\ to\ create\ steam} \tag{1.171}$$

$$Q_{produced\ \ from\ burning\ waste\ gas} = m_{water,total} \Delta H_{vap} + m_{water,total} C_{p,water} \Delta T \tag{1.172}$$

$$1.92 \times 10^{14}\ J = m_{water,total} \left(2,260,000 \frac{j}{kg} + 4,187 \frac{J}{kgK} \times 170 K \right)$$

$$m_{water,total} = 6.467 \times 10^7\ kg\ per\ year$$

This amount is added to the amount of water needed for the cooling step to get a new annual cost for water:

$$Total\ amount\ of\ water\ needed = 4,910 \frac{m^3}{year} + 64,670 \frac{m^3}{year} = 69,580 \frac{m^3}{year} \tag{1.173}$$

$$OC_{water} = 69,580 \frac{m^3}{year} \times \frac{\$1.13}{m^3} = \frac{\$78,680}{year} \tag{1.174}$$

Because the amount of steam needed for the regeneration step is only a small fraction of the total amount of steam that can be created from using all of the waste gas energy, there remains a large amount of excess steam:

$$Excess\,steam = 6.467\times10^{7}\ kg - 226,050\,kg = 6.440\times10^{7}\ kg\ per\ year \tag{1.175}$$

This excess steam can be converted to electricity using a steam turbine. A typical 500 kW steam turbine requires 21,500 lb/hr of superheated steam input at about 500 psig. The flow rate of the excess saturated steam (at 185°C and 150 psig) can be converted to high pressure superheated steam by a ratio of enthalpies:

$$6.440\times10^{7}\ \frac{kg}{year}\times\frac{1200\,Btu/lb}{1465\,Btu/lb}\times\frac{2.204\,lb}{1kg}\times\frac{1\,yr}{8765.8\,hr} = 13,270\,\frac{lb}{hr} \tag{1.176}$$

This flow rate suggests that the excess steam created from the waste gas combustion energy of two 85 MW gas turbines can fuel one 500 kW steam turbine, such that the equivalent amount of electricity produced by the waste gas combustion energy of one 85 MW turbine is:

$$\frac{0.5MW}{2}\times\frac{3.155\times10^{7}\,s}{1yr}\times\frac{1kWh}{3.6MJ} = 2.19\times10^{6}\ kWh\ per\ year \tag{1.177}$$

And the profit from producing this electricity at \$0.04/kWh is:

$$2.19\times10^{6}\ \frac{kWh}{year}\times\frac{\$0.04}{kWh} = \$87,640\ per\ year\ profit \tag{1.178}$$

Totaling the annual operating costs and profits of the system with heat integration returns a net profit on the system:

$$Net\ profit = profit - cost \tag{1.179}$$

$$Net\ profit = \frac{\$87,640}{year} - \frac{\$78,680}{year} = \frac{\$8,920}{year}$$

B.6 Final System Economics

The yearly cost of the adsorption system (capital cost distributed over lifetime plus annual operating cost) is translated to cost per MMBtu by taking into account the flow rate of natural gas through a single turbine as shown below for the fiber system without heat integration:

$$Yearly\ Cost = \frac{TCI}{system\ lifetime} + OC_{total} = \frac{\$857,020}{5 years} + \frac{\$60,840}{year} = \frac{\$275,000}{year} \quad (1.180)$$

$$\frac{\$275,000}{year} \times \frac{1 year}{525,949 mins} \times \frac{1 min}{15,000 SCF} \times \frac{1,000 SCF}{MMBtu} \cong \frac{\$0.03}{MMBtu} \quad (1.181)$$

The capital cost of the 85 MW GE turbine was also estimated using information given in an EPA turbine report, giving the turbine installed cost in 2007 $/kW for five turbines of various capacities[9]. From four of these, a correlation was fitted to the data and extrapolated for the GE turbine used in this system:

$$Installed\ Cost = -467.8 \times \ln(Turbine\ Capacity\ in\ kW) + 6255.1 = \$945 / kW \quad (1.182)$$

To get the final capital cost, simply multiply by the capacity of the turbine (85 MW) and use the cost indices to bring the cost from 2007 dollars to 2011 dollars:

$$Turbine\ Capital\ Cost = \frac{\$945}{kW} \times 85,000\ kW \times \left[\frac{585.7}{525.4}\right] \cong \$89,540,000 \quad (1.183)$$

The capital cost of the turbine can now be compared against the capital cost of the fiber sorbent system:

$$\frac{Fiber\ System\ Capital\ Cost}{Turbine\ Capital\ Cost} = \frac{\$857,000}{\$89,540,000} = 0.01 \quad (1.184)$$

The savings per year on the system can be estimated by the following equation for various estimates of original turbine lifetime ranging between 5-20 years and various

estimates on the turbine lifetime extension with the implementation of the fiber adsorbent system ranging between 1-5 years:

$$Savings = \left(\frac{Turbine\ Cap\ \$}{Turbine\ Orig\ Life} \right) - \left(\frac{Turbine\ Cap\ \$}{Turbine\ New\ Life} \right) + \left(\frac{Fiber\ Cap\ \$\ +\ Op\ \$}{Fiber\ Life} \right) \quad (1.185)$$

B.7 References

1. Tedder, D.W., *Preliminary chemical process design and economics*. 2005, ill. ;: xxii, 396.
2. Peters, M.S., *Plant design and economics for chemical engineers*. 4th ed. ed. McGraw-Hill chemical engineering series, ed. K.D. Timmerhaus. 1991, McGraw-Hill: New York.
3. Guthrie, K.M., *Process plant estimating, evaluation, and control*. 1974, Craftsman Book Co. of America: Los Angeles.
4. Popper, H., *Modern cost-engineering techniques; an economic-analysis and cost-estimation manual, with comprehensive data on plant and equipment costs in the process industries. edited by herbert popper and the staff of chemical engineering*, ed. e. chemical and e. chemical. 1970: New York, Mcgraw-hill 1970.
5. Page, J.S., *Conceptual cost estimating manual*. 1984, Gulf Pub. Co. Book Division: Houston.
6. Welty, J.R., *Fundamentals of momentum, heat, and mass transfer*. 5th ed. ed. 2008, Wiley: Hoboken, N.J. ;.
7. *Georgia Gas Marketers' Price Chart*, 2013, Georgia Public Service Commission.
8. Humphreys, P., *The Benefits of On-site Nitrogen Generation*, 2013, Atlas Copcp Compressors.
9. *Technology Characterization: Gas Turbines*, 2008, Energy and Environmental Analysis: Arlington, VA.